2003-06-01

The Influence of Surface Treatments and Surface Finish on the Fatigue Properties of Elastomers

Amir Tabakovic
Technological University Dublin, amir.tabakovic@tudublin.ie

Recommended Citation

Tabakovic, A. (2002). *The Influence of Surface Treatments and Surface Finish on the Fatigue Properties of Elastomers*. Masters dissertation. Dublin Institute of Technology. doi:10.21427/D7R62V

THE INFLUENCE OF SURFACE TREATMENTS AND SURFACE FINISH ON THE FATIGUE PROPERTIES OF ELASTOMERS

by

Amir Tabaković, Dip. Eng., B. Eng.

A Thesis Submitted in fulfilment of the Degree of Master of Philosophy

School of Mechanical and Transport Engineering
Dublin Institute of Technology

June 2003

Dr. Jim McGovern
Head of School

Dr. Steve J. Jerrams
Dr. Brian Bowe
Project Supervisors

Declaration

I certify that this thesis which I now submit for examination for the award of the Degree of Master of Philosophy, is entirely my own work and has not been taken from the work of others save and to the extent that such work has been cited and acknowledged within the text of my work.

This thesis was prepared according to the regulations for postgraduate study by research of the Dublin Institute of Technology and has not been submitted in whole or in part for an award in any other Institute or University.

The Institute has permission to keep, to lend or to copy this thesis in the whole or in part, on condition that any such use of the material of the thesis be duly acknowledged.

Signature Amit Vaidya **Date** 13/10/2003

Candidate

Acknowledgements

Thanks are extended to the following people and organisations for their assistance in various ways over the course of this study:

- Dr. Steve Jerrams, project supervisor. His advice, support and encouragement are gratefully acknowledged.
- Dr. Frank Abraham for his assistance and constant support throughout.
- Deutsches Institut für Kautschuktechnologie e.V.Hannover, Germany for allowing use of its test and manufacturing equipment and for supplying this project with raw and testing material.
- Dr. Miriam McConnell from Enterprise Ireland who helped me with the DLC coating and Dr. David Kennedy for his valuable comments during the coating stage of the research.
- Mr. James Vahey for machining the Elastomeric Clamps and for allowing use of his Shot Peening Test Rig.
- To all the technical support staff in the Mechanical Engineering Department and Chemistry Laboratories in DIT Bolton Street (Mr. Derek McEvoy, Mr. Denis McKeown, Ms. Ann Reid) for their help with the experimental work.
- Dr. Brian Bowe second supervisor and Dr. Emilia Mitkova Mihailova from DIT Kevin Street for facilitating access to the White Light Interfermeter and ESPI System.
- To my fellow researchers in DIT, especially John Hanley.
- To my girlfriend Niamh for her support and editing with meticulous attention at multiple stages.
- Last but not least to my parents and family. This thesis would not have been completed without their constant support via phone calls, e-mails and letters.

Abstract

Recent research has shown that fatigue life in non strain-crystallising rubber increases if the material is subjected to pre-loading. The central research question posed in this project is `whether preloading and surface treatments improve the surface finish of rubber components, reduce stress concentration and can this reduction partially account for greater fatigue resistance`.
The specific objectives of the research are: -

i) To assess surface finish measurements and to investigate the changes in stress concentration in preloaded rubber samples using White Light Interferometry.

ii) To consider other non-contact methods of observing changes in stress concentration in preloaded samples through use of:
i) Electronic Speckle Pattern Interferometry (ESPI) methods, ii) Ultrasonic methods.

iii) To examine whether coatings or other surface treatments can play a part in diminishing the surface flaws produced in the various manufacturing processes. The coatings/treatments investigated were:
i) Diamond Like Carbon Coating (DLC), ii) Sol-gel Coating Technology and iii) Surface Peening treatments.

iv) To use MSC/MARC Non-linear Finite Element software to model:
i) fatigue behaviour of DLC coated EPDM rubber, ii)EPDM rubber elastomeric crack propagation, iii) flaw behaviour in EPDM rubber,

v) To advise on design standards for pre loaded rubber components and to establish criteria for selecting elastomers that will minimise the likelyhood of fatigue failures in the light of the aforementioned research and of this study.

The Deutsches Institut für Kautschuktechnologie (DIK) supplied the test material for this research and provided facilities for the rubber vulcanisation process described in this work. DIK also allowed use of their test equipment. The Research involved the design of a clamp for tensile testing of elastomers, a compression mould and an ESPI in-plane test rig.

An initial investigation determined that stress concentration diminishes with prestressing rubber components. White Light Interformetry was found to be the most suitable method of non-contact analysis. The only disadvantage proved to be the small field of view. The ESPI Method did not show results as positive as those achieved using WLI, however further investigation is required before this method is discounted. The Ultrasonic non-contact method was not evaluated but a schematic system is recommended for further research. Analyses for surface roughness and stress concentration at the surface flaws of EPDM rubber using the WLI confirmed that prestressing decreases surface roughness values. The measurement of stress concentration at surface flaws using the WLI method was not successful, because the test rig used was inappropriate to perform this test. However, it was shown that WLI could detect surface defects. Another method was evaluated which uses the Olympus BX60M System Microscope in combination with the Omnimet Archive Digital

Imaging System. This method was used to measure stress concentration at the tip of an initiated edge crack. The Griffith theory for measuring stress concentration at the crack tip was employed. The results showed that pre-stressing of rubber samples results in reduction in stress concentrations at the crack tip.

The first surface treatment applied was Diamond Like Carbon (DLC) coating. This coating was used because carbon particles exhibit an appropriate size to fill the surface defects present in rubber. The coating process was performed in the laboratories of Enterprise Ireland (EI). The coating procedure involved heating the samples to a temperature of 120°C and this caused a change in the physical properties of the rubber samples. The fatigue test results show that DLC treatment does not improve the fatigue life of elastomers. However, data from the same tests also show that the complex modulus E* fell to approximately 76% of the first cycle. This supports the hypothesis in the earlier research that the complex modulus can be used for safely predicting the service life of rubber components.

Following these tests, further coating was attempted, this time employing a rubber like material using Sol-gel technology. Tetraoxidsilicate (TEOS) liquid solution was chosen as the coating material because it has a low crystallisation temperature. The results were disappointing because the coating did not react with the rubber material and so did not successfully crystallise on the surface of the rubber specimen.
Shot Peening was also used to treat the EPDM rubber surface of same samples prior to tensile testing. The tests showed that no change in tensile properties of EPDM rubber occurred in comparison with untreated EPDM rubber. However, Microscopic analysis showed improvement in the surface roughness (R_a).

For carrying out a Finite Element Analysis (FEA), material data was obtained from uniaxial tests. The first test was an axisymmetric analysis of fatigue behaviour of the DLC coated EPDM rubber. For these analyses data was used from the first recorded cycle and the last recorded cycle of the fatigue tests. Material models were determined for implementation in the analysis using MSC/MARC software. The axisymmetric analysis of the fatigue specimen simulated the model being subjected to the same displacements that produced values of maximum stress in the tests. FEA reasonably accurately predicted the physical test results. The axisymmetric FEA of the crack models showed a large concentration of stress at the tip of the crack. The FE plain strain analysis of the EPDM rubber sample, with a flaw of 60μm in diameter modelled, gave the best correlation with physical tests. The Ogden material model represents the most plausible model and is the most popular function using stretch ratios. For the Ogden model, a two-term function was used and constants were calculated from uniaxial tests. In future an emphasis must be placed on creating appropriate material models.

Conclusions can be summarised as follows.

- White Light Interferometery is the best metrology method considered for measuring surface roughness and profiling the geometries of surface defects in rubber materials.
- Tensile loading reduces stress concentration.
- Surface finish improvements may contribute to improved fatigue life.

- An exponential decay formula is proposed for determining improvement in surface finish with tensile load.
- The coatings or surface treatments did not increase fatigue life.
- The dynamic stored energy theory of fatigue in non strain-crystallising rubbers is supported.
- That 'loss in complex modulus' can be used as a predictor of fatigue life for non-strain crystallising rubbers is cofirmed.

Table of Contents

Table of Contents

Table of Contents

List of Figures

List of Figures

List of Figures

List of Figures

List of Figures

List of Tables

List of Tables

Abbreviations

A	Width of a flaw
B	Length of a flaw
E	Young's modulus
E*	Complex modulus
F	Force
G	Shear modulus
I_1,I_2,I_3	Strain invariants
j	Volumetric ratio in Ogden Formula
k_f	Dynamic stress concentration
k_t	Stress concentration
l	Depth of edge flaw
l	Crack length
l_g	Critical crack length
l_n	Test specimen gauge length
n	Fatigue life, service life
r	Radius of the dumbbell test specimen
R	Tip radius
R_a	Average surface roughness
R_{as}	Surface finish at stretch ratio λ (μm)
R_{ao}	Surface finish of unstrained rubber (μm)
t	Time
tan δ	Loss factor
T	Strain energy release rate

δ	Displacement
ε	Strain
$\lambda, \lambda_1, \lambda_2, \lambda_3$	Stretch ratios, principal stretch ratios
σ	Stress
σ_t	Stress at the tip of a sharp flaw
W	Strain energy (density)
α_n, μ_n, β_n	Ogden Constants
ν	Poisson's ratio

Chapter 1

Introduction

In material science, investigation of the behaviour of non-linear materials has had insufficient consideration when compared with conventional solids. Unlike linear materials such as metals, relatively little is known about how non-linear materials behave under dynamic load.

Elastomers can withstand very large reversible strains without permanent deformation. This makes them an ideal design material for sealing and damping applications. Elastomeric materials can withstand large static and dynamic strains for long periods of time. Virtually all rubber components in service will be subjected to dynamic loading conditions. Typical examples of dynamic loaded components used in industry today are: V-belts, conveyor belts, seals, engine mounts, tyres, etc. As with other materials, elastomeric components are deformed according to their stiffness and an important property for all rubber components is Elastomeric Fatigue Behaviour.

Currently, an acceptable method of calculating and predicting the fatigue life of elastomeric components does not exist, though much work has been devoted to studying the energy released in crack propagation [1,2]. These methods rely on inducing a cut in the specimen and are thus not easily applied to actual un-notched components. Therefore the designer must produce prototypes and test them under service conditions. Such procedures can prove to be very expensive and time consuming. A solution often used is to design components larger than required so

that they easily attain the expected service life. This practice results in material wastage and component design and manufacture become expensive and inefficient. To improve the quality of manufactured elastomeric parts there is a need to calculate and simulate the fatigue behaviour of rubber components. Currently it is still not clear what criteria are applicable to the prediction of the service life of typical rubber components.

1.1 Aims and Objectives

Research carried out by Abraham [3-6] in the Deusches Institut für Kautschuktechnlogie (DIK), showed great improvements in fatigue life with increases in the minimum stress from zero applied to non-strain crystallising rubbers (pre-loading). Related research, undertaken in Dublin Institute to Technology (DIT) [7] considered the stress concentrations at the surface of the rubber specimens. The results showed that the stress concentration around surface flaws in Natural rubber (NR) and Ethylene Propeylene Diene Rubber (EPDM) produced in the manufacturing processes diminishes with pre-loading (see chapter 5).

Consequently this work focused on the following research objectives:

i) Surface finish measurements were assessed and the changes in stress concentration in preloaded rubber samples were investigated using White Light Interferometry. The question posed: was whether preloading could improve the surface finish of a rubber component and whether this could partially account for greater fatigue resistance?

The research also considered other non-contact methods of observing the changes in stress concentration in preloaded samples.

The Electronic Speckle Pattern Interferometry (ESPI) [8] method is considered to be a reliable non-contact method of observing surface flaws. It provides an accurate display phase distribution over the object surface subjected to stress (load).
Previous research undertaken on ceramics and metals showed that the ESPI method is well suited to the study of crack propagation. To date ESPI has not been used for detecting or measuring crack propagation in rubber materials. Therefore this research examined the suitability of ESPI in the investigation of crack propagation.

The Ultrasonic technique is another method that is well known in the inspection of metal and ceramic material surfaces. An ultrasonic analyser has been developed for the non-contact analysis of non-liner materials, the NCA 1000 Ultra sonic non-contact analyser [9]. Therefore an additional research aim was to examine the use of ultrasonic technology in the measurement of changes in the stress concentration of preloaded samples.

ii) A further objective was to examine whether coatings or other surface treatments could play a part in diminishing the surface flaws produced in the manufacturing process. Coating processes are often used in the treatment of metal surfaces. However, for rubber materials coatings have only been used for the purpose of wear resistance. As research to date has not considered whether coating would improve the fatigue properties of rubber, this became another research question.
To complete the coating processes successfully, high temperatures are required. Heat treatment can be expected to change the properties of rubber material. The heat involved in the procedures will invariably result in a deterioration of rubber properties. Hence an aim of the research was to investigate the rubber coating

treatments and technologies available. It was hoped to find a suitable surface coating treatment that would improve the fatigue properties of Rubber materials without causing deterioration in other rubber properties. The process must also be economically viable. The influence of both the surface finish and surface treatments on the fatigue life of rubber will be evaluated. The results should show whether a simple surface finish treatment can increase the service life of an elastomeric product

iii) A further objective was to use MSC MARC Non-linear Finite Element software, to model: i) fatigue behaviour of DLC coated EPDM rubber, ii) elastomeric crack propagation, iii) flaw behaviour in the EPDM rubber. Using stress/strain data from physical tests and applying the rules for curve fitting to give plausible material models [10], the analysis ascertained the most suitable data for FEA modelling and simulation of the notch dimensions to model actual material behaviour.

iv) The final objective of this research project was to advise on design standards for pre-loaded rubber components and to establish criteria for selecting elastomers that should minimise the likelyhood of fatigue failures in the light of the results of this research and Abraham's research.

Chapter 2

Literature review

2.1 An Introduction to Elastomeric Materials

2.1.1 Properties and definitions of Elastomers

The terms elastomer and rubber have the same meaning in science, although the latter is used by some to refer only to natural rubber which comes from the latex contained in some trees and other plants, as opposed to synthetic rubber which is generally a by-product of oil. Some standards attempt to reserve the term elastomer for a crosslinked material, but there is no general agreement on this. In fact, the terms elastomer and rubber are generally synonymous.

Elastomers are a class of materials which differ substantially from all other solid materials because they can be easily stretched and from a state of high extensions, they are almost completely reversible. An ordinary rubber band illustrates this behaviour. Rubber bands are generally made from natural rubber, and can be stretched almost seven times their original length after which, providing they have not reached their ultimate breaking elongation, they can be released and will rapidly recover to almost their original lengths. This material is said to be hyperelastic.

Most synthetic elastomers are not as elastic as natural rubber, but all can be stretched (or otherwise deformed) in a reversible manner to a large extent. This distinguishes elastomers from most other solid materials. (Although a metal spring appears to be similar, in that a metal spring exhibits high reversible elasticity, this is simply a feature of its wound shape. The actual metal of which the spring is made only

deforms slightly, by twisting locally, at any particular point and without experiencing the high deformations of which elastomers are capable.)

Elastomers are a special subgroup of the wider group of materials known as polymers. Polymers are not made up of discrete compact molecules like most materials, but are made of long, flexible, chain-like or string-like, molecules [11]. At this scale, the inside of a piece of rubber can be thought of as resembling a serving of cooked spaghetti. However in spaghetti the chains, though intertwined, are all separate but if you leave them to cool the spaghetti sticks together and act in the same way as chains of rubber molecule (except that the deformations are not reversible). In most elastomers, each chain will be joined to one or more nearby chains by a few chemical bridges, known as crosslinks. So the whole structure forms a coherent network which stops the chains from sliding past one another indefinitely although leaving the long sections of chain between crosslinks free to move. The process by which crosslinks are added is known as vulcanisation. To achieve vulcanisation, the raw rubber is mechanically mixed with a number of compounding ingredients, carefully chosen to give the properties required for the particular application. The reason that elastomers behave as they do is due to the type of molecular structure described above [11].

Against this background, the reason that rubber can stretch so much is that, at normal temperatures, each long chain-like molecule (like any molecule) is in a constant state of agitation (thermal motion) [12]. The lateral forces between the molecules are weak and hence the molecules can readily slide over one another when deformed. For these flexible long chain molecules the movement is considerable, and the molecule is agitated to such an extent that it can take up a highly distorted shape. Because of this distorted shape, the distance between the two ends of the chain is much less than

its fully stretched length. This gives the rubber its flexibility. When a rubber band is extended, some of the highly distorted chains are simply being stretched out. Stretching can then continue until many of the chains are fully extended, or until the rubber breaks.

This describes why elastomers can stretch, but does not explain why, when the stretching force is removed, the material returns to its original shape. This can be explained by thermodynamics, and a simplified description is given here. When the rubber is at rest at normal temperatures, the chain-like molecules are in a constant state of agitation and are highly random in configuration due to thermal energy. This is a highly disordered state described thermodynamically as being in a state of maximum entropy [12]. When the chains are stretched, a higher level of order is obviously being imposed. In other words, the chains are being forced into a state of lower entropy. As it is a fundamental law of thermodynamics that entropy strives for a maximum, the driving force returns to the disordered state and as soon as the stretching force is removed, the rubber will retract.

2.1.2 High temperature behaviour

The highest temperature at which an elastomer may be used is generally determined by its chemical stability, and will vary for different elastomers. Elastomers can be attacked by oxygen or other chemical agents, and because the attack results in a chemical reaction, its potency will increase with temperature [13]. Degradative chemical reactions are generally of two types. The first are those which cause breakage of the molecular chains or crosslinks. These result in a softening of the rubber because they weaken the network. The second are those, which result in additional crosslinking, which harden the rubber and are often characterised by the

formation of a hard, degraded, skin on the rubber component. Using a selection of a suitable elastomers and using chemical anti degradants can reduce the rate of chemical attack.

2.1.3 Fluid resistance

As already outlined, the structure of an elastomer comprises of a network of chains which means that there are gaps between the adjacent chains. The elasticity of rubber relies on substantial thermal motion of the chains, which would not be possible if the chains were tightly packed together. This free volume available within the rubber means that some liquids can enter the rubber and cause swelling [14]. For example, the ability of oil to swell natural rubber is well documented. The potential for swelling is largely controlled by a thermodynamic property known as the solubility parameter. All rubbers and all liquids have specific solubility parameter values, a knowledge of which enables designers to avoid excessive interaction between an elastomer and the fluids which it will come into contact with in service.

2.1.4 Incompressibility

Another property of elastomers that distinguishes them from other solid materials is their virtual incompressibility. For most practical purposes, other than use under very high pressures, elastomers do not change their volume significantly when deformed [15]. A rubber band may stretch 600%, but if its volume were measured in the stretched state, it would be found to be almost identical to its unstretched volume.

This has important implications for designing with elastomers, as the stiffness of components can be controlled, not just by altering the rigidity of the rubber itself, but also through the use of various techniques of restricting volume changes. This

phenomenon is known as shape factor effects and leads to greater versatility in design. In particular, it enables rubber components to be designed with different, and controlled, stiffnesses and other properties, in two or even three different directions.

2.2 Physical Properties of Rubber

2.2.1 Hyperelasticity

Virtually all research characterising the behaviour of rubber derives from observing rubber under different conditions of homogenous strain [16]. This phenomenological approach assumes that the material will behave isotropically and that the initial orientation of the chain molecules is random. Elastic strain energy density functions are obtained from experimentation. Strain energy (W) can be expressed as a polynomial function of strain invariants (I) or alternatively in terms of principal stretch ratios (λ). A component manufactured from a hyperelastic material will exhibit large localised strains in service and the nature of the applied loads will influence the accuracy of the model. Stretch ratios (λ) are determined by adding the unit one to values of "engineering strain" hence $\lambda = 1 + \varepsilon$ [16].

2.2.2 The Viscoelastic Properties of Rubber

Viscoelasticity is defined as stress response of a material which behaves as though it were a combination of an elastic solid and a viscous liquid [17]. The chain rotation process gives rise to a wide spectrum of relaxation times in the polymer, varying with the temperature. With stress at high temperatures, flow properties are emphasised, but with stress at low temperatures, solid properties dominate. In

properties other than those associated with mechanical deformation, rubbers resemble liquids as revealed by scattering of X-rays (representing molecular disorder) [16].

Common mechanical tests for rubber subject the specimens to tensile, compressive or shear forces, to measure properties which will determine behaviour in service. The loading may be transient or periodic (dynamic). These tests are time dependant and provide information on viscoelastic properties.

2.2.3 Creep

All rubbers exhibit some degree of creep. Creep is usually defined as the increase in deformation which has occurred after a specific time interval, during the application of constant force [18]. The deformation due to creep is not recoverable and, unlike in metals, is not confined to high strains and high temperatures, but will occur for any form of loading. Creep in elastomers will usually increase linearly if plotted against time having a logarithmic scale. However, if a stress is maintained for a very long time, the rate of creep will eventually rise sharply and this will result in an associated oxidative breakdown and failure of crosslinks, as can be seen in Figure 2.1. The amount of creep varies greatly in rubbers and is dependent on a number of factors, the principal ones being that:

i) Vulcanised synthetic rubbers tend to creep more than vulcanised natural rubbers;

ii) Generally, the greater the amount of filler in a compound, the greater the incidence of creep;

iii) Hard rubbers creep more than soft rubbers;

iv) Rubbers containing more crosslinks creep less than those with fewer (hence less well vulcanised rubber) [16].

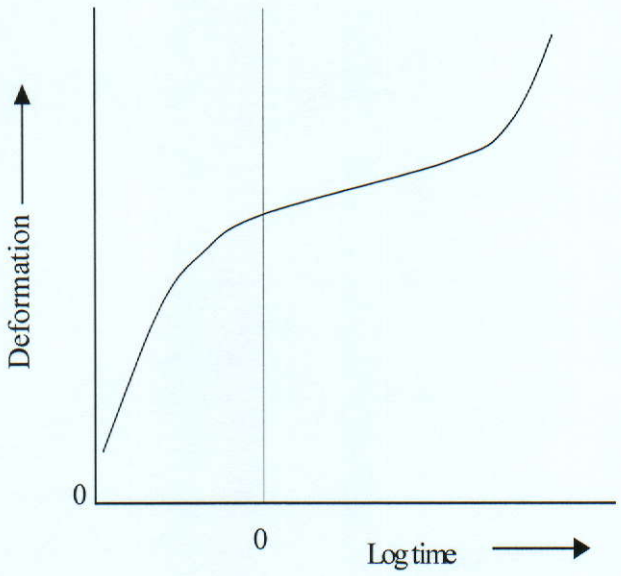

Figure 2.1 Typical Creep Curve for Rubber at High Stress [16]

Two phenomena closely related to creep are **work softening** and **fatigue**.

Work softening is a reduction in static shear modulus resulting from cyclical loading. It can go unnoticed because no permanent deformation of the rubber occurs and, on the removal of the load, a work softening rubber will appear to return to its original state. However, if work softening and set are present in the same component, their effects will tend to cancel each other out. If a rapidly fluctuating stress is applied to a rubber, the modulus gradually reduces. This process, termed **fatigue** can be considered a form of stress relaxation that is comparable to an increase of strain at constant stress, or creep. Plotted against log time, the modulus gives a straight line, similar to that of creep [16].

2.2.4 Stress Relaxation

Stress relaxation and creep are physical changes resulting from the same viscoelastic phenomenon. Whereas an ideal elastic solid subjected to a fixed strain for a specific period of time will record a constant stress, a viscoelastic material having nominally instantaneous strain applied will experience a reduction in the initial stress with time [18].

Figure 2.2 "shows stress relaxation occurring in a uniaxial tensile test. The test was on a sample of 60 IRHD rubber of a gauge length 15mm, extended to a stretch ratio of 4 at a rate 120 mm/min and held at that extension for 10 minutes. After 3 minutes the tensile stress in the sample had fallen by 14%. Most of this reduction occurred in the first 20 seconds of dwell at $\lambda = 4$" [16].

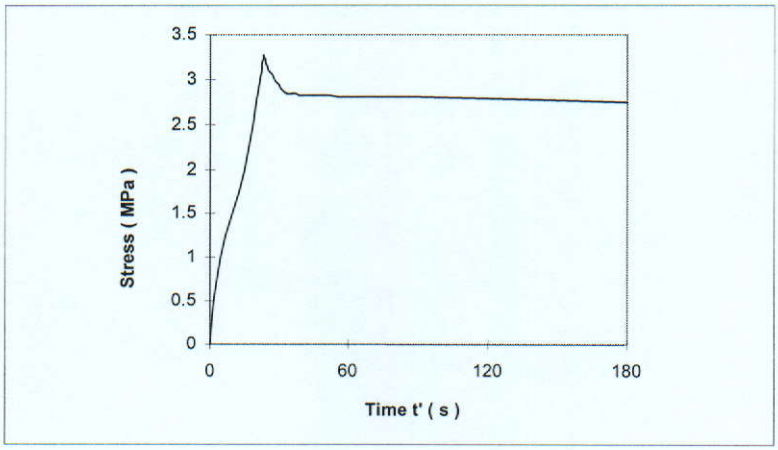

Figure2.2 Stress Relaxation in a Medium Hard Rubber [16]

Many mathematical models have been proposed to describe viscoelastic behaviour. The Kelvin (Voigt) model, as shown in Figure 2.3a, uses a Hookean spring and

Newtonian dashpot in parallel to represent the time dependent component of creep, whilst the Maxwell model, as shown in Figure 2.3b, places the spring and dashpot in a series and is of value when considering stress relaxation. Zener added a second spring in parallel with the Maxwell unit to provide an approximation of the behaviour of polymers in the viscoelastic range, as shown in Figure 2.3c. This three-element model is known as the standard liner solid (SLS). Often, to give an approximation of linear viscoelastic behaviour the analyst will use a combination of these models. However, the models cannot adequately represent time dependent, non-linear viscoelastic rubber and, in practice FEA codes have frequently employed modified forms of Mooney-Rivlin, Ogden and other polynomial strain energy functions which are described further in reference [19].

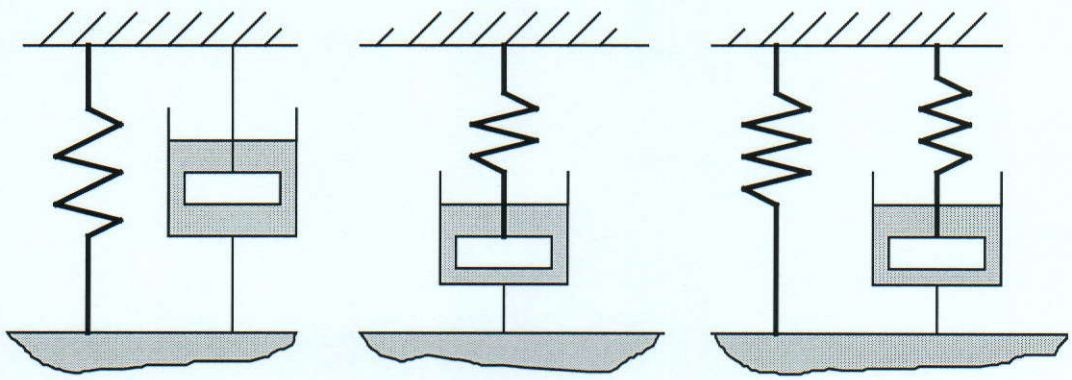

(a) Kelvin (Voigt) Model (b) Maxwell Model (c) Zener SLS Model

Figure 2. 3 Alternative Representation of Viscoelasticity in Polymers [16]

2.2.5 Set

Set is a measure of deformation in a material after load has been removed. Unlike models made of conventional solid, which will normally be considered to have failed when they have fractured or reached a level of wear that impairs their function, a rubber component can fail for a variety of reasons. Creep, work softening or set could all cause an elastomeric component not to fulfil its function. Since set is an important parameter when maintaining component function, for instance sealing efficiency, the rubber industry has tended to focus on measuring recovery. The notion of 'permanent set' in relation to rubbers is virtually meaningless since its measurement would require an infinite recovery time. Hence, set will normally be expressed as a percentage of the applied deformation for a given recovery time, as shown below [18].

$$\text{Set} = (t_o - t_r / t_o - t_s) * 100\% \quad \text{(compression set)} \qquad (2.1)$$

Where: t_o = initial thickness, t_r = recovered thickness and t_s= compressed thickness.

2.2.6 Stress Softening

When subjected to stress cycles, rubber dissipates energy as a result of hysteresis effects. Filled rubbers stress soften and a rubber component will have a 'steady state' response markedly different from its initial response. Carbon black is added to rubber to reduce costs and because it enhances stiffness and toughness. However, strain induced stress softening in such rubbers result from a break down of crosslinks and a gradual detachment of the reinforcing fillers from the long chain molecules. This

phenomenon is known as the Mullins' effect [16] in recognition of the research he conducted into history dependent stiffness.

2.2.7 The Hardness of Rubber

Hardness is most simply defined as 'resistance to indentation`. The hardness of rubber has been used widely as a control test and many product specifications quote hardness as a guide to the type of compound required. Indeed in many cases, this may be the only property specified. Hardness tests may indicate the state of vulcanisation or degradation in use. Compound hardness is largely determined by the type and amounts of reinforcing fillers and softeners used and by the use of cross-linked resin systems [20]. The hardness quoted for rubber is usually either IRHD or Shore A values [20,21]. In both systems, increasing hardness is represented by increasing numbers and the International Rubber Hardness Degree (IRHD) is found by indenting a rubber block with a steel ball to a specified force; a dead load test. This method is popular for characterising rubber as the indentation depth is assumed to be related to the initial shear modulus by equation 2.2.

$$d = (3P_2 / 16\, G^* r^{0.5})^{2/3} - (3P_1 / 16\, G^* r^{0.5})^{2/3} \qquad (2.2)$$

Where G is the initial shear modulus, d is depth of indentation, P_1 is a small initial load, P_2 is final load and r is the indentor radius.

Shore A readings are used worldwide, although they have poor reproducibility. Readings are taken using a durometer which utilises a spring to give the indenting

force. Shore A and IRHD scales correspond approximately and are used across the normal range of rubber hardness'; from 30 to 85 IRHD. Very hard rubbers in excess of 90 IRHD are measured for hardness using durometers calibrated on the Shore D hardness scale [21].

2.2.8 Early Theories of Rubber Elasticity

Figures 2.4 a) and 2.4 b) show, the ordering of long chain molecules of rubber in the unstrained and strained state respectively. In reality, the chain segments are disordered in a three dimensional matrix but are of course shown in two dimensions in the figures. Thus, a piece of unloaded rubber comprises a tangled mass of long chain molecules which are free to rotate about the cross-links that join them together. Intermolecular attractions between molecules are small (van Der Wahl's forces), allowing them to move readily past one another. The atoms in the long chain molecules are in constant motion due to thermal vibrations. This causes the individual molecules to assume their irregular sinuous shape. If loaded in any way, the molecules will become more or less aligned with the loading b). The rubber resists this alignment and, if the load is removed, it will return to its more natural random state a). The rubber has its maximum entropy in this state and always tends to assume its original shape when unconstrained [22].

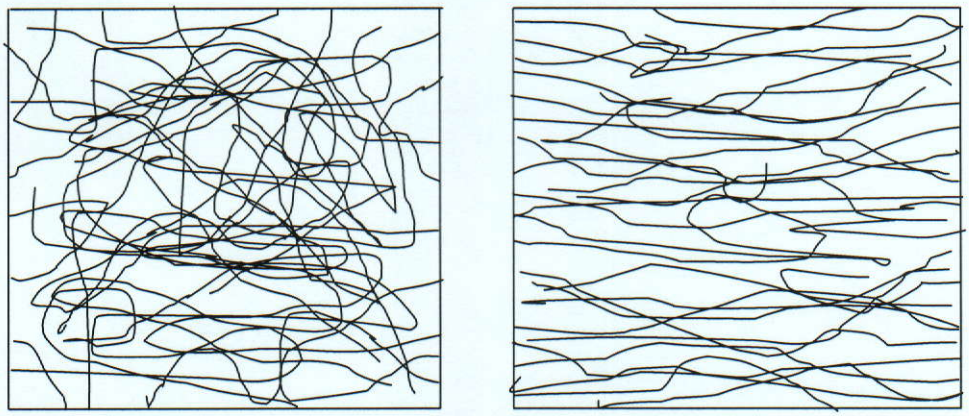

a) b)

Figure 2.4 Rubber in the Unstrained and Strained State [16]

It is unsurprising that initial attempts to characterise this behaviour met with enormous difficulties. A classical solid was thought of as a group of atoms or molecules held in fixed relative position by inter-atomic forces. The magnitude of these forces is dependent upon the distance between atoms and hence large deformations beyond 10% could not be supported. Two alternative hypotheses were advanced to permit large deformations without inducing large stresses in elastic elements. The first suggested some kind of open network and the two-phase theory postulated by Ostwald (1926) [23] was typical of this approach. Increased elasticity was attributed to a structure in which a network of micelles or molecular aggregates were suspended in a semi-liquid medium of rubber hydrocarbon having a lower molecular weight. Fikentscher and Mark (1930) [23] developed a theory which was indicative of the second alternative. They envisaged helical spring molecules wherein residual forces between neighbouring turns of the helix produced retractive tendency in polyisoprene. Similarly, Mack (1934) [23] proposed a model, capable of extensions of 300%, which consisted of folded molecules. Constrained chains form their random directionality allowed extensibility to reach 600%.

2.3 Strain Energy Functions

In finite element software analysis the most common polynomial strain energy function is the James, Green and Simpson (Equation 2.3) [16]

$$W = C_{10}(I_1 - 3) + C_{01}(I_2 - 3) + C_{11}(I_1 - 3)(I_2 - 3) + C_{20}(I_1 - 3)^2 + C_{30}(I_1 - 3)^3 \quad (2.3)$$

This polynomial strain energy function can be used in many different forms, dictated by the requirements of an analysis. Alternatives are summarised bellow.

2.3.1 Strain Energy Functions for Uniaxial Extension

i) **Neo- Hookean model** this is a one parameter model that simulates a material possessing a constant rigidity modulus (G) [16].

$$W = C_{10}(I-3) \quad (2.4)$$

or

$$W = E/6(I_1 - 3) \quad (2.5)$$

The strains at high pressures could be over estimated as the up turn in the stress strain curve associated with the finite extensibility of the chains and the break of the cross links is not modelled.

ii) **Two term Mooney-Rivlin** formulation cannot model complex loads cases since I_1 and I_2 vary greatly with differing modes of load application. The function is largely based on even powered strain invariants and assume a constant value of G. This function overestimates stress for moderate strains and underestimate for high strains [16].

$$W = C_{10}(I_1 - 3) + C_{01}(I_2 - 3) \quad (2.6)$$

iii) The three term Mooney-Rivlin formulation allows some variations in shear modulus.

$$W = C_{10}(I_1 - 3) + C_{01}(I_2 - 3) + C_{11}(I_1 - 3)(I_2 - 3) \quad (2.7)$$

iv) **Yeoh** a development of James, Green and Simpson function that assumes $\delta W/\delta I_2 \approx 0$, which is not unreasonable for filled rubbers in some loading modes. This means that only the C_{10}, C_{20} and C_{30} terms are used in the strain energy function. Yeoh argues that data from a test (Uniaxial Tension) is capable of modelling other deformation modes [16].

$$W = C_{10}(I_1 - 3) + C_{20}(I_1 - 3)^2 + C_{30}(I_1 - 3)^3 \quad (2.8)$$

v) **Two term Ogden** [16] is based on stretch ratios (λ_s) and non strain invariants (I_s). Ogden argues for the use of a three term model derived from testing in a number of deformation modes. Even a two term model based on uniaxial tensile test derives reasonable results for most analysis. This model underestimates stress at small stains.

$$\sigma_1 = \Sigma\, \mu_n/\lambda_1\, (\lambda_1^{\alpha n} - j^{\beta n}) \quad (2.9)$$

Where: β_n is a material constant and j is a volumetric ratio derived from λ_1, λ_2 and λ_3 and hence equals one for incompressibility.

2.4 Fatigue

2.4.1 Fatigue Analysis Methods for Rubber

Fatigue is a reduction of strength as a result of cyclic stressing over a period of time. The question of fatigue in materials is not new. Fatigue has been recognised as a problem for 200 years, from the age of sailing vessels and later when steam engines were invented. However fatigue in polymers is not nearly as well understood. In 1971 [20], it was stated that fatigue in polymers constitutes one of the unsolved problems in polymer science. Our knowledge has advanced since then, but much research is now underway to characterise fatigue for different polymetric materials [24].

2.4.2 Fatigue Failure and Testing

Fatigue failure can be caused by two different mechanisms. In some cases, damping (internal friction) causes a rapid temperature increase. The high temperature can produce a deterioration of the mechanical properties or can lead to thermal breakdown. The risk of thermal failure increases with increasing frequency, strain amplitude and increasing component thickness [25].

In other cases, fatigue failure occurs due to the initiation and growth of one or more cracks. These cracks are usually initiated from defects (pores, particle inclusion, impurities, surface defects, etc., as shown in Figure 2.9, and grow initially at a low rate, but subsequently at an increased rate until the component separates into two or more parts or no longer fulfils its purpose [25].

The fatigue properties of rubbers can be tested in two different ways. When testing unnotched specimens [26], (as described in chapter 6) the material is subjected to a

periodic, often sinusoidal load – usually at a constant strain amplitude. The loads in testing can be either bending or direct, usually at frequencies less than 5 Hz in order to avoid excessive heat build up and resulting thermal failure. Fatigue failure data are often presented in diagrams as shown in Figure 2.5, where the number of cycles to failure is plotted as a function of applied strain or stress. Such Wöhler or S-N curve requires many tests at different strain levels in order to give a complete illustration of fatigue properties and are usually both time consuming and expensive to produce. The scatter of data is usually great and this can often be explained by a variable defect size, (see results in Chapter 6). Since the defect size is usually unknown, the results become unreliable when it comes to grading different materials in respect of fatigue resistance.

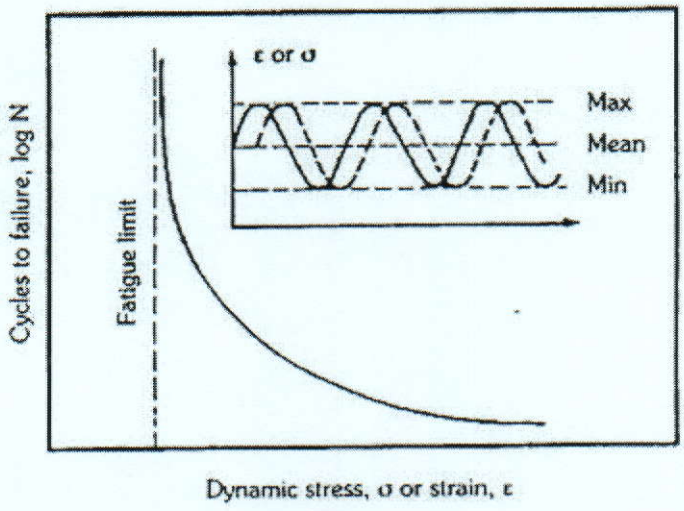

Figure 2.5 "Wöhler" (S-N) Curve for Rubber, where fatigue lifetime is plotted vs dynamic strain or stress. Inset shows maximum, minimum, mean stress and strain. N is the number of cycles [27]

An alternative method that has become increasingly popular is fracture mechanics testing (see Chapter 6). Test specimens are produced with sharp notches and the growth of cracks from the roots of the notches are measured as a function of the

number of load cycles [28]. This method provides more fundamental material data that can be applied to many different types of deformation and geometries [29].

Richard *et al* [30] outlined three major problems in understanding fatigue in polymers:

i) The continuum-mechanics approach to fracture developed by the physicist or engineer does not in it self describe the atomic and molecular processes familiar to the chemist,

ii) The ultimate phenomenon of fracture involves large, irreversible, and non-linear deformations, in contrast to the small scale, reversible and linear deformations often measured in order to characterise the effects of molecular properties and polymer composition,

iii) Our understanding is unclear of the precise nature of the competitive processes that are balanced out in fatigue, and that give rise to the especially damaging effect of intermittent loading.

2.4.3 Approaches for predicting fatigue life

As previously outlined, fatigue is what happens when cyclic loading is present in an object over a long period of time. Fatigue failure can occur at stresses well below the ultimate tensile strength of a material. In essence, the repeated loading / unloading helps a crack (on the surface, or internal, such as a flaw, knot, or inclusion) to grow, and eventually the crack becomes large enough to spontaneously and rapidly propagate across the entire cross section of the object. Typically, the fatigue failure process involves two distinct phases. The first phase is a period during which cracks nucleate in regions that were initially free of observable cracks. The second phase is

a period during which nucleated cracks grow to the point of failure. Mars and Fatemi [25] outlined two approaches for predicting fatigue life in rubber. One approach focuses on predicting crack nucleation life and the other approach is based on the principles of fracture mechanics.

2.4.3.1 The Crack Nucleation Approach considers that the material has intrinsic life determined by the history of stress or strains at a point. This approach is convenient because it is formulated in terms of stresses and strains, which are familiar to designers. The approach is particularly appropriate in applications where the initial flaws that decay component life are several orders of magnitude smaller than component features and where it is desired to analyse the spatial distribution of fatigue life.

Two widely used fatigue life parameters for crack nucleation prediction in rubber are those at maximum principal strain (or stretch) and strain energy density. Neither of these parameters have been very successful in correlating results from different strain states, especially simple tension-compression and equibiaxial tension-compression. The nucleation approach has received less attention in the literature, although many engineers still use this approach for its simplicity and familiarity [25].

2.4.3.2 The Crack Growth Approach explicitly considers pre-existing cracks or flaws. Focusing attention on individual flaws was an idea introduced by Inglis in 1913 [31] and Griffith in 1920 [32]. Griffith proposed a fracture criterion based on the energy of a cracked body and the energy associated with the crack surfaces, which is described later in the text. Griffiths approach was further developed for rubber by Thomas, Greensmith, Lake, Lindley, Mullins and Rivlin [1, 33, 34] in the

1950s and 1960s. The original application of this approach to rubber was to predict static strength. In the late 1950s, Thomas furthered this approach by analysing the growth of cracks under cyclic loads in NR. Thomas [35] showed the first two important developments in the fracture mechanics of rubber, the connection between the energy release rate and the strain concentration at the crack tip.

Some success has been achieved in developing and applying the crack growth approach to rubber. Robust numerical procedures are required. When the crack is small, another problem is in determining the initial size and shape of the crack. Small flaws are often of particular importance, since most of a component's life may be spent on the growth of small flaws. For uniaxial situations in which failure initiates from a small flaw, the strain energy density can be used to estimate the energy release rate of the flaw, from which fatigue life can be computed, given the fatigue crack growth curve. For multiaxial situations, the strain energy density is not generally appropriate because not all of the energy is available to be released by the growth of a flaw. An adequate multiaxial nucleation life approach is needed to accurately predict fatigue life in rubber components.

2.5 Crack Growth

2.5.1 The Energy Release Rate

Griffith's [32] hypothesis was that crack growth is due to the conversion of a structure's stored potential energy to surface energy associated with new crack surfaces. He was able to show that the surface energy associated with new crack faces of a broken glass filament was equal to the elastic energy released by the fracture. In the rubber, the potential energy released from surrounding material is

spent on both reversible and irreversible changes to create the new surfaces [33, 36]. Griffith's approach was further developed by Rivlin and Thomas [33]. They defined a quantity known as tearing energy, denoted 'T', which is defined as the decrease of elastic strain energy. In any case, the energy release rate is simply the change in the stored mechanical energy dU, per unit change in crack surface area dA.

$$T = - (dU/dA) \qquad (2.10)$$

The energy release rate was first applied to analysis of rubber specimens under static loading [25]. Rivlin and Thomas showed that tearing energy is a true material property, independent of specimen geometry and type of load.

Commonly used test specimens for determining tearing energy of rubbers are shown in Figure 2.6. For an edge notched tensile specimen ("Tensile strip" or "Single Edge Notched (SEN) specimen") in Figure 2.6a it has been shown [33, 36] that the energy release rate in simple extension is given by:

$$T = 2kWl \qquad (2.11)$$

Where W is the strain energy density in the bulk of the material and for large strains, l is a crack length, k departs from the classical value of π, being given approximately by:

$$k = \pi / \lambda^{1/2} \qquad (2.12)$$

Where λ is extension ratio.

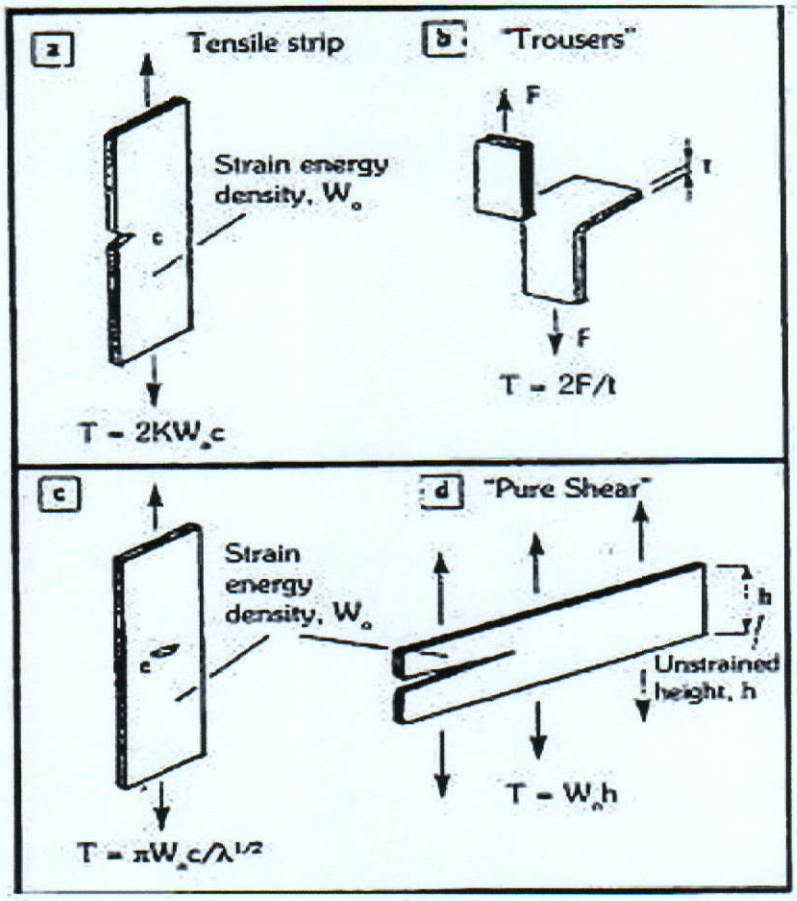

Figure 2.6 **Crack Growth Test Specimens: a) Single Edged Notched (SEN) Specimen or Tensile Strip, b) Trouser Specimen, c) Centre Notched Specimen, d) Pure Shear Specimen [1]**

2.5.2 Tensile strength

Tensile failure can be treated essentially as a single cycle of a fatigue test, although there are complications for both crystallising and non-crystallising rubbers [36]. Some of these also apply when calculating relatively short fatigue lives but with suitable modification in this region the theory works reasonably well for lives ranging from some 10^8 cycles down to the single cycle tensile failure.

2.5.3 Griffith Criterion and Critical Crack Length

As previously stated fatigue is a deterioration in the physical properties and eventual failure of rubber when repeatedly subjected to a stress well below its ultimate tensile strength. The onset of fatigue in rubber is characterised by the appearance of a series of cracks on the surface, which enlarge on repeated deformation, and which eventually cause failure. Drastic section changes in the stress-strain cycles, or the rubber going through zero displacement (relaxation) in a plus-minus straining cycle will lead to fatigue failure of rubber.

In 1920 A. A. Griffith [32] undertook a novel approach to the whole problem of fracture by considering the available energy to propagate crack. Griffith stated that two conditions must be fulfilled if a crack is to propagate. Firstly, there must be a molecular mechanism by which the energy transformation can take place. Consider however the transformation that occurs during the intermediate stages of fracture. When a crack appears in strained material, it will open up slightly, so that the two faces of the crack are separated. This implies that the material immediately behind the crack is relaxed and the strain energy in that part of the material is released. If we think of the crack as proceeding inwards from the surface of a stressed material, we should expect the area of material in which the strain is relaxed to correspond roughly to the two shaded triangles, as shown in Figure 2.7.

Figure 2.7 Griffith Criterion for Crack Propagation

Now the area of the two triangles is roughly l^2, where l is the length of the crack. The relief of strain energy would be expected to be proportional to the square of crack length, or depth, and this rough guess is confirmed by calculation. Thus a crack two microns deep, releases four times as much strain energy as a one micron deep crack and so on.

Also, surface energy, 2Gl (where G is the free surface energy which is measured in J/m^2), is needed to form the new surfaces. This increases only as the first power of the depth of the crack. Thus, the crack two microns deep has twice the surface energy of a crack one micron deep. The consequences of this are very clear; when the crack is very shallow it consumes more energy as surface energy than it is releasing as relaxed strain energy and therefore the conditions are energetically unfavourable for it to propagate. However, as the crack becomes deeper, these conditions are reversed and beyond the 'critical Griffith length' l_g, the crack is producing more energy than it is consuming, and it may start to grow in an explosive manner.

At the theoretical maximum stress the critical crack length l_g is extremely short and at zero stress it is infinitely long, which is expected.

$$l_g = 1 / \pi * \frac{\text{Work fracture per unit area of crack surface}}{\text{Strain energy stored per unit volume of material}} \qquad (2.13)$$

Algebraically, this can be shown to be equivalent to

$$l_g = 2WE / \pi s^2 \qquad (2.14)$$

Where:

W = work of fracture in J/m^2 for each surface, E = Young modulus in N/m^2,

s = average tensile stress in material near the crack in N/m^2,

l_g = critical crack length (m).

The stress concentration at the tip of a crack is approximately:

$$k = 2 (1/R)^{0.5} \qquad (2.15)$$

Where: l = crack length, R = tip radius.

2.5.4 Linear Elastic Fracture Mechanics

Linear elastic fracture mechanics (L.E.F.M.) was developed from the early work of Griffith who sought to explain why the observed strength of a material is considerably less than the theoretical strength, based on the forces between atoms. He concluded that real materials must contain small defects and cracks which reduce their strength. These cracks cause stress concentrations but they cannot be allowed for by the calculation of a linear elastic stress concentration factor k_t. The elliptical defect is shown in Figure 2.8 and has its stress concentration factor defined by equation 2.16.

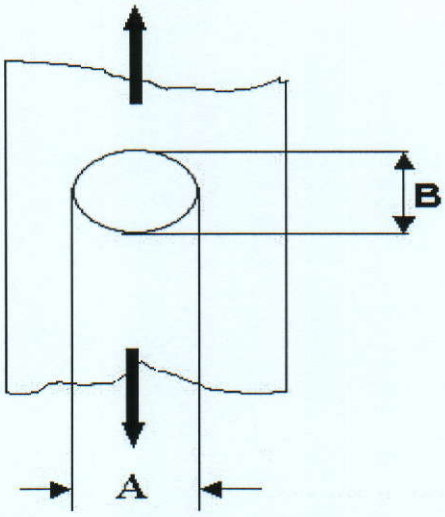

Figure 2.8 Elliptical Defect in a Stressed Plate

$$k_t = 1 + 2A/B \qquad (2.16)$$

Griffith developed a concept to explain how a stable crack could exist in a material. He postulated that a crack only becomes unstable if an increment of crack growth results in more stored energy being released than can be absorbed by the criterion of new crack surface.

2.5.5 Surface Crack Propagation

Under repeated tensile deformations cracks appear, generally at the edges of the specimen, and rapidly increase in size, as shown in Figure 2.9. This process is known as fatigue failure. It has been treated quantitatively in terms of stepwise tearing from an initial flaw, as follows: every time a deformation is imposed, energy T becomes available in the form of strain energy which causes growth by tearing of a small flaw in the edge of the specimen.

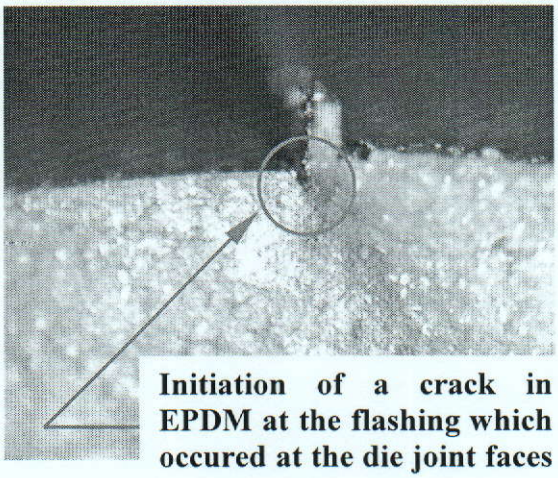

Figure 2.9 Fatigue Crack Initiation in an EPDM Dumbbell Specimen

The value of T for tensile pieces is given by equation:

$$2klU \geq T_c \qquad (2.17)$$

The corresponding growth step Δl is assumed to obey equation (2.18):

$$\Delta l = BT^2 \qquad (2.18)$$

i.e. to be proportional to T^2, so that the crack growth law becomes

$$\Delta l / l^2 = (4k^2BU^2)\,\Delta n \qquad (2.19)$$

Where n is the number of times the deformation is imposed, and k is a numerical constant. The depth of the crack after n strain cycles is obtained by integration,

$$l_0^{-1} - l^{-1} = 4k^2BU^2N \qquad (2.20)$$

where l_o is the initial depth of flaw.

If the crack grows to many times its original depth, so that $l >> l_0$ before fracture ensues, then the corresponding fatigue life may be obtained by setting $l = \infty$ in equation (2.20), yielding

$$1/N = 4k^2BU^2 l_o \qquad (2.21)$$

This is the quantitative prediction for the fatigue life, N in terms of one material property, the crack growth constant B, which can be determined in a separate experiment. It is particularly noteworthy that similar sizes are deduced for natural flaws for both strain-crystallising and non-crystallising elastomers (eg. SBR) althrough the crack growth law is quite different from the main tearing region equation.

$$\Delta l = BT^4 \qquad (2.22)$$

and the fatigue life relation becomes;

$$1/N = 48k^4DU^4 l_0^3 \qquad (2.23)$$

in place of equation 2.21. Abraham's [6] measurements of the fatigue lives for an SBR elastomer have been found to be suitable for a wide range of initial cut sizes l_0

and deformation amplitudes. The different crack growth laws for strain-crystallising and noncrystallising elastomers thus lead to quite different fatigue life relations, equation 2.21 and 2.23.

The fatigue life of a noncrystallising elastomer is more dependent on the size of the initial flaw and the magnitude of the imposed deformation, so that such elastomers generally have a longer service life at small deformations with no accidental cuts, but much shorter service life under more severe conditions. The fatigue life is also drastically lowered at high temperatures as a result of the sharp increase in the cut growth coefficient D as the internal viscosity is decreased. In contrast, the hysteresis associated with strain induced crystalisation is retained, provided that the temperature does not become too high (about 100^0C for natural rubber) for crystallisation to occur. The fatigue life for natural rubber is therefore not greatly affected by a moderate rise in temperature.

A more striking difference was previously claimed between strain crystallising and non-strain crystallising elastomers when stress is not relaxed to zero during each cycle. The fatigue life of natural rubber is greatly increased when the minimum strain is raised from zero to, say, 100 % because the crystalline barier to tearing at the tips of random flaws do not then disappear in the minimum-strain state.

As a result, the growth of flaws is virtually stopped unless the total applied strain is very large, say about 400-500%. No comparable strengthening effect on raising the minimum strain level had previously been found for non-strain crystallising elastomers.

Reinforcing fillers greatly enhance the tear strength and tensile strength of elastomers, but do not cause an equivalent improvement in the crack growth and fatigue properties. At a given strain energy input, the measured lives are appreciably

longer, but if compared at equal available energy levels, they will probably be quite similar. The initial flaw size and threshold tear energy T_o are therefore deduced to be similar to those for unfilled materials.

The growth steps are apparently too small for pronounced deviation of the tear, and hence "reinforcement" against fatigue failure by this mechanism does not seem to occur.

2.5.6 Surface Cracking by Ozone

In an atmosphere containing ozone, stretched samples of unstrained elastomers develop surface cracks, which grow in length and depth until they eventually sever the test piece. Ozone reacts rapidly with carbon-carbon double bond and causes a direct cleavage of the bond [37]. An attack on un-stretched rubber is therefore restricted to a very thin surface layer and it is of no practical consequence. Nevertheless, if rubber is stretched above the threshold strain, cracking will occur. Even when cracks are quite small, they can cause a serious reduction in strength and fatigue life of rubber. The approximately applied tensile stress necessary for an ozone crack to appear may be calculated from equation 2.24.

$$\sigma_b = (T_c E/\pi l)^{1/2} \qquad (2.24)$$

The fracture energy T_c is only about 0.1 J/m^2, representing the small amount of energy needed for the fracture of a liquid medium, i.e., about twice the surface energy for hydrocarbon liquid. Molecular scission apparently occurs readily by reaction with ozone, and does not require mechanical energy to be induced.

Taking a representative value for E for a soft rubber of 2 MPa and a value of 40 μm for the effective depth *l* of a chance surface flaw, equation. 2.24 yields a critical tensile stress for ozone cracking of about 50 kPa and a critical tensile strain of about 5%. These predictions generally concur with experimentally observed minimum values for ozone attack.

As the stress level is raised above the minimum value, numerous weaker stress raisers become effective and more cracks form. Actually, a large number of small, mutually interfering cracks are less harmful than a few widely separated cracks, which develop into deep cuts, so that the most harmful condition is just above critical stress. The rate at which cracks grow when the critical energy condition is satisfied depends on two factors:

1. The rate of incidence of ozone at the crack tip.
2. The rate of segmental motion in the tip region.

When either of these processes is sufficiently slow it becomes rate controlling. The overall rate R of crack growth is thus given approximately by

$$R^{-1}\ (\text{sec/m}) = 8 \times 10^{13} \varphi_T^{-1} + 1.2 \times 10^{5} C^{-1} \qquad (2.25)$$

Where φ_T (sec^{-1}) is the natural frequency of Brownian motion[1] of molecular segments at the temperature *T*, given by the Williams-Landel-Ferry (WLF) relation [37].

[1] Brownian motion; Einstein's explanation for Brownian Motion: little particles batting about a more massive one.

For a typical outdoor atmosphere, C is of the order of 10^{-4}mg/L, and the second term in equation 2.25 is then dominant for values of φ_T greater than about $10^4 sec^{-1}$, that is, at temperatures more than 25°C T_g. However in static tests the threshold strain at which cracking occurs may be increased substantially by dialkyl p-phenylene diamine antiozonants. These antiozonants also can induce dependence of the threshold strain on the ozone concentration so that static tests in high concentrations of ozone may not be reliable guide to performance at ambient ozone concentrations [37]. Hydrocarbon waxes may also prevent ozone cracking under static conditions and the effect can be particularly improved when used together with p-phenylamine antiozonants. The effect of waxes largely depends on the temperature and this must be kept in mind when choosing the temperature of accelerated tests. Larger bulky components will have the advantage of a large surface. If the threshold is exceeded, antiozonants can reduce the rate of cracking [37]. Protection against ozone attack under dynamic conditions is more difficult than under static conditions. P-pheyanediamine antiozonanats are particularly helpful in reducing the dynamic growth rate, but the dynamic strain below which no cracking occurs, remains too low to be of practical significance [37]. One of the aims of this research is to improve surface performance under dynamic loading. Unfortunately ozone attack was not investigated in this research project as suitable equipment is not available.

Chapter 3

The Rubber Vulcanisation Process

3.1 Rubber production

Rubber production requires the synthesis of monomers, or small petrochemicals molecules, followed by the polymerisation of long chain molecules. For example, butadiene-styrene requires two monomers for production, styrene (a liquid), and butadiene (a gas) at normal temperatures; upon polymerisation, the monomers combine to form the polymer, butadiene-styrene. Catalysts are required to initiate polymerisation and, after initiation, polymerisation occurs continuously.

Emulsion polymerisation is the most frequently used process, with the monomer dispersed in water as an emulsion. The process leads to aqueous suspension of raw rubber particles called latex. The latex is coagulated to form solid granules of rubber. It is usually performed in two stages.

1. First, a brine (salt water) solution is added and mixed with sulphuric acid or aluminium sulphate.
2. Second, the fine raw rubber granules are washed and the rubber is dried with vacuum filtration

The manufacturing process for this project was performed in the laboratories of Deutsches Institut für Kautschuktwchnologie (DIK).

The manufacturing procedure was conducted in the following order:

1) Initial preparation,
2) Mixing and blending with other vulcanising chemicals,
3) Vulcanisation.

3.1.1 Initial Preparation

This involves cutting up bales for the mixer and occasionally heating the bales.

3.1.2 Mixing and Blending with the Vulcanising Chemicals

Protecting and vulcanaising agents such as carbon black, sulphur, etc are added to the mixed raw rubber. Figures 3.1 a) and 3.1 b) show the two mixing machines used for the manufacture of EPDM rubber. The chemical composition of EPDM rubber is described in Table 3.1.

Rubbers containing only processing aids and chemicals for protection, colouring and effecting vulcanisation are known as unfilled rubbers. The majority of rubbers used for engineering applications contain fillers. One such filler is Carbon black, which can comprise up to one third of the total volume of a vulcanisate.

These black fillers fall into two groups:

1) Reinforcing fillers improve the tear and abrasion properties of the unfilled rubber as well as increasing the Young's Modulus, hysterises and creep.
2) Non-reinforcing fillers have little effect on the tear and abrasion resistance and give only moderate increases in modulus, hysterises and creep. These fillers can be added in greater volume than reinforcing fillers.

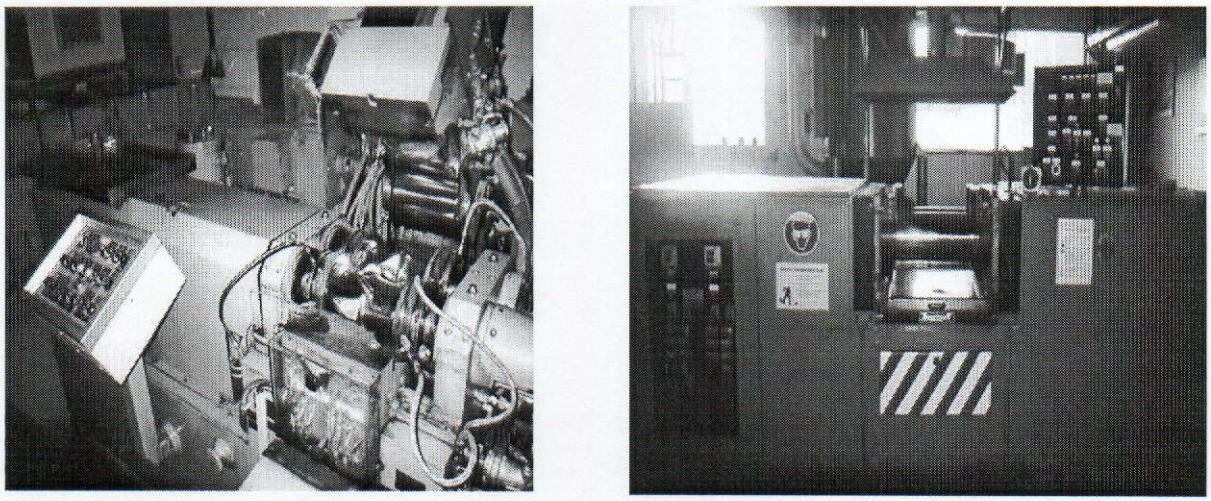

a) b)

Figure 3.1 Rubber Blending Machines, Laboratories of DIK, Hannover, Germany

3.1.3 Vulcanisation

The vulcanisation process, involves the cross-linking of polymer chains. Without the cross-linking agents, rubber is thermoplastic and lacks elasticity. Vulcanisation or cross-linking gives rubber almost complete elasticity over a wide range of deformation.

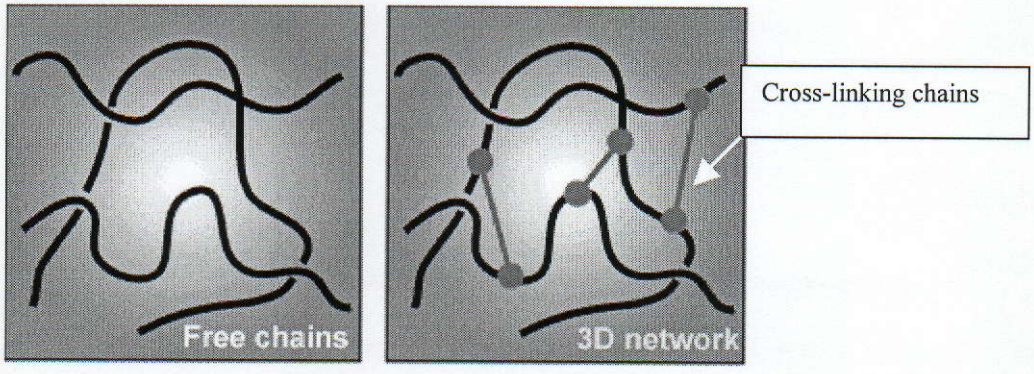

a) b)

Figure 3.2 Rubber molecular chains a) free molecular chains, b) cross-linked chains

A test preformed before Cross-linking / Vulcanisation was to define viscosity. This test is performed to ascertain the processability of the compound and is the most important cross-linking parameters. This test is necessary to control the quality of the finished product. It can be performed just after cross-linking or after aging at extreme environmental conditions of temperature or chemical aggression.

For this test an **Oscillating Disc Rheometer (ODR)** was used. The ODR is a useful tool in the study of peroxide cross-linking kinetics. It is used to determine the vulcanisation time. ODR torque is directly related to the number of cross-links formed during the peroxide vulcanisation. As vulcanisation proceeds, the torque required to shear the rubber increases and a curve of torque versus vulcanisation time can be obtained (as shown in Figure 3.3).

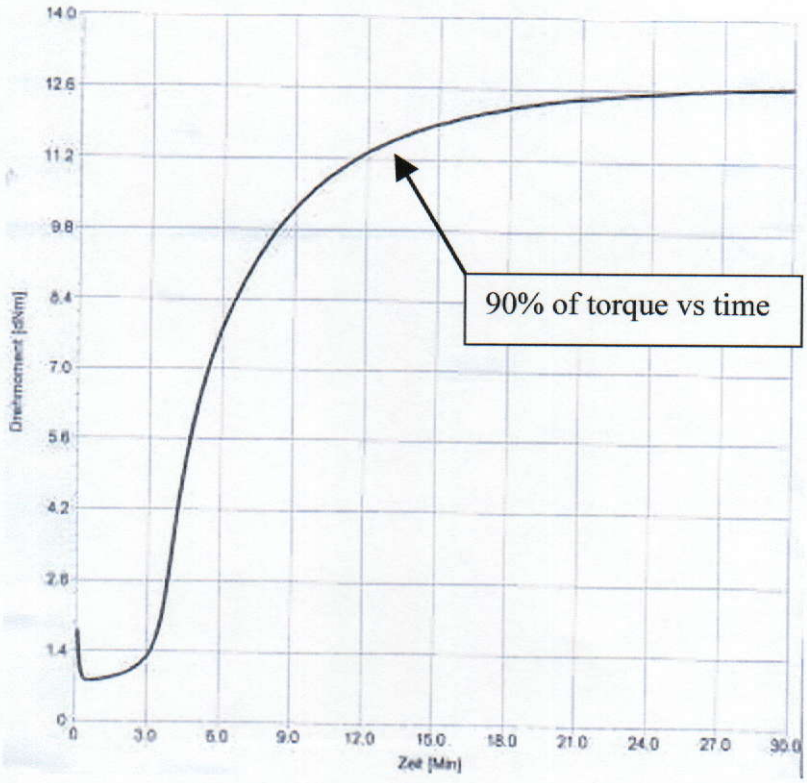

Figure 3.3 Graph of Torque Vs Time

The viscosity test was used to determine the vulcanisation time. The vulcanisation time was calculated to be 90% of the maximum torque vs time and found to be 12.69 minutes, which was rounded up to 13 minutes. To ascertain the correct vulcanisation time, it was necessary to add 1 minute for every 1mm of specimen thickness. For example, for a specimen 2mm thick, the vulcanisation time was calculated to be 15 minutes. The vulcanisation temperature was 160^{O}C and the pressure was between 200 and 300bar. A compressive moulding machine was used in the vulcanisation process, as shown in Figure 3.4a.

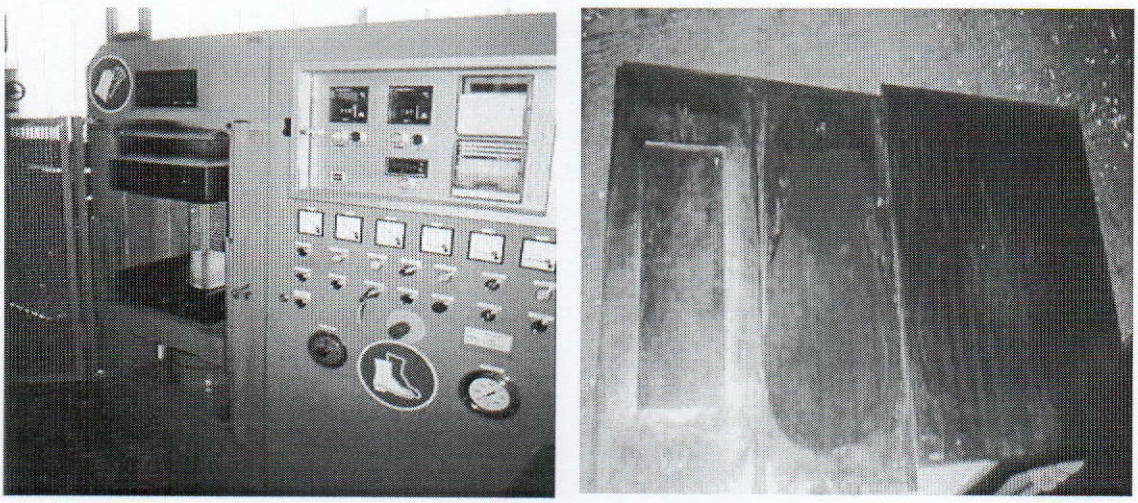

a) **b)**

Figure 3.4 **Vulcanisation, a) Compressive Moulding Machine, b) Compression mould, DIK Hannover, Germany**

3.2 Elastomers and their applications

Elastomers used in this research are:

3.2.1 Ethylene Propylene Diene (EPDM), which is a synthetic rubber produced by the copolymerisation of ethylene and propylene using catalysts such as titanium and vanadium.

For this project, an Ethylene Propylene Rubber (EPDM) was used because its non-strain crystallising behaviour and this material was provided by DIK. The chemical composition of EPDM is outlined in Table 3.1. The carbon blacks used for the filled material were chosen to represent a material with an average level of reinforcement.

Ingredient	Amount (phr[1])
EPDM	100.0
Carbon black N550	70.0
Carbon black N772	40.0
Stearin acid	1.0
Zinc-oxide	5.0
Oil Sunpar2280	70.0
Sulphur	1.5
Vulcanising agent CZ (CBS)	1.0
Vulcanising agent Thiuram (TNTD)	0.8

Table 3.1 Chemical Composition of EPDM Carbon Black Filled Rubber

This material is not typical for dynamic applications, but it is used in DIK to show the influence of different mixing procedures on the physical properties of cured rubber. For the fatigue test specimens, an optimised mixing procedure, which assures good carbon black dispersion, was chosen. Previous research shows [38] that well

[1] phr- Parts by weight per 100 parts by weight of rubber [39].

mixed and softer materials have an increased service life under displacement control, compared with less thoroughly mixed materials (eg. EPDM). Latter research found that the harder material has similar fatigue properties to the well mixed rubber under load controlled tests.

3.2.1.1 Applications for EPDM rubber

The EPDM rubber is exceptionally resistant to heat and oxygen. Therefore it has many applications. In the car industry it is used for weather strips, radiator hoses, circuit breaks, gaskets, sound insulating sheets, car bumpers and car spoilers.

It is also used in electric cable insulation, for domestic gaskets and pipes for washing machines, buildings for door and window seals and water proofing.

3.2.2 Natural Rubber (NR), which is a material made from natural latex, a white milky liquid which is tapped from rubber trees. The latex is dried by adding acetic acid which thickens the solution. The product is then rolled into sheets and bales.

Table 3.2 shows a typical chemical composition of Natural Rubber (NR) [39].

Ingredient	Amount (phr)
Natural Rubber	100
Process Oil	5
Stearic Acid	2
Zinc Oxide	5
N-550 Carbon Black	25, 50, 75
Phenylamine antioxidant	1.5
Sulfur	2.5
Cure Accelerator: Benzothiazyl disulfide	1.0
Cure Accelerator: Tetramethyl thiuram disulfide	0.1

Table 3.2 Chemical Composition of Natural Rubber Carbon Black Filled

Most NR is produced in South East Asia with smaller amounts coming from South America and Africa.

NR is used in the manufacture of tyres, resilient mountings in automobiles and machines, insulated cables, flexible hoses for air and water, etc.

3.2.3 **Styrene Butadiene (SBR),** is commercially the most important rubber of all synthetic rubbers. It is cheap and its production does not require the destruction of natural resources, ie. Rubber trees. There is not enough Natural rubber produced to satisfy world demand.

SBR can be produced with hot or cold polymerisation. The polymerisation process is controlled by the process temperature. Cold SBR has fewer branched polymer molecules. Another form of SBR is the oil extended type. Oil extension is the process of adding oil to the mix in amounts of up to 35% prior to vulcanisation. The action of oil on rubber is not destructive in the chemical sense, oil swells the rubber and softens it. The properties of oil extended and cold polymerised SBR are improved by softening action combined with the mixture of other additives. More than 50% of all SBR produced is in an oil extended form.

Table 3.3 shows a typical chemical composition of Styrene-Butadiene Rubber (SBR) [39].

Ingredient	Amount (phr)
SBR-1500	100
Process Oil	4
Stearic Acid	2
Zinc Oxide	5
Antioxidant: DPPD	1.5
N-330 Carbon Black	50
Sulfur	2
Cure Accelerator: Benzothiazyl disulfide	2
Cure Accelerator: Tetramethyl thiuram disulfide	0.15

Table 3.3 Chemical Composition of SBR Rubber

SBR is used in tyre treads (passenger vehicles often in direct competition with Natural rubber) transmission belting, electrical products, rollers and moulded and extruded items. Hot polymer is used in the side walls of tyres, light coloured household goods, sporting goods and other products where colour is important.

3.3 Elastomeric Clamp Design

Dumbbells are generally used for simple tension test and covered by ISO standards [40]. However, the die for cutting the dumbbell test specimens was not available. Therefore the dumbbell specimens were not used, instead rectangular strips were used conforming to the following dimensions: length: 80mm, width: 15mm, thickness: 2mm. Rubber specimens are not easy to grip and considerable ingenuity has been devoted to the design of clamps to allow tests to take place. The Elastomeric Clamps had to be designed to prevent slippage and also to grip the end of a specimen with uniform pressure across its width without setting up local strains

liable to cause failure. The drawings for the Elastomeric Clamp design are shown in Appendix A.1, pp.163.

Chapter 4

Surface Characteristics Methods

4.1 Surface Roughness

Over the past 50 years or so, the attention of the engineering industry has become increasingly engaged with the subject of the surface roughness. With this came a realisation that an improvement in surface finish often leads to an enhanced product performance or increased service life. This led to an increased understanding of the influence of roughness on functionality and the need to more closely specify surface finish in order to ensure an acceptable level of product function.

Theory of Surface Roughness

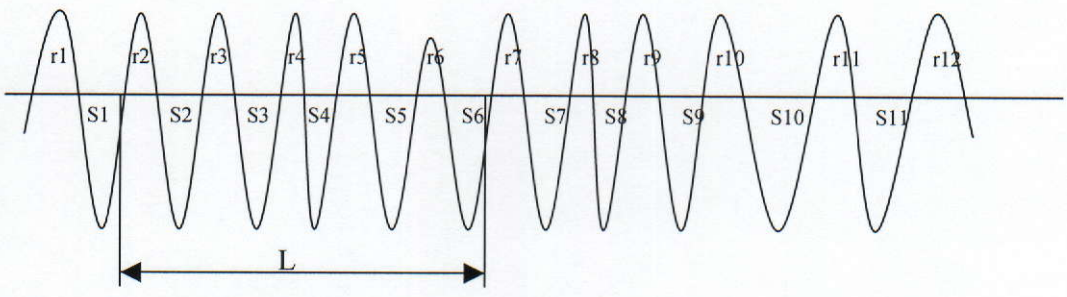

Figure 4.1 Diagrammatic Representation of a Trace from a Surface Finish Test

$$\text{Surface roughness average Ra} = \frac{\text{sum of areas 'r' + sum of areas 'S'}}{L} \quad (4.1)$$

Surface roughness is measured in micrometers (μm).

The measurement of surface roughness is concerned with both:

i) The lay of the surface and

ii) The roughness of the surface.

The lay of any surface is generally determined by the manufacturing process, which produces the surface finish. Roughness refers to fully spaced surface irregularities. A machined surface is in reality not smooth, as it appears to the naked eye, but consists of a series of minute peaks and valleys caused by the manufacturing process.

Substantial research has been undertaken since the inception of measuring instruments like the Taylor-Hobson Talysurf [41]. The Taylor-Hobson Tallysurf uses a mechanical probe to detect surface roughness. This method is successful in measuring the roughness of hard surfaces like those of most metals. However, for measuring the surface roughness of soft surfaces like some rubbers, the Taylor-Hobson Talysurf is of limited use. Therefore in this chapter a number of non-contact methods for measuring and profiling the surface of rubber like materials are described.

4.1.1 Taylor-Hobson "Talysurf"

This method was used at the beginning of the research for profiling the surface of Natural Rubber (NR). The NR had a hard surface, which allowed the stylus to traverse the surface. The movement of the stylus was converted into electrical impulses, which were amplified and fed into a recording machine or computer. In practice, the vertical movement of the stylus is magnified on the printout to a much greater extent than the horizontal movement of the stylus. The section of the surface over which the stylus is moved is known as the sampling length. The sampling

length can vary from 0.25 mm to 8 mm depending on the method used to produce the surface finish.

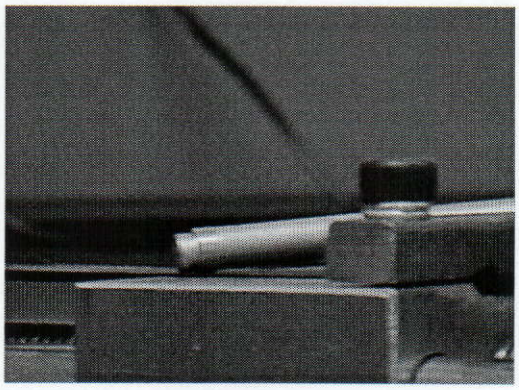

Figure 4.2a Talysurf Probe

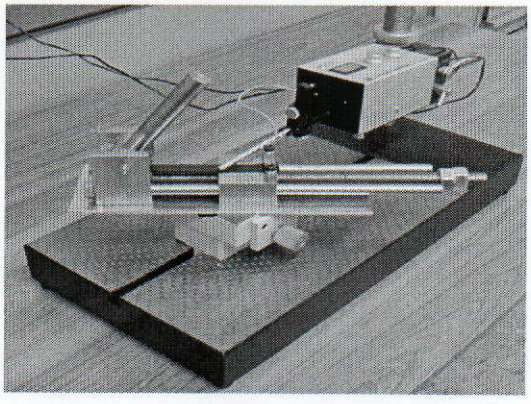

Figure 4.2b Taylor-Hobson Talysurf with Test Rig

The physical properties of EPDM are different from those of NR. Without additives, EPDM rubber is a copolymer that is weak and soft. A large amount of filler is added during mixing and poor shear properties are exhibited during this process that mean that the ingredients are less well dispersed than in NR. Oil is added to improve the usefulness of the compound and to reduce levels of dispersion. In terms of these physical properties, EPDM behaves in a totally different manner to NR. The surface of EPDM is very soft and during the Talysurf testing the probe scraped the surface of the EPDM. Therefore the results obtained using the Talysurf are unreliable. On the basis of this research, it is recommended that non-contact surface methods, such as

'White-light interferometry' (WLI), be employed for measuring surface characteristics of EPDM rubber. The technique is non-contact and covers the whole surface, unlike stylus profilometry. It also offers very high precision and computer algorithms are developed to cope with rough surfaces.

4.1.2 White Light Interferometery

For noncontact surface analysis of the EPDM rubber surfaces finishes two profilers were used:

i) The New View 100 (Figure 4.3), c) is a scanning white light interferometer [43], located in the CMA Laboratory of Trinity College Dublin. It has a maximum vertical step height of: 100μm and a minimum vertical resolution of: 0.1 nm.

ii) The MicroXAM S/N 8038 (Figure 4.3), b) optical profiler has an lateral resolution in the region of 0.5 μm and a vertical resolution of 1nm [44].

Interferometry is a traditional technique in which a pattern of bright and dark lines (fringes) result from an optical path difference between a reference and a sample beam. Incoming light is split inside the interferometer, one beam going to an internal reference surface and the other to the sample [42]. After reflection, the beams recombine inside the interferometer, undergoing constructive and destructive interference and producing the light and dark fringe pattern. A precision translation stage and a CCD camera together generate a three-dimensional interferogram of the sample, which is stored in the computer memory. The 3D interferogram is then transformed by either frequency domain analysis or into a quantitative 3D image as shown in Figure 4.4 and 4.5.

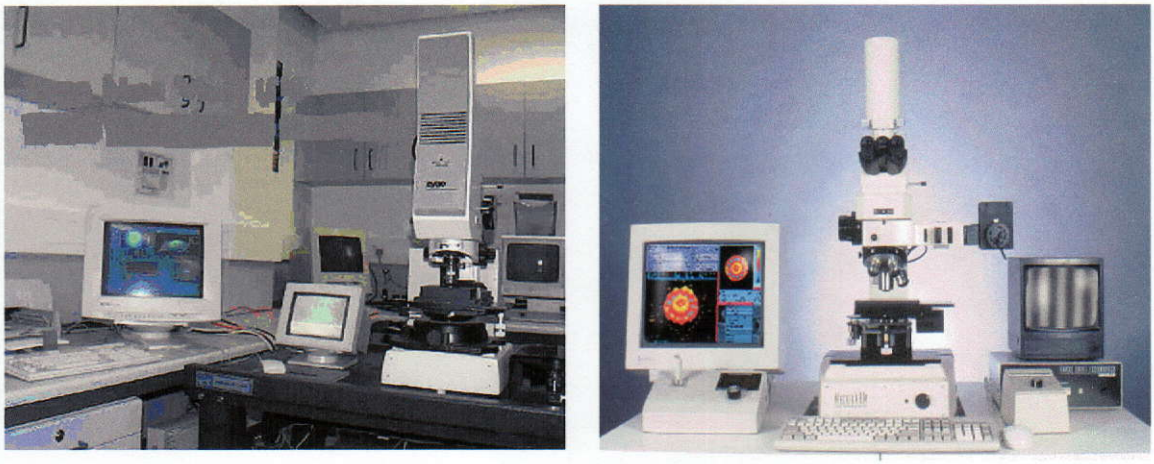

a) b)

Figure 4.3 a) Zygo New view 100 White Light Interferometer CMA Laboratory TCD [43], b) MicroXAM 3D While Light Profiler [44]

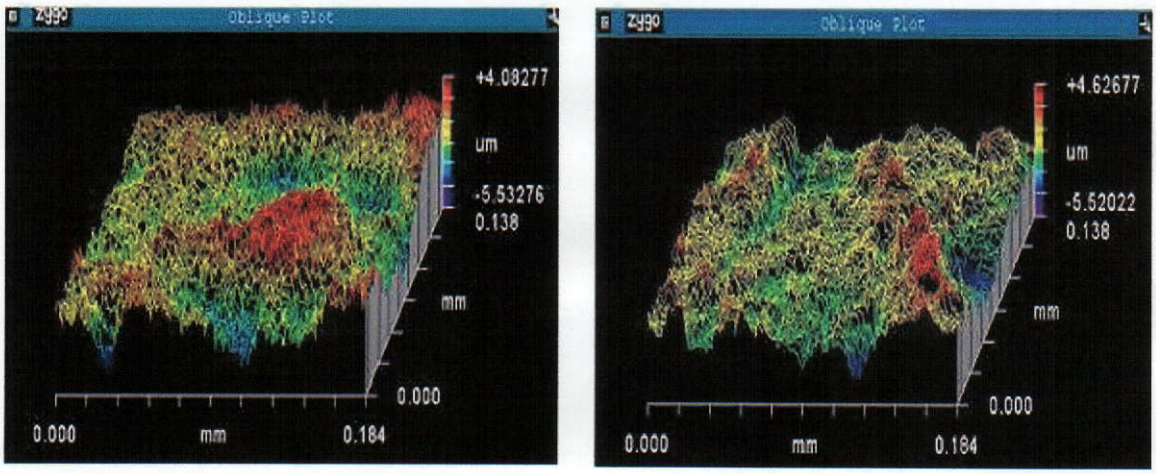

a) b)

Figure 4.4 The EPDM Rubber Surface impression captured using The New View 100 Scanning White Light Interferometer a) DLC Uncoated EPDM Rubber, b) DLC Coated EPDM Rubber

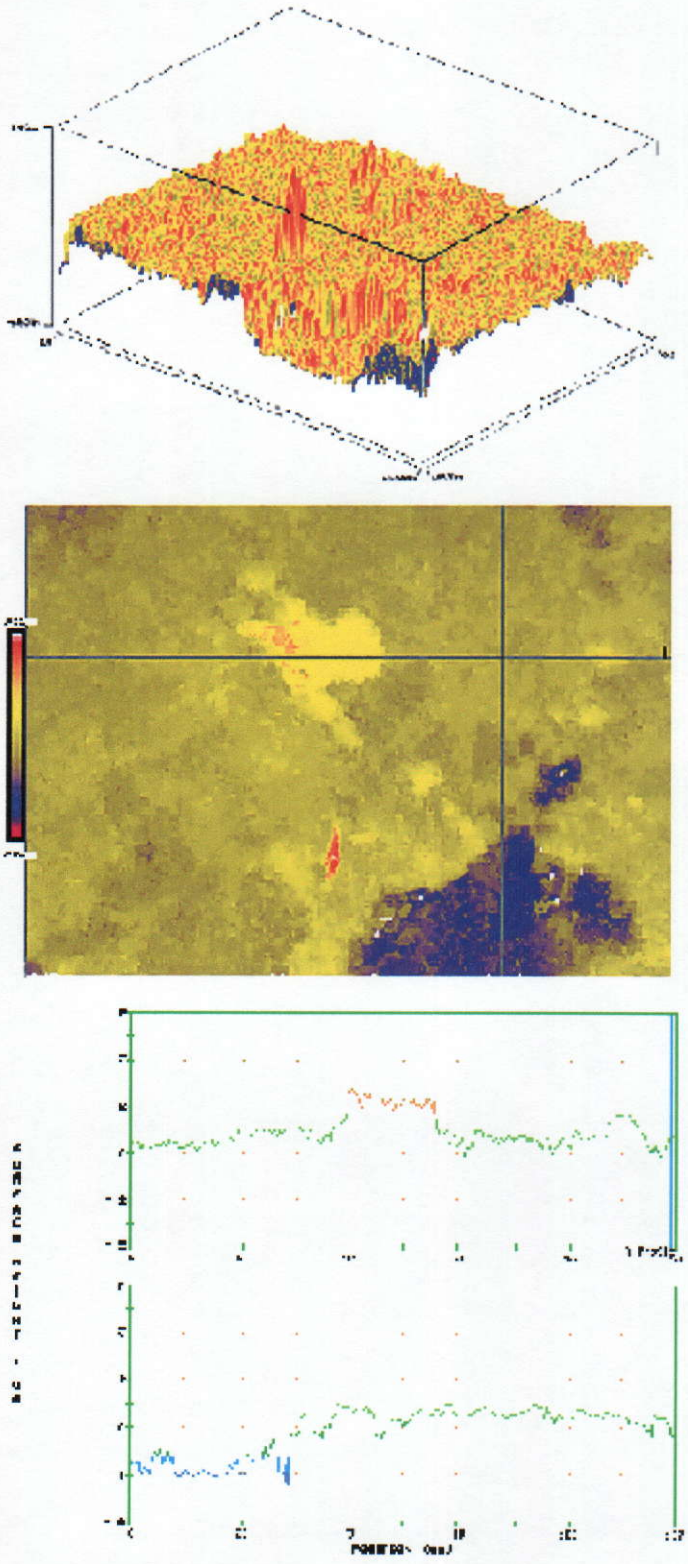

Figure 4.5 EPDM Rubber Surface profiled using MicroXAM 3D While Light Profiler a) 3D Surface profile, b) 2D Image of the Surface 260.51µm X 197.27µm, Average Surface Roughness R_a= 0.75µm, c) X-Y Surface Profile of EPDM Rubber Sample

4.2 Method of Measuring Surface Flaws and Defects

This study describes methods used to profile dimensional changes in the flaws on the surface of elastomers. Rubber preloaded in tension reduces stress concentration at surface defects (see Chapter 5). This can partially explain their improved fatigue properties.

4.2.1 Olympus BX 60M UIS optical system Microscope

(UIS – Universal Infinity System)

An Olympus BX60M System Microscope incorporating a universal infinity system (UIS infinity-corrected optical system), as shown in Figure 4.6, was used for profiling geometries of flaws on the surface of NR and EPDM rubber.

Magnified images of the rubber were captured using a video printer, as seen in Figure 4.7.

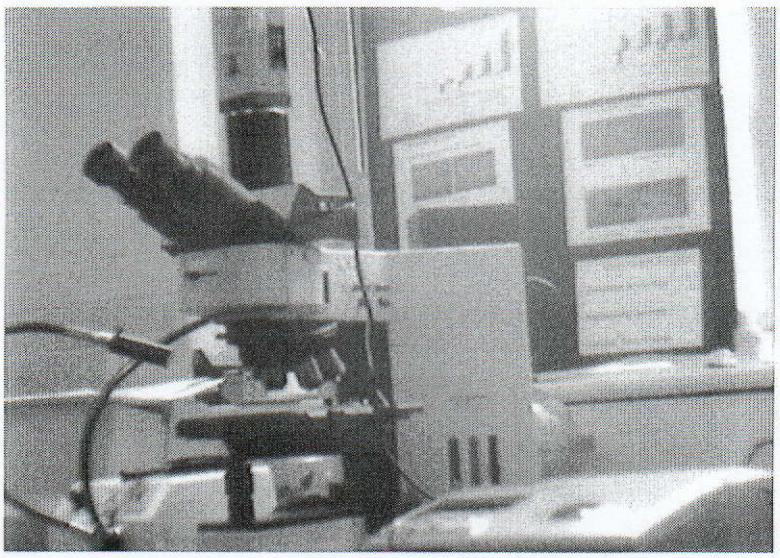

Figure 4.6 Olympus BX60M System Microscope with the Video Printer

Figure 4.7 Magnified Image of a Flaw in Natural Rubber (NR) captured using Olympus BX60M System Microscope with the Video Printer

4.2.2 Analysis of a Flaws and an Initiated Cracks in EPDM Rubber Specimens Using Omnimet Archive Digital Imaging System (86-4000)

The Olympus BX60M System Microscope's lacked an accurate measuring system. This problem was solved by introducing the Omnimet Archive Digital Imaging System (86-4000). The software is capable of producing accurate measurements on line as shown in Figure 4.8. The samples were gripped in the elastomeric clamps previously discussed (see Appendix A.1, pp.163).

The Omnimet Archive Digital Imaging System (86-4000) was used for measuring the crack deformations. For measuring geometries of the flaw the Olympus BX60M System Microscope was linked to the full system. The Olympus BX60M System Microscope had to be linked because camera was not capable of detecting small surface defects (30 μm to 60 μm), as shown in Figure 4.9. The Omnimet Archive Digital Imaging System is a modular system and is capable of capturing high resolution colour images. The high Resolution module works at 1600 x 1200 pixels. The Omnimet is comprised of a medium resolution monochrome video camera, a

specially configured high specification PC with an image capture card, Windows 98 operating system, Microsoft Office 2000, Beuehler proprietary imaging software and connecting cables [45], as shown in Figure 4.10.

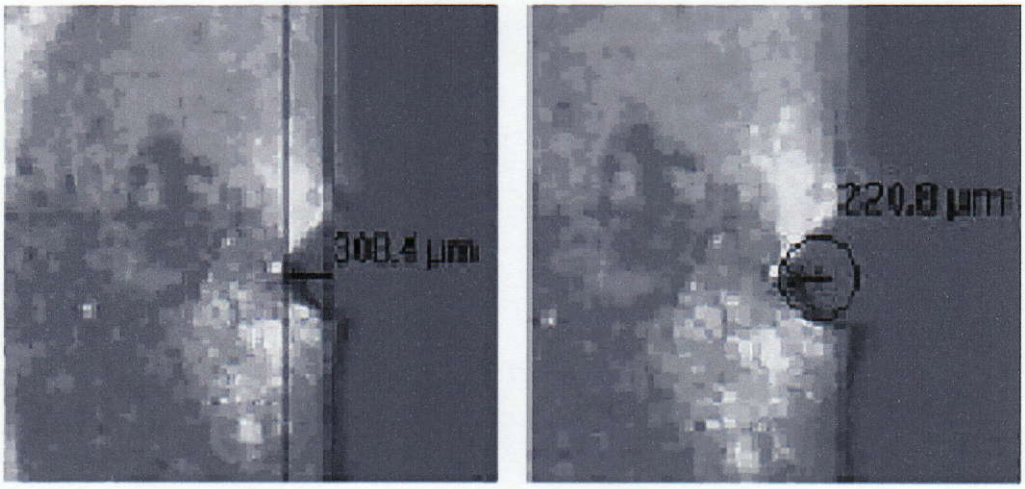

a) b)

Figure 4.8 Measuring Crack Propagation using the Omnimet Archive Digital Imaging System, a)length, b) radius

Figure 4.9 Magnified Image of EPDM Rubber Surface captured using Omnimet Archive Digital Imaging System (86-4000)

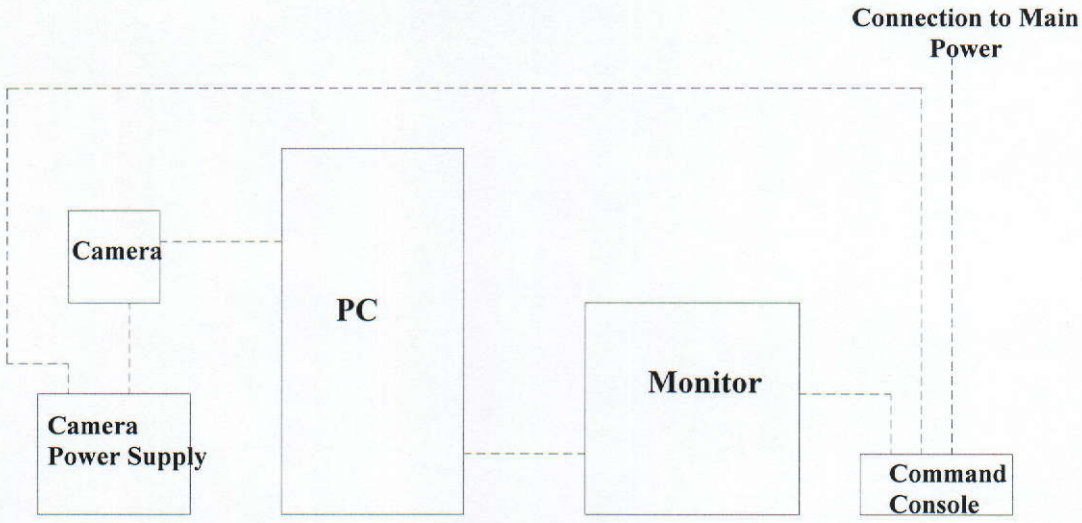

Figure 4.10 Layout of the Omnimet Archive Digital Imaging System (86-4000)

4.2.3 White Light Interferometer

The previously described system profiles the surface flaws in two dimensions X and Y. A more accurate method was required and therefore the MicroXAM S/N 8038 (Figure 4.3, b) optical profiler was used. The same equipment was used to profile the surface roughness of the EPDM rubber.

The White Light Interferometric Profiler provides 2D and 3D visual data of the rubber surface. Figure 4.11 shows a surface flaw that is about 60 μm wide and about 5 μm deep. Figure 4.12 shows a flaw of 30 μm and 5 μm deep. Using the dimensions of the flaw shown in the Figure 4.8 FEA model is drawn and tested.

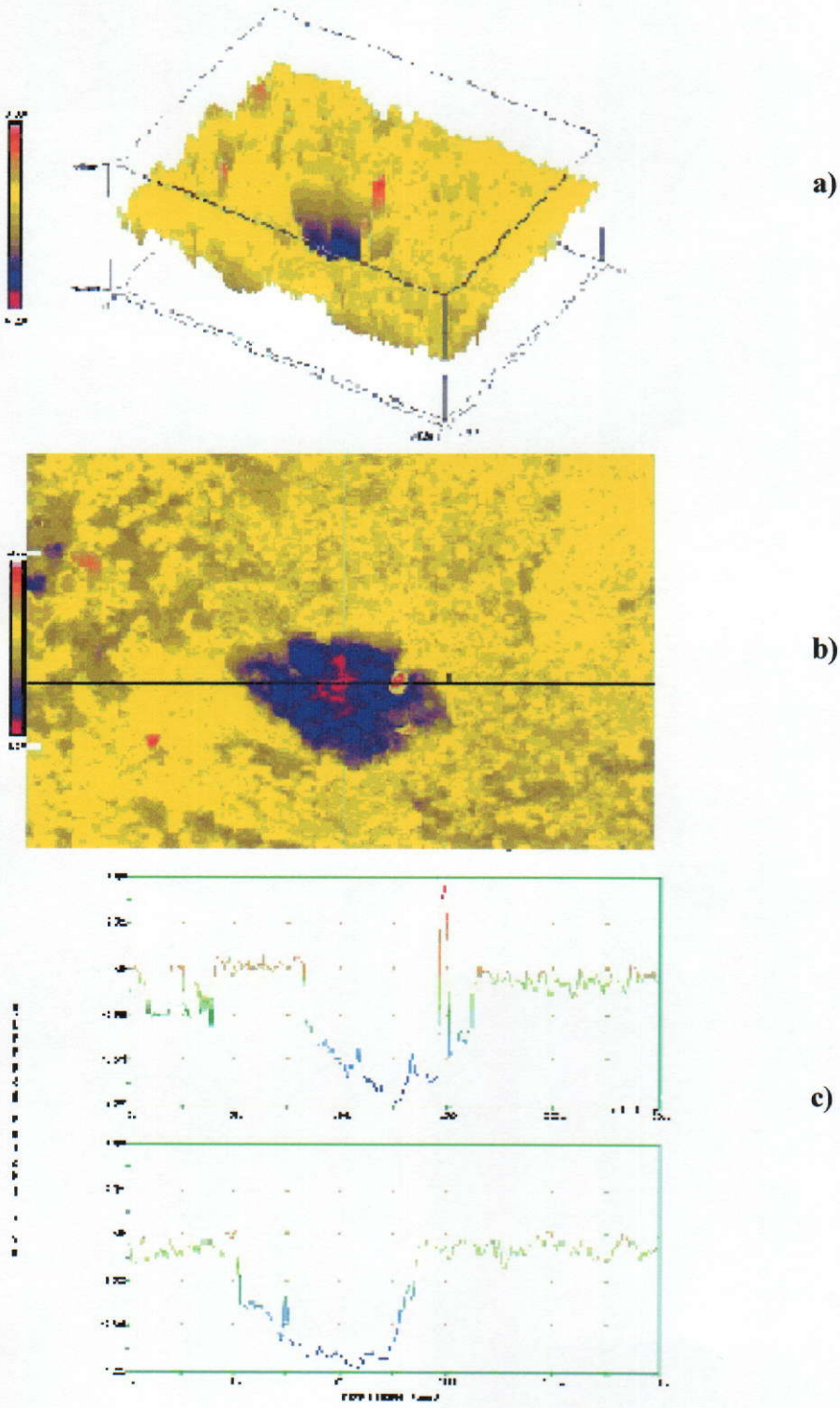

Fgure 4.11 EPDM Rubber Surface profiled using MicroXAM 3D While Light Profiler a) 3D Surface Flaw Profile, b) 2D Image of the Surface Flaw 260.51µm X 197.27µm (Magnification: 31.5, Average Surface Roughness R_a= 0.67µm), c) X-Y Profile of the Surface Flaw

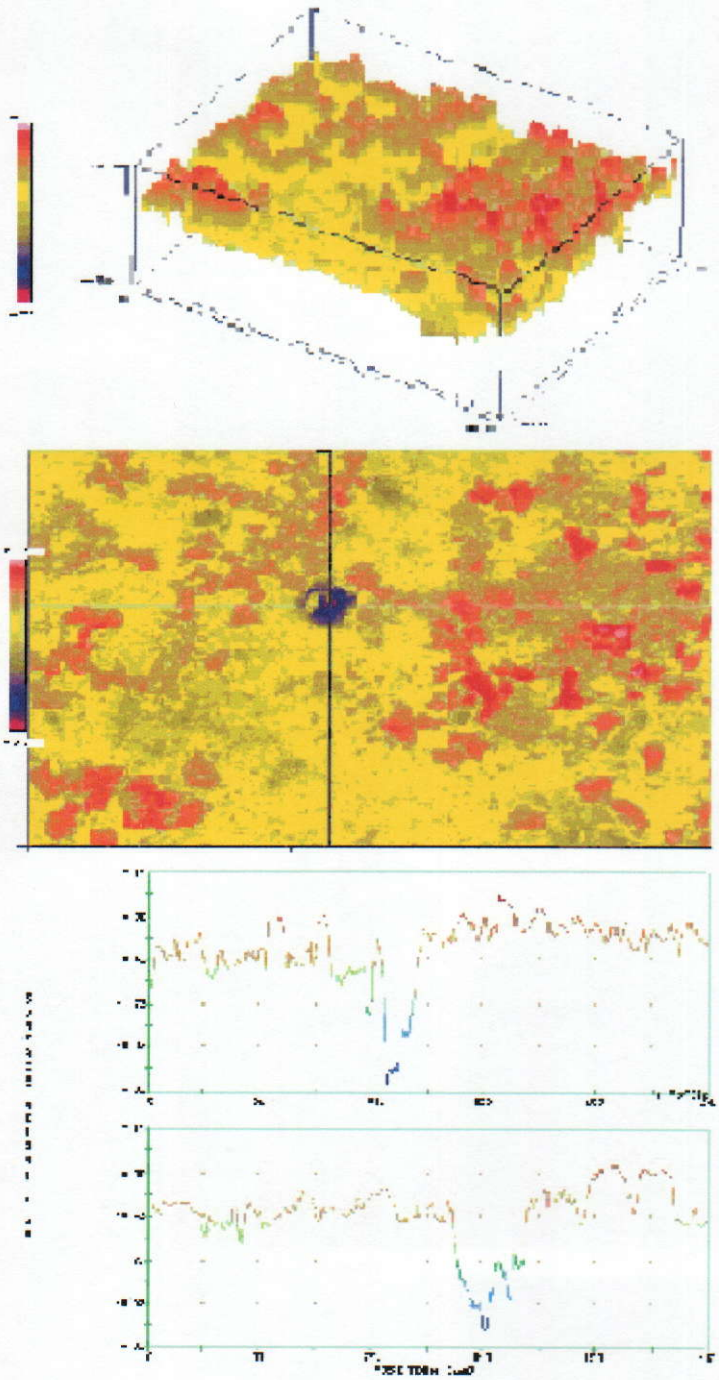

Figure 4.12 EPDM rubber surface profiled using MicroXAM 3D While Light Profiler a) 3D Surface Flaw Profile, b) 2D Image of the Surface Flaw 260.51µm X 197.27µm (Magnification: 31.5, Average Surface Roughness R_a= 0.55µm), c) X-Y Profile of the Surface Flaw

4.2.4 Electronic Speckle Pattern Interferometry (ESPI)

The third method used was Electronic Speckle Pattern Interferometry (ESPI). The Electronic Speckle Pattern Interferometry (ESPI) [8] method is considered to be a reliable non-contact procedure for observing surface defects. It provides an accurate display of the phase distribution over the object surface subjected to stress (load).

ESPI is a technique that was first demonstrated by Butters and Leendertz [46]. The ESPI system is capable of providing information about the dynamic changes of surface characteristics. This optical metrology technique has been used for inspection of cracks in materials in a vast number of industries, eg.: Aviation, Ship building, Construction [8]. Using a CCD camera as a recording instrument and with the electronic processing of interferometric information, ESPI is a rapid and practical method when compared with conventional investigation methods [8]. ESPI is a non-contact optical interference technique, which is able to record surface displacement in response to an applied stress. This is achieved by using laser light to illuminate the surface of the test specimen. Referring to the diagram in Figure 4.13, the process can be described as follows:

Firstly the emitted laser beam is split into two separate beams via the beam splitter. The beams are used to illuminate the test specimen surface and then produce an optical interference pattern. A CCD camera, linked via a digitiser card to a computer, is then positioned in front of the test sample and focused onto the illuminated sample. The CCD video camera captures the speckle interference pattern and stores it in the computer.

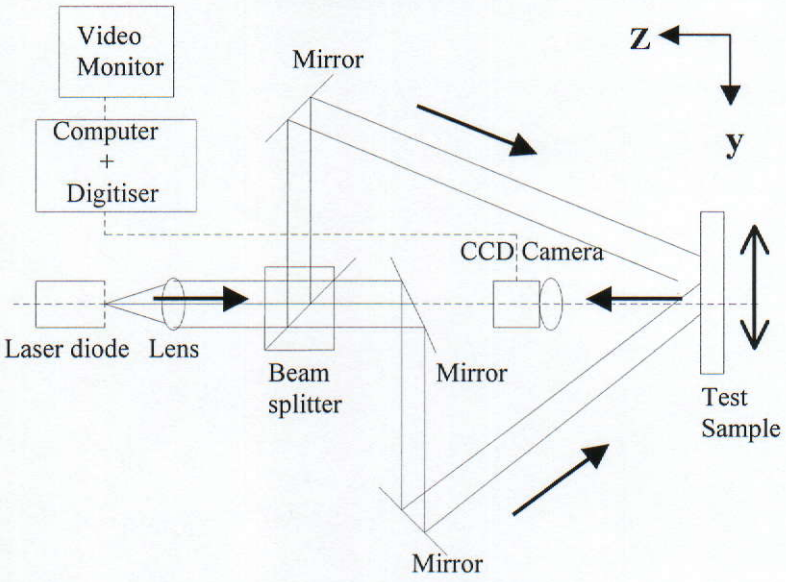

Figure 4.13 Typical Layout of the In-plane ESPI System

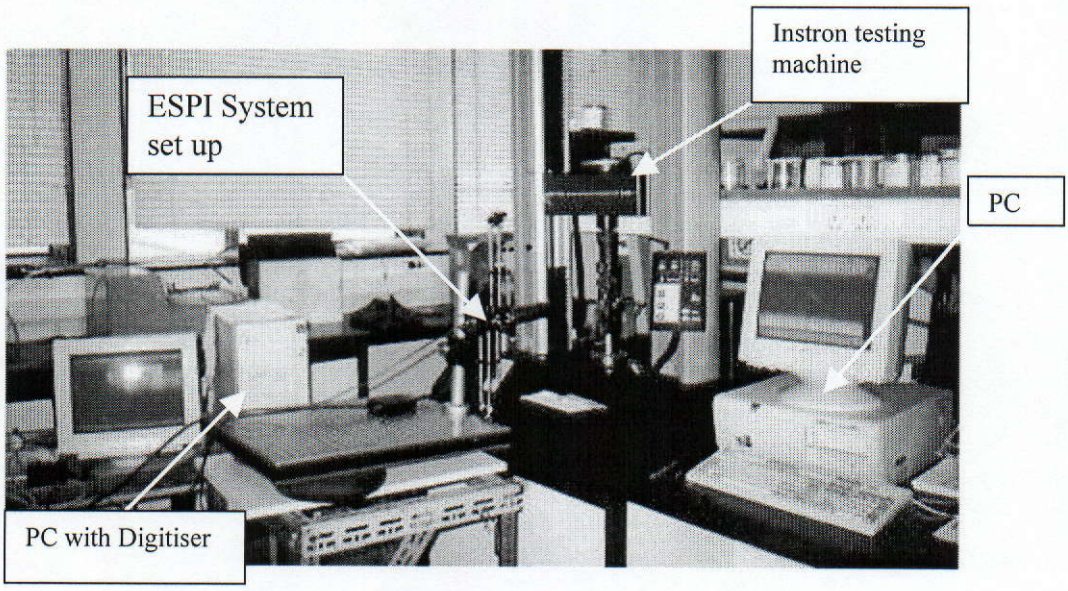

Figure 4.14 Laboratory Set-up of ESPI System and Instron Instron 5569 Testing Machine

If the test specimen is then stressed mechanically, its surface will deform. This causes the path length of the optical beam to change. The speckle pattern produced

by the interference of the test specimen and the unaltered reference beam changes accordingly. The new speckle interference pattern is also captured and stored. The images are then correlated with each other to produce an image which contains zebra like, black and white fringes which can be evaluated using equation 4.2 [47].

$$d = n\lambda / (2\sin\alpha) \qquad (4.2)$$

Where:

d = in-plane displacement of the object due to the applied stress,

α = angle between the direction of object displacement and camera viewing angle,

n = number of fringes.

The black and white fringes are a direct indication of the magnitude of surface deformation as represented by equation 4.2. If a flaw is present in the area under inspection, it will cause stress to increase in that region of the material. This presence weakens the structure of the material. During inspection it will be detected directly as an increase in fringe density, as shown in Figure 4.15.

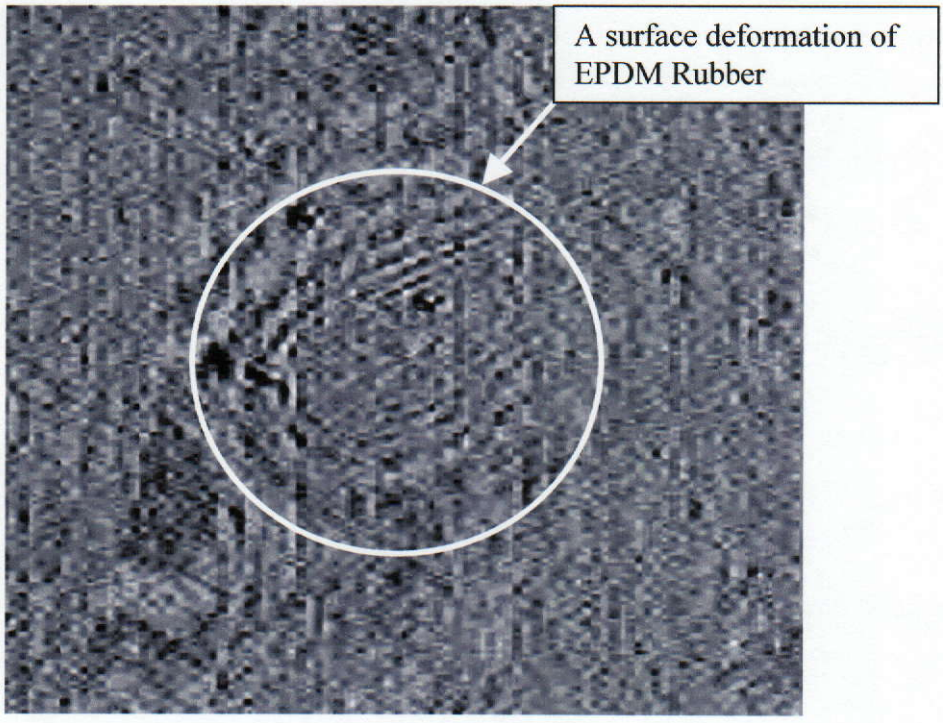

Figure 4.15 Fringes showing a Surface Deformation of EPDM Rubber

ESPI was used for the inspection of EPDM rubber surface flaws. ESPI can be used in arrangement with either in-plane or out-of-plane displacement, the in-plane method was used for this investigation. For the preliminary test a special test rig was built. The initial results were positive, and it was therefore decided to proceed with further testing of the rubber. The ESPI system tested for measuring dimensional changes in the flaws on the rubber surface. A laser diode with a wavelength of 785 nm and a maximum output power of 500mW was used as the light source for the ESPI system. The Instron testing machine 5569 used is shown in Figure 4.16. Elastomeric Clamps were also designed and these are seen in position in Figure 4.16.

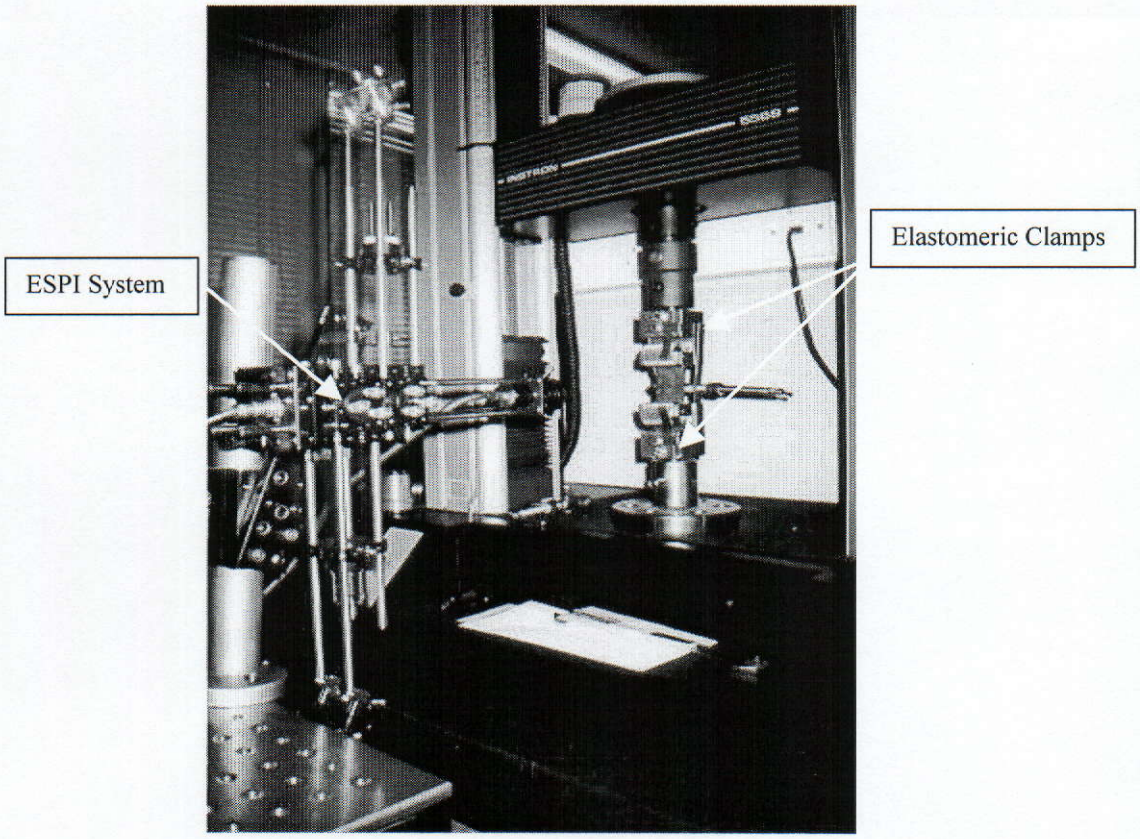

Figure 4.16 Instron 5569 Testing Machine with ESPI System

The formation of the fringes is directly related to the difference in beam path length. Any change between the object and reference beam during the inspection process and any background `noise` that occurs will destroy the image acquisition procedure. Noise was a major problem during the test. A small vibration produced from the electric motor of the Instron machine or even people walking in the corridor outside the laboratory caused problems for detecting any changes in deflection. Problems were partially solved by separating the two instruments, as shown in Figure 4.14. An optical table was employed with three small tyres filled with air. The optical table was placed on a mobile bench opposite the Instron machine. The ESPI system is very sensitive to noise, vibration and movement. The fastest cross head speed of the Instron machine at which fringes could be detected was somewhere between 0.06

mm/min to 0.09 mm/min. Because of slow stretching of samples it was not possible to cause any deflection changes on the rubber surface. Later samples were pre-strained to 100% of the original gauge length. When fracture occurred on one of the samples it was possible to detect some fringes. It was not possible to follow the fracture's progress. After fracture stopped, it was possible to detect fringes, as shown in Figure 4.17. It was later decided to drill a small hole in the test sample as previously it was seen that larger defects could be detected. The diameter of the hole was 1 mm as shown in Figure 4.18. Samples were strained to 200% of the gauge length. However the ESPI system could not work during the stretching process. Every time the sample was stretched, the machine had to be brought to a full stop. It was only then that the ESPI system could detect some deflection. The fringe pattern is shown in Figure 4.18 a) after 5s and b) after 20s.

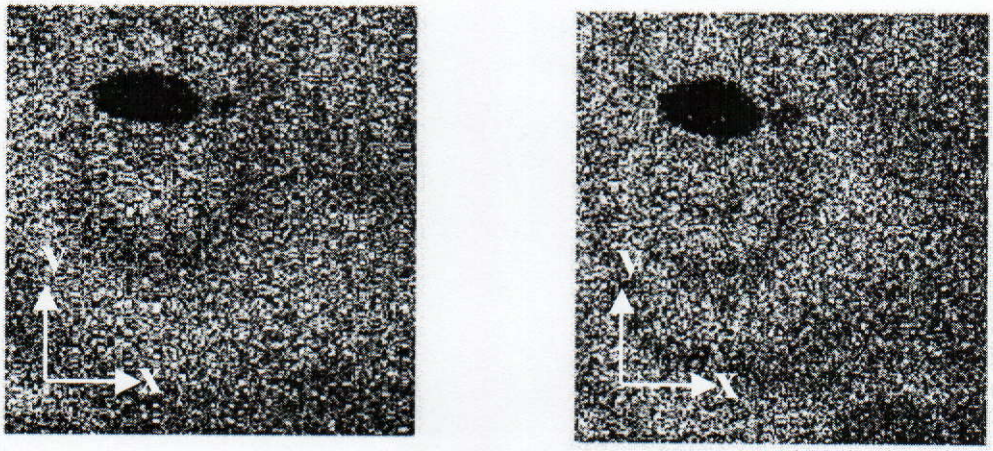

a) b)

Figure 4.17. Surface crack in the EPDM rubber test sample showing some fringes during ESPI testing: x = 2.5cm, y= 2.5cm; a) fringes 5 seconds after rubber being pre-stretched, b) fringes 20 seconds after rubber being pre-stretched

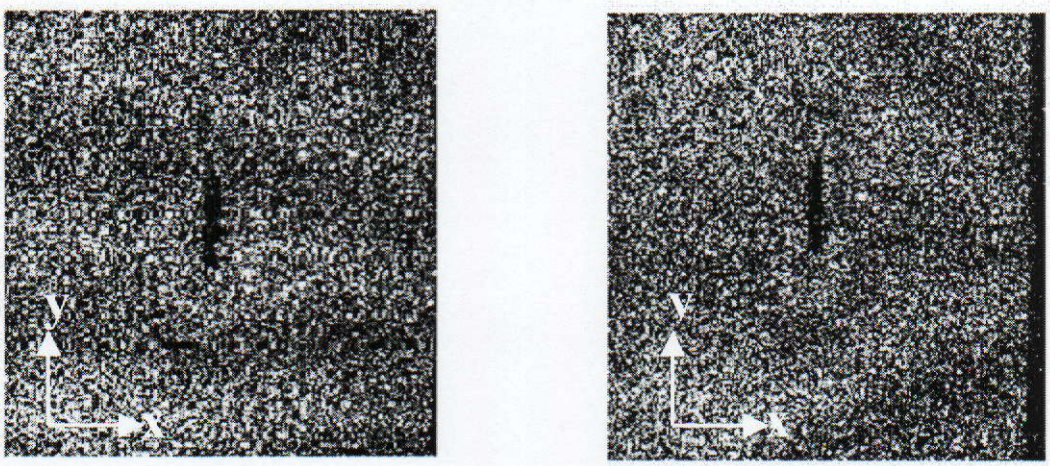

a) b)

Figure 4.18 Initiated Surface hole, Φ=1mm in the EPDM rubber test sample showing some fringes during ESPI testing: x = 2.5cm, y= 2.5cm; a) fringes 5 seconds after rubber being pre-stretched, b) fringes 20 seconds after rubber being pre-stretched

All three methods described above were tested. The White Light Interferometer produced the best results for measuring surface roughness and profiling the geometries of the surface defects. The ESPI System did not seem to be a very successful method of detecting the surface flaws (30μm to 60μm) resulting from the vulcanisation process. The performance of the ESPI system could be improved with the introduction of a high speed camera and the eliminating of background noise. Only then could the ESPI system become a valid method for measuring the surface displacement of Rubber.

It was hoped that the ultrasonic technique could be used in this research to measure surface roughness and detect any defects that occur in the body of the rubber specimen or on the surface of the rubber during the vulcanisation process. An advantage of this method is that defects inside the specimen could be detected [48,

49, 50]. Unfortunately this method was not evaluated, as the equipment is not available, it would be necessary to build a full system. The development of a Non-Contact Ultrasonic Analysis System could be the focus of future research in this field, a Non-Contact Ultrasonic Analysis System is proposed, as shown in Figure 4.19.

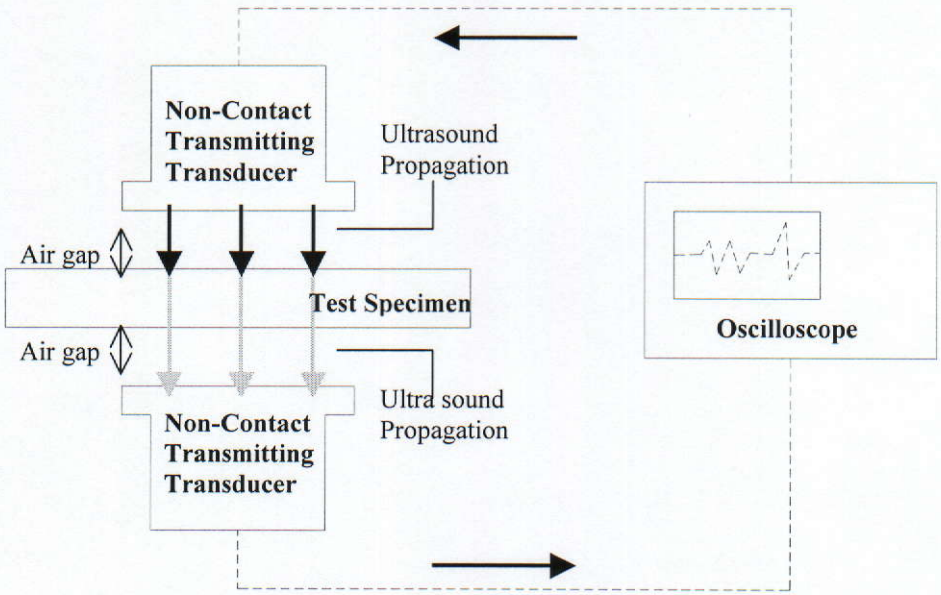

Figure 4.19 Schematic set-up of the proposed Non-contact Ultrasonic Analysis System

Chapter 5

The Influence of Pre-stressing on the Surface Finish and Stress Concentration (k_t) of Elastomers

5.1 Introduction

The design of a dynamically loaded rubber component conforms to different criteria than those for a metal component when subjected to fatigue. For instance, if the tensile cycles incurred by an elastomeric part are strain (displacement) controlled, the designer will choose the softer of two appropriate compounds. However, if the cycles are stress (load) controlled, the harder material will be selected. This choice is based on the amount of strain energy available to propagate a crack in each cycle, as shown in Figure 5.1. For a repeated displacement, the area under the load/displacement curve, repeating the work done is smaller for the less rigid rubber (Figure 5.1a), but for repeated load application, the opposite is true (Figure 5.1b).

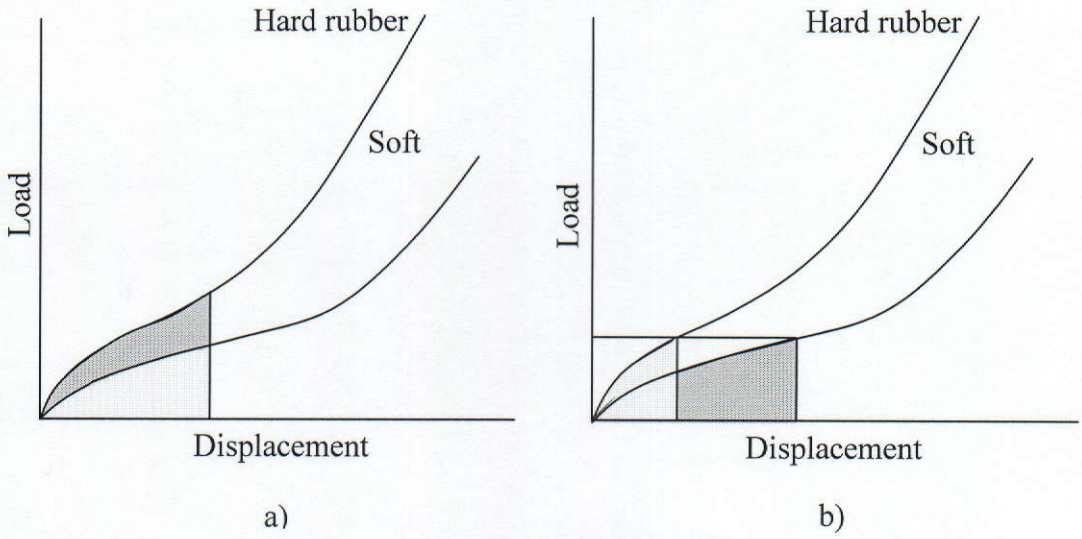

Figure 5.1 Available Strain Energy for Crack Propagation in Elastomeric Fatigue

In fatigue, metal components experience micro-strains and such considerations are irrelevant. Also, the reduction in fatigue life in metals when tensile mean stresses are increased has been comprehensively researched and explained [51, 52]. Strain crystallising rubbers exhibit greater fatigue resistance if tensile mean stresses are increased, providing the stress is not fully relaxed between loading cycles [53]. Hence improved fatigue properties can be achieved by pre-loading Natural Rubber (NR) components. The increase is attributed to crystallites inhibiting crack growth at the crack tip in a component under load. If the load in the rubber is not fully removed, then the crystalline region at the crack tip does not melt and the crack cannot propagate in the subsequent load applications. However, increased fatigue resistance, associated with higher tensile mean stress in the absence of full load relaxation, has also been observed in non-strain crystallising rubbers. The predominant reason for this increase in fatigue strength is related to the 'dynamic' strain energy available to propagate a crack, but the influence of changes in stress concentration in elastomeric fatigue has not been researched. In metal fatigue, the geometry of notches and flaws are barely changed by repeated strain cycles, but rubber undergoes large reversible strains. Fatigue cracks in rubber are thought to emanate from naturally occurring surface defects of 40 μm ± 20 μm across [53]. These flaws occur in rubber components, irrespective of the production process.

This study describes dimensional changes in the flaws on the surface of elastomers, preloaded in tension and considers whether a reduction in stress concentration in preloaded rubbers can partially explain their improved fatigue properties. The rubber compound used in the physical test was carbon filled, sulphur cured NR, produced in nine hardness values between 38 IRHD and 75 IRHD. EPDM rubber samples were also tested. It is hypothesised that the fatigue resistance in a component can be

improved by pre-stressing the surface finish at the predicted point of failure. A prediction of the elastomeric fatigue properties can be gained by comparing the surface finishes of samples. Both unstrained and strained surface finish were measured for each hardness of NR. Thereafter, microscopy was used to compare geometry and stress concentration of individual surface flaws at different levels of strain. Different non-contact methods were analysed for profiling the surface finish of rubber. They were also used for profiling geometry and stress concentration of the surface flaws as well as for investigating changes in the stress concentration at the tip of the crack.

5.2 Natural Rubber (NR) Surface Finish Test Results

Figure 5.2 shows variation of surface finish with tensile loading and Tables: 5.1- 5.4 present the results from the first surface finish testing of NR for the hardness range 38 – 75 IRHD.

Test 1:

	Relative roughness, R_a (μm)								
Extension %	38 IRHD	41 IRHD	48 IRHD	53 IRHD	58 IRHD	63 IRHD	68 IRHD	73 IRHD	75 IRHD
λ	2.36	1.7	2.25	1.44	2.21	2.04	1.53	1.67	1.23
2λ	1.38	1.21	1.92	1.22	1.77	1.53	1.45	0.9	0.86
3λ	1.16	1.06	1.52	1.05	1.31	1.44	1.32	0.78	0.8

Table 5.1 Measured Surface Finish for Natural Rubber Samples, R_a (μm)

	Relative roughness, R_a (%)									
Extension %	38 IRHD	41 IRHD	48 IRHD	53 IRHD	58 IRHD	63 IRHD	68 IRHD	73 IRHD	75 IRHD	Average (%)
λ	100	100	100	100	100	100	100	100	100	100
2λ	58	71	85	85	80	75	94	54	70	74
3λ	49	62	67	73	60	70	86	46	65	64

Table 5.2 Measured Surface Finish for Natural Rubber Samples, R_a (Percentages)

Test 2:

	Relative roughness, R_a (μ)								
Extension %	38 IRHD	41 IRHD	48 IRHD	53 IRHD	58 IRHD	63 IRHD	68 IRHD	73 IRHD	75 IRHD
λ	2.2	1.56	1.79	1.8	1.49	1.81	2.31	1.84	2.42
2λ	1.89	1.36	1.2	1.38	0.8	1.69	1.54	1.2	1.69
3λ	1.3	1.08	1.07	1.08	0.66	1.25	1.21	0.94	1.57

Table 5.3 Measured Surface Finish for Natural Rubber Samples, R_a (μm)

	Relative roughness, R_a (%)									
Extension %	38 IRHD	41 IRHD	48 IRHD	53 IRHD	58 IRHD	63 IRHD	68 IRHD	73 IRHD	75 IRHD	Average (%)
λ	100	100	100	100	100	100	100	100	100	100
2λ	85.9	87.17	67	76.66	53.69	93.37	66.66	65.21	69.91	73.96
3λ	59.09	69.23	59.77	60	44.29	69.06	52.38	46.70	65.04	58.39

Table 5.4 Measured Surface Finish for Natural Rubber Samples, R_a (Percentages)

Stretch ratios, λ	% Of unstrained surface finish
1	100
2	74.39
3	61.41

Table 5.5 Average Percentage Change of Surface Finish vs Stretch Ratio of Two Tests

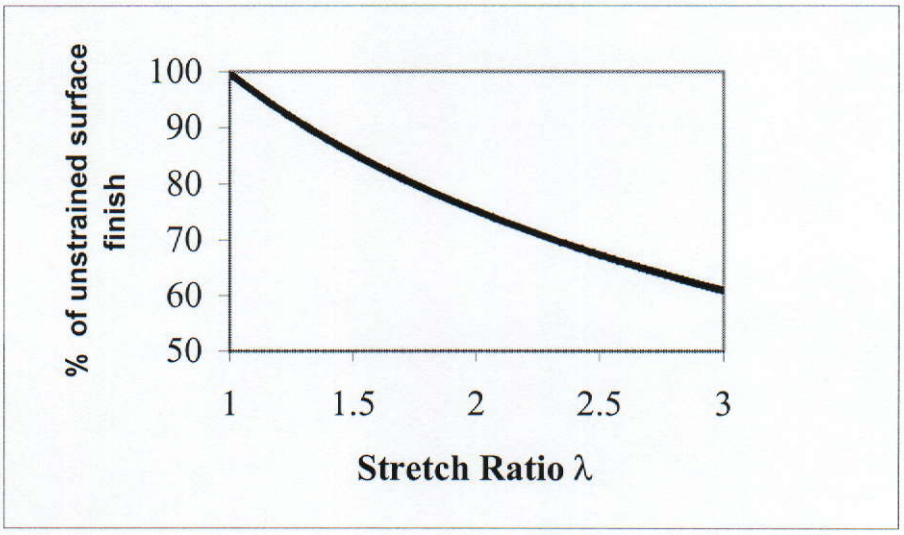

Figure 5.2 Improvement in Surface Finish of NR Subjected to Tensile Strain

It is significant that surface finish was seen to improve in each of the eighteen tests on the rubber stretched to $\lambda = 2$ and improved further in the eighteen tests on the rubber stretched to $\lambda = 3$. Surface finishes intermediate stretch ratios ($\lambda = 1.5$ and $\lambda = 2.5$) were determined in a small number of tests to corroborate the test outcomes. The mean changes in surface finish with increased strain are shown as percentages in Figure 5.2 and equation 5.1 gives an approximate relationship between tensile strain and surface finish.

$$R_{a_S} = R_{a_0}(1 - 0.35 l_n \lambda) \qquad (3.1)$$

where R_{a_S} = *surface finish at stretch ratio* λ (μm)

R_{a_0} = *surface finish of the unstrained rubber* (μm)

5.3 EPDM Surface Finish Test Results

As previously stated, in terms of physical properties EPDM behaves in a totally different manner to NR. The surface of EPDM is very soft, and during the Talysurf testing, the probe scraped the surface of the EPDM while measuring surface roughness. The results obtained were not reliable. For this reason it is recommended that a non-contact surface method, such as "White Light Interferometry", be employed for testing EPDM rubber.

5.3.1 White Light Interferometry (WLI)

The Micro XAM Surface Mapping WLI was used to profile the surface roughness of EPDM rubber. It is significant that surface finish was seen to improve in the tests on the rubber stretched to $\lambda = 2$ and improved further in the test on the rubber stretched to $\lambda = 3$. The mean changes in surface finish with increased strain are shown as percentages in the Table 5.6.Only few tests were carried out and more testing would be required to establish if the changes in surface finish were typical. The rest of the tests showed increases in surface roughness. The reason is related to the small field of view. Also each time the test rig had to be taken out to pre-stretch the rubber. After returning the rig, it was hard to pin point the exactly where the surface had been scanned previously. However from the results obtained, it can be seen that White Light Interferometry is one of the best options for profiling the surface finish without contact with the surface of the test specimen. White light Interferometry provided a complete profile of a test specimen surface.

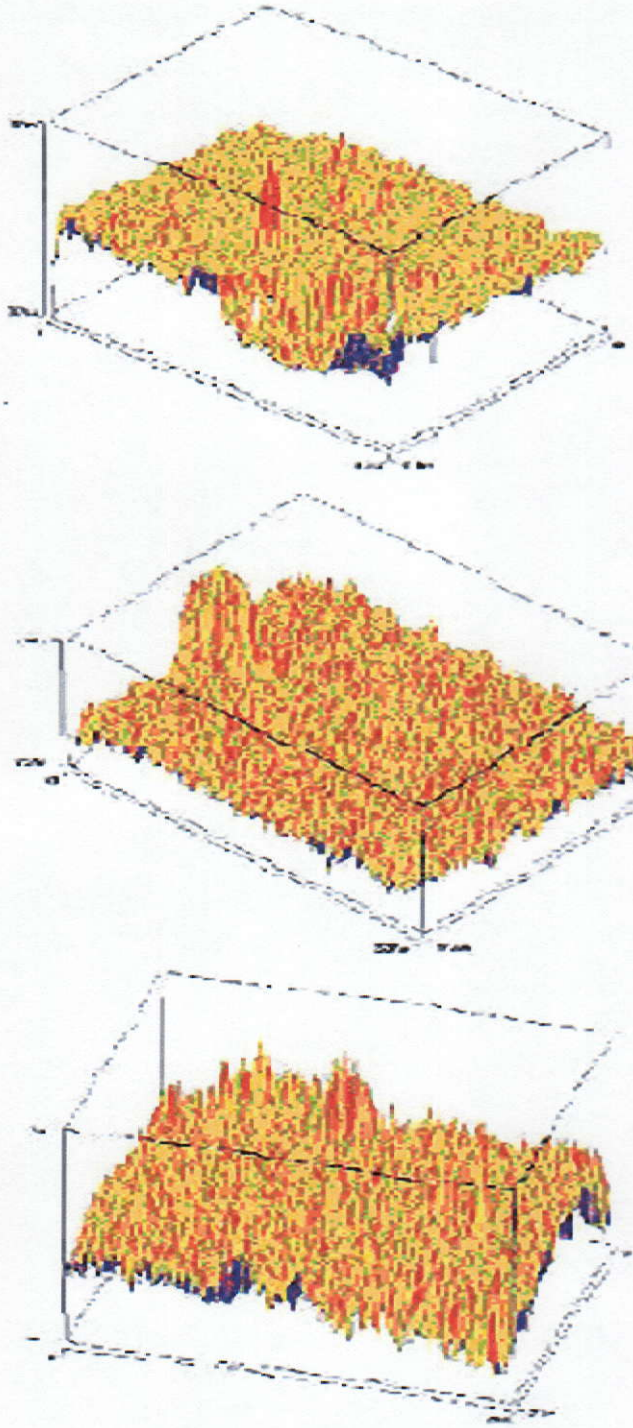

a) λ=1 (R_a=0.75μm)

b) λ=2 (R_a=0.52μm)

c) λ=3 (R_a=0.44μm)

Figure 5.3 3D Surface Profile of EPDM Rubber Subjected to Uniaxial Tensile Strain captured using The Micro XAM Surface Mapping White Light Interferometer

Stretch ratios, λ	% Of unstrained surface finish
1	100
2	69.3
3	58.6

Table 5.6 Average Percentage Change of EPDM Rubber Surface Finish vs Stretch Ratio

5.4 Microscopic Analysis of Surface Flaws

5.4.1 Microscopic Analysis of Surface Flaws in Natural Rubber (NR)

Figure 5.4 shows a surface flaw in a 38 IRHD NR. Figure 5.4 a) shows the flaw in the unstrained state, whereas Figure 5.4 b) shows100% strain based on a gauge length of 10 mm ($\lambda = 2$), within which the flaw is positioned and Figure 5.4 c) shows 200% strain ($\lambda = 3$). It is evident from the sequence that the flaw is a void in the material surface, as the bottom of the depression is coming into focus as the rubber is stretched and the depression becomes shallower. Initially the void is approximately circular and 80μm across. If the material is considered to behave as a linear elastic solid and the simple expression for stress concentration given by equation 5.2 is applied, then the static stress concentration k_t would reduce when strained, as shown in Table 5.7 consequently the static stress concentration k_t reduces with strain as shown in Table 5.8. For these elastic deformations it is more appropriate to use Inglis's equation in its general form for enclosed flaws equation.5.3.

a)Unstrained b) $\lambda = 2$ c) $\lambda = 3$

Figure 5.4 A Surface Flaw in a 38 IRHD NR Subjected to Uniaxial Tensile Strain

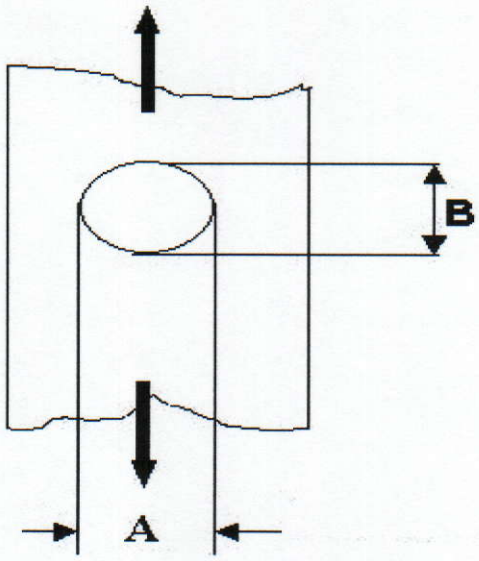

λ	k_t
1	2.6
2	1.79
3	1.46

$$k_t = 1 + 2A/B \quad (5.2)$$

Table 5.7 Changes in Stress Concentration with Tensile Strain in NR Samples (Eqn 5.2)

$$k_t = \frac{\sigma_t}{\sigma} = 1 + 2(0.5l/r)^{0.5} \qquad 5.3$$

σ_t = stress at the tip of a sharp flaw, σ = nominal tensile stress, l = depth of edge flaw, r = radius of the tip in the unstressed state.

λ	k_t
1	2.80
2	1.85
3	1.38

Table 5.8 Change in Stress Concentration with Tensile Strain in NR Samples

5.4.2 Microscopic analysis of surface flaws in EPDM

Figure 5.5 shows a surface flaw in an EPDM rubber. Figure 5.5c) shows the flaw in the unstrained state, Figure 5.5b) shows the flaw at 100% strain based on a gauge length of 10mm (λ=2), wholly enclosing the flaw and Figure 5.5a) the flaw at 200% strain (λ = 3). As with NR, it is evident that there is a void in the material surface, as the bottom of the depression is coming into focus as the rubber is stretched and the depression becomes shallower. Initially, the void is almost circular and 50μm across. As for the NR sample, the expression for stress concentration is given when equation 5.2 is applied. The static stress concentration k_t reduces as shown in Table 5.9, and as shown in Table 5.10 using equation 5.3. Again for these elastic deformations, it is more appropriate to use Inglis's equation in its general form for enclosed flaws equation.5.3.

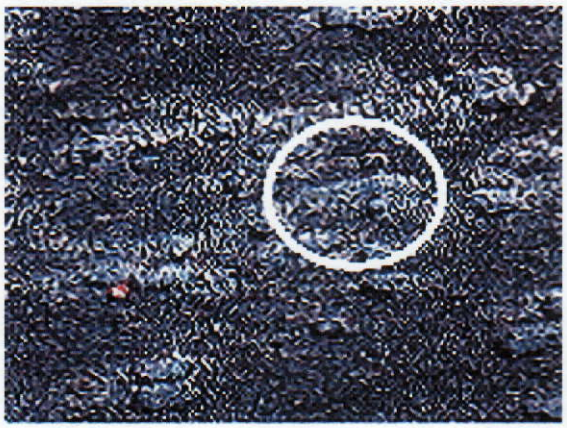

a) $\lambda = 1$

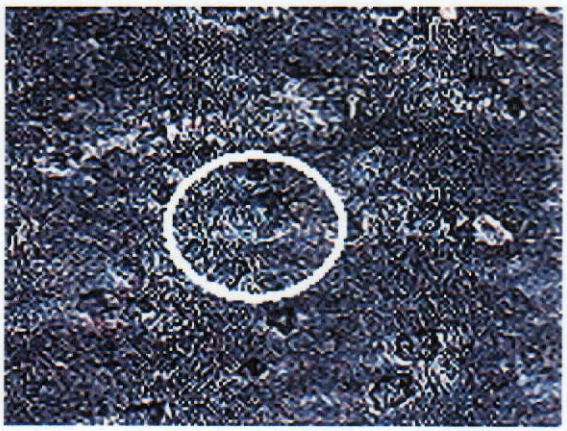

b) $\lambda = 2$

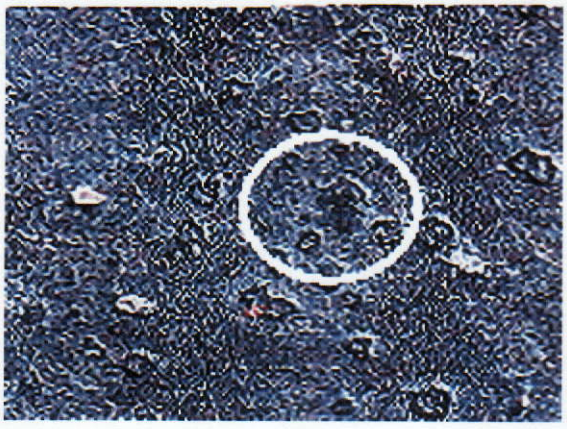

c) $\lambda = 3$

Figure 5.5 **A Surface Flaw of EPDM Rubber Subjected to Uniaxial Tensile Strain**

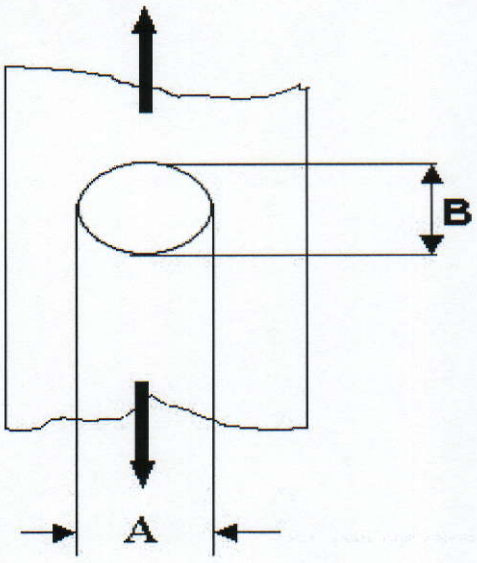

λ	k_t
1	3.44
2	2.29
3	1.73

Table 5.9 Changes in Stress Concentration with Tensile Strain in EPDM Samples (Eqn. 5.3)

λ	k_t
1	3.18
2	2.34
3	1.83

Table 5.10 Change in Stress Concentration with Tensile Strain in EPDM Samples

5.5 White Light Interferometry analysis of surface flaws in EPDM

From Figures 5.4-5.5 it can be seen that the depression of the flaws come into focus as the rubber was stretched. However more accurate observations had to be obtained the solution was found in employing a White Light Interferometer.

Figure 5.6-5.7 show a surface flaw in an EPDM rubber test sample. Figure 5.6b) shows the flaw in the unstrained state. The surface flaw is 60μm wide and 5μm deep. Figure 5.7 show another flaw 30μm wide and 5μm deep.

As previously described, the initial stress concentration can be calculated using Griffith equation (equation 5.2) and Inglis' equation (equation 5.3). The initial stress concentration at the tip of the 60μm void when equation 5.2 is applied is $k_t = 3$. Applying equation 5.3 the static stress concentration becomes $k_t = 2.41$.

Using this method of measuring the geometries of surface defects is very promising. However, the test rig used was not appropriate to perform this test. The problem was that the test rig had to be removed every time when a reading was required to be taken, and later returned and positioned under the objective. Because of its small field of view it was impossible to locate the same defect each time. This problem can be solved with the design of a special test rig that would stay in the same position throughout all the tests. This would allow the surface roughness readings to be more accurate.

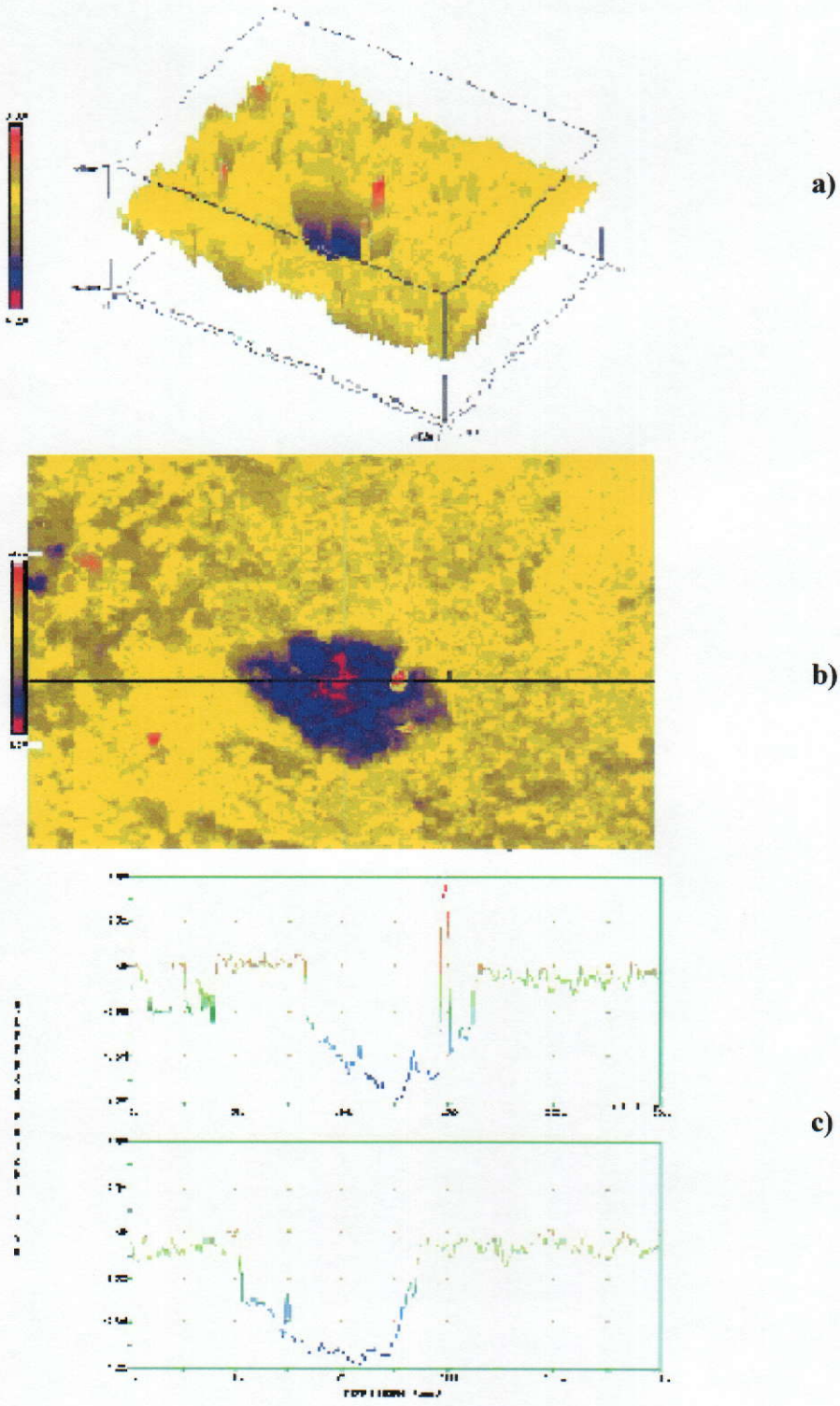

Figure 5.6 EPDM Rubber Surface profiled using MicroXAM 3D While Light Profiler a) 3D Surface Flaw Profile, b) 2D Image of the Surface Flaw 260.51µm X 197.27µm (Magnification: 31.5, Average Surface Roughness R_a= 0.67µm), c) X-Y Profile of the Surface Flaw

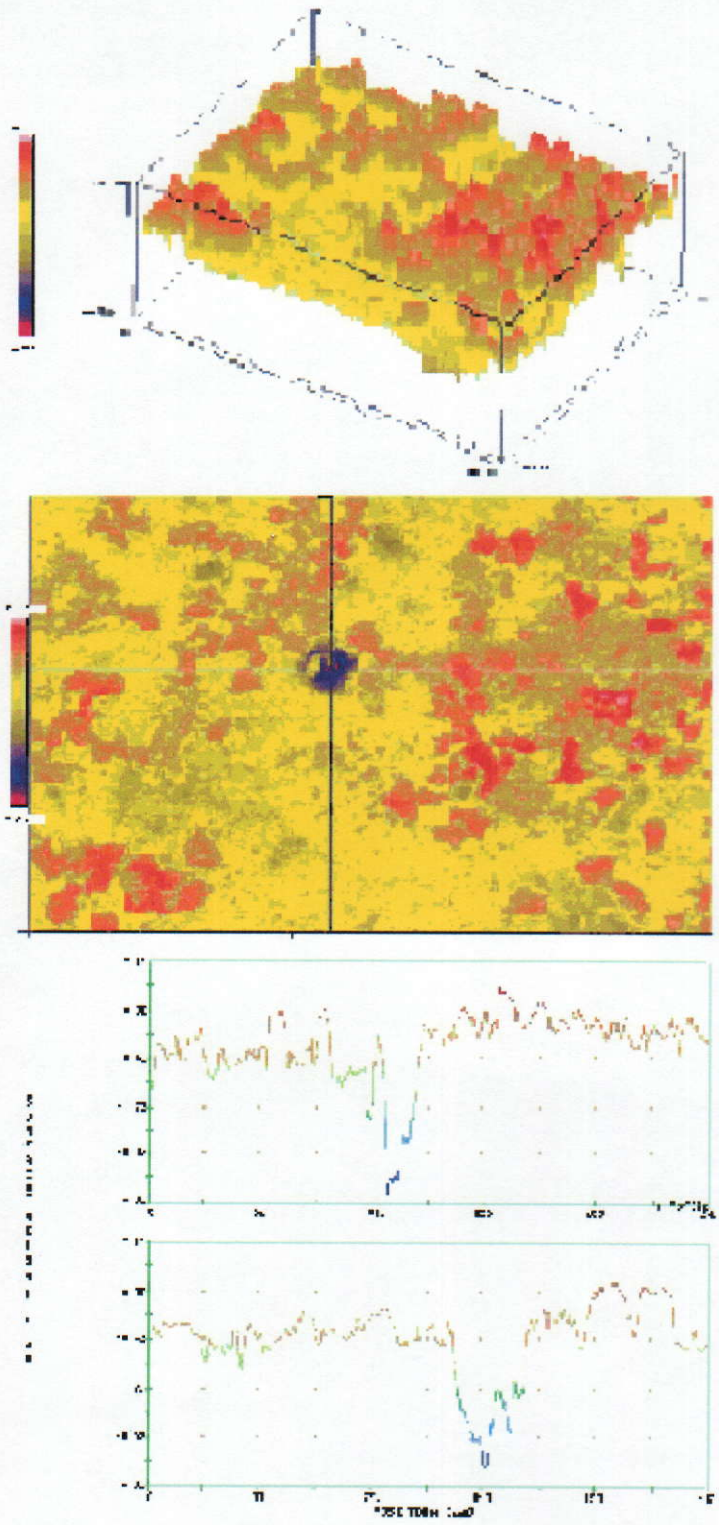

a)

b)

c)

Figure 5.7 EPDM rubber surface profiled using MicroXAM 3D While Light Profiler a) 3D Surface Flaw Profile, b) 2D Image of the Surface Flaw 260.51µm X 197.27µm (Magnification: 31.5, Average Surface Roughness R_a= 0.55µm), c) X-Y Profile of the Surface Flaw

5.6 Microscopic Analysis of Initiated Crack in EPDM Rubber Specimens

The test is preformed using a tensile test specimen of EPDM rubber, with initiated cracks. The length of the cracks varied as cuts were initiated using a sharp bladed knife and an engineers ruler. Figure 5.8a) shows a test specimen with an initiated crack in an unstrained state. Figure 5.8b) shows the specimens at 50% strain based on gauge length of 10mm ($\lambda = 1.5$), Figure 5.8c) shows specimen at 100% strained ($\lambda = 2$), wholly enclosing the crack and Figure 5.8.d) shows the specimen at 200% strain ($\lambda = 3$). It is evident that the radius of the crack increases with strain as the length of the crack reduces. Initially, the crack is approximately 140μm in length with a radius of zero. The Cracks were measured using the Omnimet Archive Digital Imaging System. In Figure 5.10a) the length of the crack is 308.4μm and in b) the radius of the crack is 220.8μm. For these elastic deformations it is appropriate to use the Griffith equation in its general form for calculating stress concentration at the tip of crack, (equation 3.4). The static stress concentration k_t at the Crack tip reduces, as shown in Table 5.11.

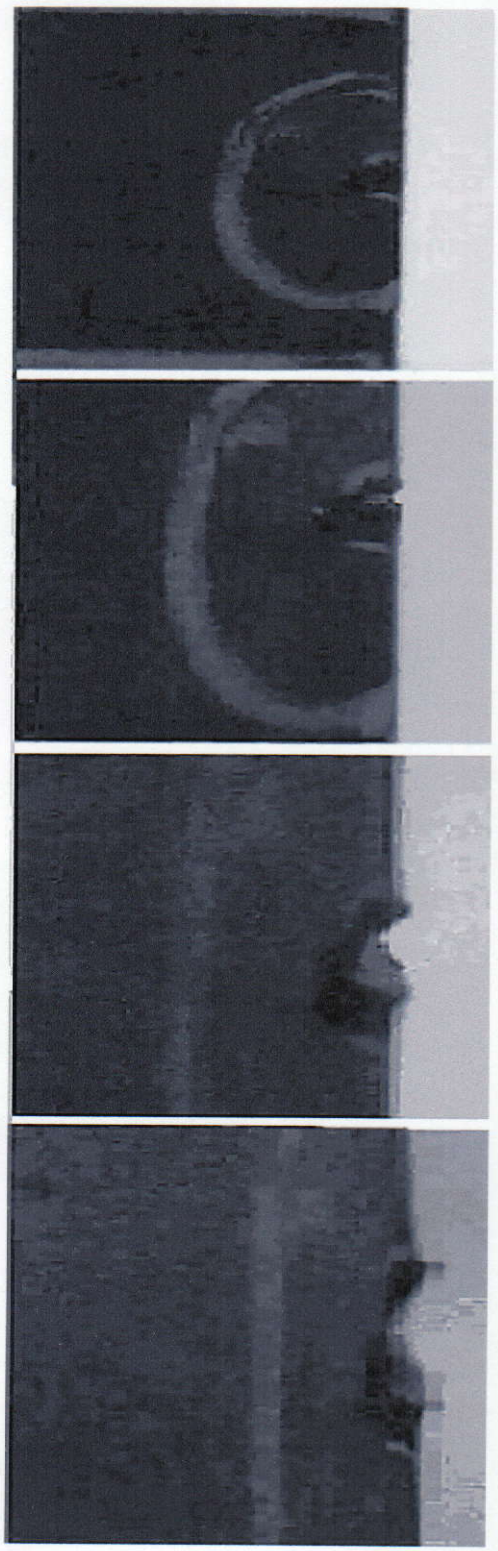

a) λ=1

b) λ=1.5

c) λ=2.5

d) λ=3

Figure 5.8 **An Initiated Crack in EPDM Rubber Subjected to Uniaxial Tensile Strain**

After the results were obtained, as shown in Table 5.11, the percentage stress concentration was calculated using Griffith formula for measuring stress concentration at the tip of the crack k_t, equation 5.4.

$$k_t=2(l/R)^{1/2} \qquad 5.4$$

Where: l = crack length, R = tip radius.

λ (%)	Average % stress concentration
50	100 (Assumed)
100	60
150	37
200	3

Table 5.11 Change in Stress Concentration with Tensile Strain in the Crack Initiated EPDM Samples using Eqn. 5.4

The loaded NR and EPDM rubber components that were produced by conventional compressive moulding process (see Chapter 3) contain surface defects that increase the stress and contribute to fatigue failure. The surface finish of NR and EPDM rubber improves with increased tensile strain, as can be seen in Tables 5.5-5.6. In fatigue higher levels of stress in the pre-stressed (pre-strained) material are partially compensated by such improvements in surface finish. From the surface flaws tests and edge crack test can be seen that stress concentration diminishes with strain in these tests, as shown in Tables 5.7- 5.11. Irrespective of the notch sensitivity of the material, dynamic stress concentration (k_f) will diminish with reduction in static stress concentration (k_t). Again, higher mean stress in fatigue cycle is partly redressed by lower stress concentration.

Chapter 6

Surface Treatments

6.1 Introduction

In service rubber undergoes large reversible strains and it is seen in previous chapter that rubber components have less severe surface flaws when preloaded than when in a stress free state. In fatigue, higher stress levels in the pre-stressed (pre-strained) material are thought to be partially compensated by improvements in surface finish. It is expected that the size of flaws introduced during the manufacturing process, irrespective of whether the part is made by compression, injection or transfer moulding, participate in early failure of the rubber specimen when it is under load. The fundamental question posed is whether surface treatments influence fatigue resistance?' Reducing the size of a flaw has the potential to reduce the concentration under load and thereby improve resistance. This chapter describes an investigation of surface treatments and their influence on the surface characteristics and fatigue life of EPDM and SBR rubber dumbbell specimens.

6.2 Material

For the test, Ethylene Propylene Rubber (EPDM) was used because of its non-strain crystallising behaviour. The EPDM used in the fatigue test, was Buna EP G 5450. The chemical composition of the EPDM is shown in Table 3.1, pp.54. Figure 6.1 shows a dumbbell test specimen. The major and minor diameters of the test-piece were 25 mm and 15 mm respectively. The fillet radius that is essential for allowing

the test-piece to be cycled between tension and compression, is 5 mm. The gauge length is 25mm.

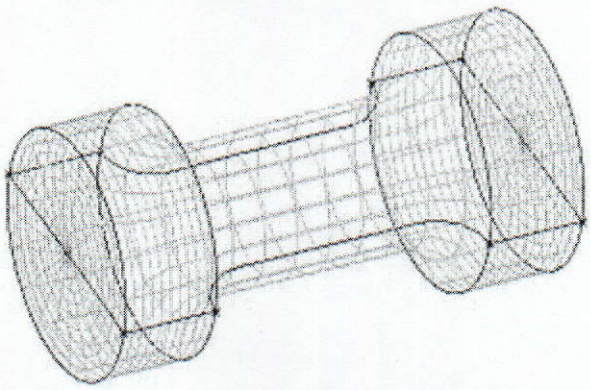

Figure 6.1. Model of a dumbbell test specimen

The geometry of this dumbbell test specimen allows compression up to 30 % without the barrelling that occurs to simple cylindrical test-pieces when compressed at much lower strains.

6.3 Coatings

6.3.1 Diamond-like Carbon Coating

The use of Diamond-like Carbon Coating (DLC) films is accompanied by two major problems: high internal compressive stresses (leading to poor adhesion properties between treated material and the coating) and a friction coefficient: μ, that is dependent on the ambient relative humidity. In this project we are solely concerned with low adhesion properties of DLC.

Carbon is a very versatile element. In graphite, carbon atoms bond strongly to each other within a plane, but weakly between adjacent planes. Graphite is soft, electrically conducting and opaque. In diamonds, the bonding is strong in all directions. Diamond is the hardest known material, electrically insulating and transparent. Diamond films with excellent protective properties can be produced by vacuum deposition but the optimum substrate temperature for coating is about 900°C, which severely limits the range of substrates to which diamond carbon can be applied.

At room temperature, an amorphous carbon containing coating can be produced in which a proportion of the carbon atoms are bonded as in diamond and this resembles diamond in many ways, hence Diamond-like Carbon Coating.

6.3.1.1 The Coating Process

The samples were initially cleaned in deionised water and placed in an oven at 50°C to remove any remaining water from the samples. The warm samples were then placed in an atom beam system, as shown in Figure 6.2 and a pump creates a base pressure of $1x10^{-5}$ mbar.

The samples were cleaned in argon plasma and the coating was deposited using acetylene gas (as the source of the carbon). The argon is ionised by the radio frequency (RF) electro magnetic field and the positive ions bombard and clean the substrates. The cleaning stage is followed by the deposition stage in which a carbon containing gas such as acetylene is introduced to provide the energetic carbon ions.

Diamond-like carbon is produced when carbon is deposited under energetic bombardment.

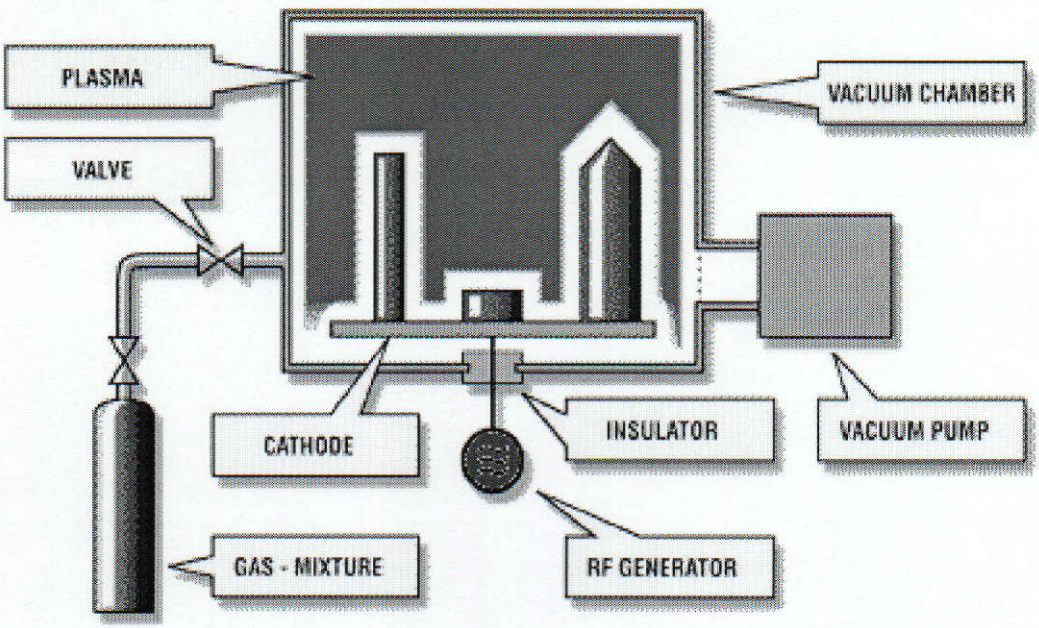

Figure 6.2 DLC Coating chamber [54]

The instantaneous local high temperature and pressure cause a proportion of the carbon atoms to bond as diamond. These conditions are obtained during plasma assisted chemical vapour deposition (PACVD).

The samples were rotated during deposition. Coating thickness is around 150nm - 200nm.

a) b)

Figure 6.3 a) EPDM dumbbell specimen DLC uncoated, b) EPDM dumbbell specimen DLC coated

6.3.2 Sol-gel Coating

Thin film or coating deposition represents the oldest commercial application of sol-gel technology. Sol-gel processing begins with a colloidal dispersion, or sol, of particles or polymers in a liquid. Through subsequent cross linking the fluid, sol may be transformed into a rigid gel. The first patent based on sol-gel processing was granted to Gen *et al* [55], in 1939 for silicate sol-gel films formed by dip coating. Today, sol-gel technology is used extensively for applications as diverse protective and optical coatings. As this technology is based on applying a thin film of material onto a surface, it is essential to understand the basics of surface science. The interaction between two solids or between a solid and its environment is through the material surface. The properties exhibited by the surface are largely determined by the composition of the outer most layers of the material. Metals are often coated with sol-gel films to protect surfaces from damage by acids and oxidation. Dense

zirconium films are used to protect steel from corrosion [55] and silica films are used for corrosion protection of aluminium [56]. Sol-gel films can also be used for fracture protection of ceramic substrates [57-59]. The function of the film is usually to fill surface flaws that can otherwise lead to fracture initiation. Dip sol-gel coating will be used for this research and Tetraoxidsilicate $Si(OC_2H_5)_4$, (TEOS) as a coating material. The central research question is whether the flaws in the surface of the rubber samples will be successfully filled with TEOS and whether this treatment will prevent the start of crack propagation and therefore improve the fatigue life of specimens?

6.3.2.1 Coating Process

The Initial part of the Sol-gel coating process involved the preparation of the coating solution. This area of the sol-gel process is considered to be the most important, as the end product is very dependent on details such as precursor, reaction conditions, solubility (R) value and heat treatments. Apart from pH[1] and R_r[2] value, important other parameters which affect the overall coating structure are: precursor type, nature of the catalyst, ageing time, ageing temperature, drying time and drying temperature. For this project, Tetraoxidsilicate, $Si(OC_2H_5)_4$, known as TEOS, was used as a coating material. The solution was prepared according to guidelines provided by Enright [60]. The solution was prepared using the Tetraoxidsilicate (TEOS) liquid solution, de-ionised water pH1 and ethanol. The molar ratio of the mix was considered and the amount of precursor calculated to give proportions quoted below.

---

[1] PH; is a unit of measure which describes the degree of acidity of a solution it provides the needed quantitative information by expressing the degree of the activity of an acid or base in terms of hydrogen ion activity

[2] R_r; Water: Precursor ratio

Solution composition contains:

Water = $22cm^3$,

TEOS = $91cm^3$,

Ethanol = $62cm^3$.

The solution was mixed together and stirred for an hour using a magnetic method for stirring. After an hour the solution was covered and left to age for 24 hours.

Rubber test specimens were cleaned in de-ionised water and dried in the oven at a temperature of 50 °C. Following the cleaning process the specimens were ready for coating. Each specimen was coated separately.

The specimen was dipped in the solution for 10 seconds and withdrawn at a speed of 4mm/s. Then specimens were placed in the furnace at a temperature of 100°C and left for an hour which is the recommended crystallisation time.

6.3.3 Fatigue Test

The fatigue tests were performed using MTS 831.50 Servo-Hydraulic Elastomer Test System, Deutsches Institut für Kautschuktechnologie, Germany (see Figure 6.4). This Machine has the capability of applying frequencies up to 100 Hz under load or displacement control. For tests under load control, it is necessary to optimise the control parameter (PID and MTS added F-Parameter) for each material or test specimen design. Otherwise the system cannot drive an exact excitation (sinus) for extreme non-linear and soft test pieces. A special elastomer software TestWare SX under the TestStar control software allows for the online analysis of the tested specimen.

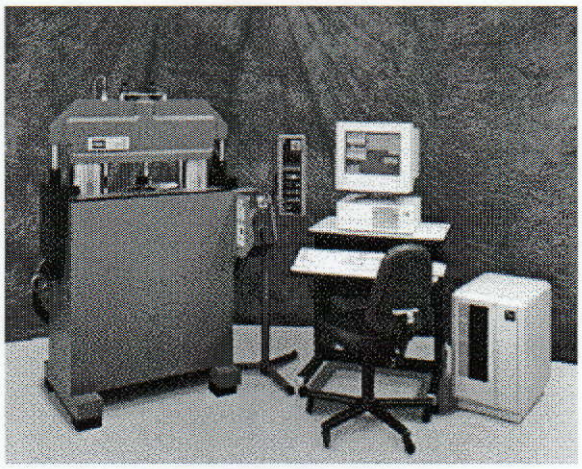

Figure 6.4 MTS 831.50 Elastomer [61]

Samples were tested under load control with 0 N minimum load and 500N maximum load. All tests were to failure at a frequency of 1 Hz. The frequency was chosen to induce failure due to the initiation and growth of cracks as opposed to internal friction causing large increases in temperature and consequent thermal break-down [62].

6.3.3.1 Procedure

Each specimen was subjected to tensile cycles with zero minimum load. The peak load in a test was kept constant, but increased in subsequent tests on different specimens over a range of 500 N.

During the tests, the dynamic visco-elastic properties of the test specimens were recorded to evaluate the influence of the coating on the fatigue life of EPDM rubber. To calculate the elastomeric behaviour of the test materials the sinus regression was

chosen. This method uses the main sinus oscilation for the calculation of the dynamic properties. The only problem with the sinus regression method is that the height of harmonic contributions to the signal are neglected in the calculation which causes a small deviation or error in the case of non-linear material properties. The main problem in the calculation of the dynamic properties of elastomers is the high non-linearity of the material for which principally no E-modulus is defined. The sinus regression method is however, the best compromise in commercially available software solutions.

An experimental problem was to achieve a valid mean value of the fatigue properties of the samples. Only 6 samples were tested, 3 coated and 3 uncoated. There was high scatter in fatigue life, even though the specimens were produced and coated under the same laboratory conditions.

6.3.4 Results Analysis

6.3.4.1 DLC Results

The results of the fatigue tests of the coated and uncoated EPDM are shown in Figures 6.5 and 6.6. Filled EPDM undergoes changes in physical properties during the load controlled cycles. Dynamic load cycles induce an increased permanent set as the tests progresses. The modulus of the tested specimens decrease as a result of stress softening [63]. The fatigue tests on coated and uncoated samples, show that the stiffness as well as the loss factor (tan δ) of the material decreases throughout, until fracture occurs, as shown in Figures 6.7-6.9.

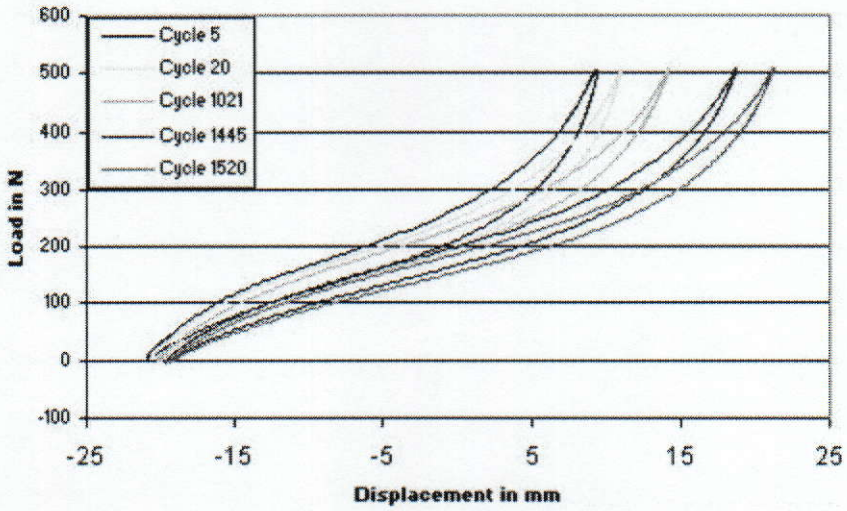

Figure 6.5 Hysteresis Loops during Fatigue Test, DLC Coated EPDM

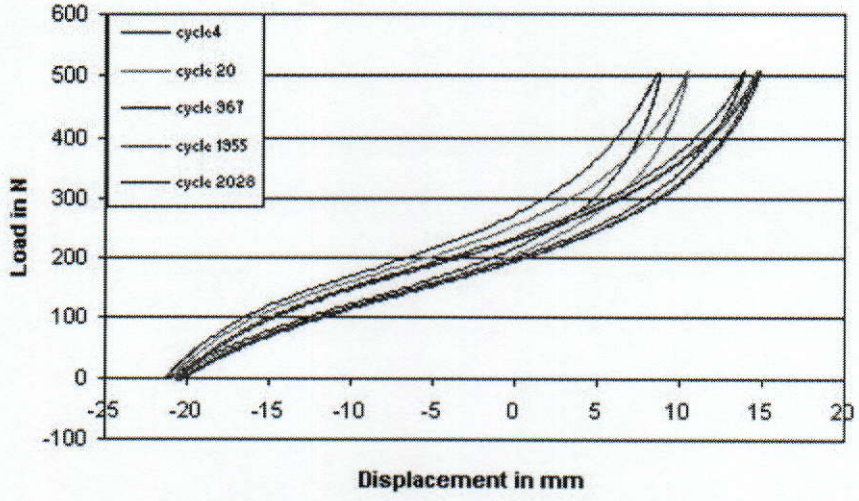

Figure 6.6 Hysteresis Loops during Fatigue Test, DLC Uncoated EPDM

The test results of the coated samples showed that dissipated energy per cycle reaches a plateau after a few hundred cycles as a consequence of the strain behaviour and the change in tan δ. It is only immediately before fracture, as the crack propagates, that the dissipated energy per cycle and tan δ increase, see Figure 6.7.a).

The same phenomenon can be observed under less severe conditions when test specimens fail after a thousand cycles [64]. Uncoated specimens did not display the same behaviour, see Figure 6.7.b).

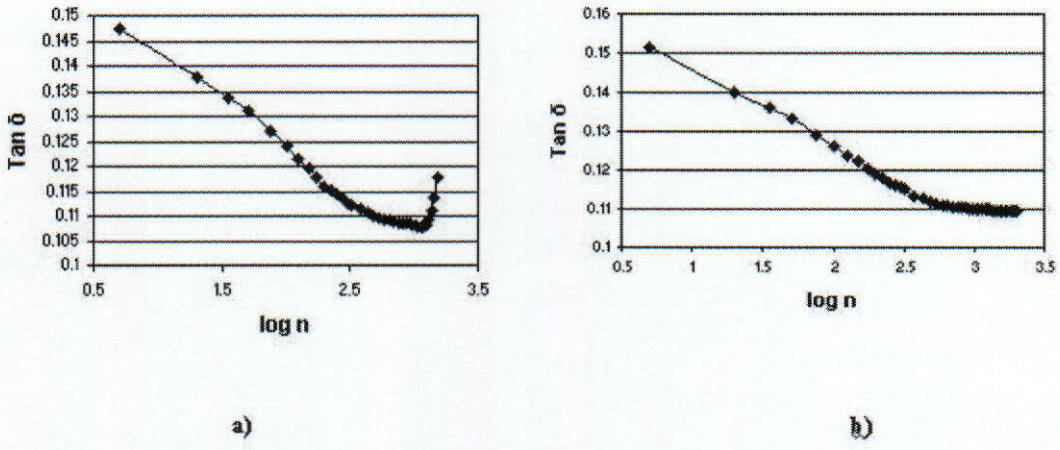

Figure 6.7 Tan δ vs log n cycles a) EPDM DLC Coated, b) EPDM DLC Uncoated

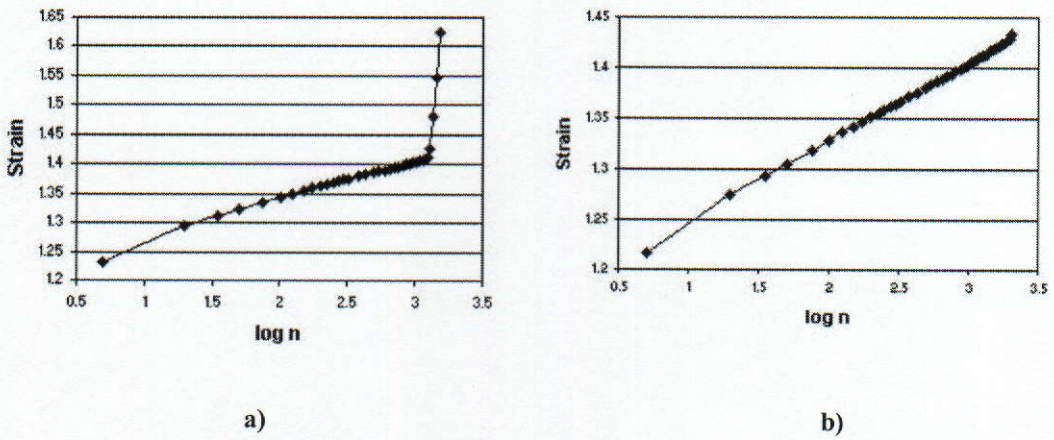

Figure 6.8 Strain vs log n cycles, a) EPDM DLC Coated, b) EPDM DLC Uncoated

Previous research suggests that the component will fail when the complex modulus E* has fallen to approximately 76% of the first cycle [64]. This can lead to a determination of stiffness loss at which any rubber component manufactured from

any particular material will fail. This finding has important consequences for the maintenance and replacement of elastomeric components prior to failure. Test results for coated and uncoated specimens confirmed this observation, see Figure 6.9.

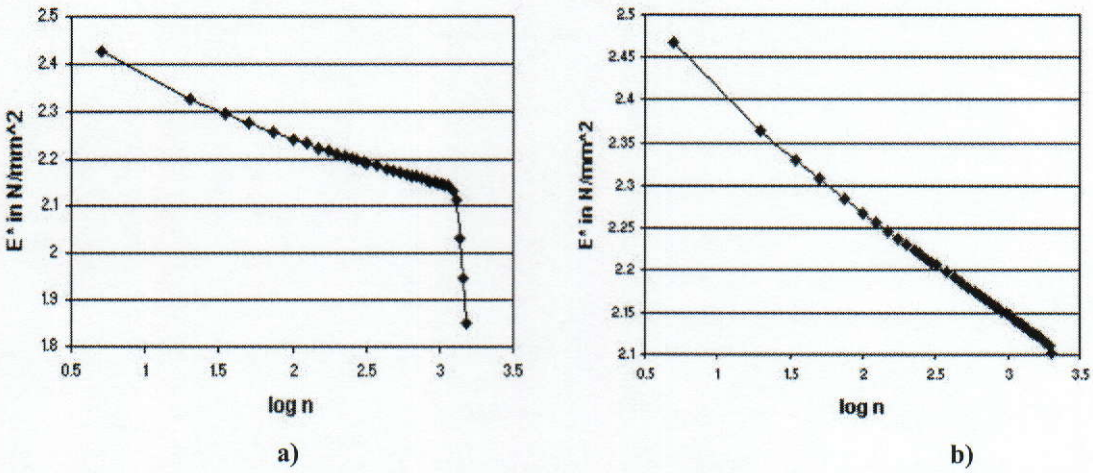

Figure 6.9 Complex Modulus E* vs log n Cycles, a) EPDM Coated, b) EPDM Uncoated

The fatigue test results of EPDM rubber coated with the DLC coating show that the fatigue life does not improve.

6.3.4.2 Sol-Gel coating Results

Unfortunately in both cases, the coating procedure was unsuccessful, because during the crystallisation time the coating began to peal off from the specimens. It did not crystallise on the surface. For this reason, the sol gel coating had to be disregarded as a possible rubber coating. The crystallisation temperature had to be increased above 200°C, which is not a suitable temperature for rubber specimens. High temperatures would negatively impact on the properties of the rubber.

The fatigue test results using a DLC coating and Sol-gel coating show that these coating treatments do not have positive effect on the fatigue life of elastomers. The coating procedure involved heating the samples above critical temperature levels, at above 120°C and this caused a change in the physical properties of the rubber.

6.4 Shot Peening

6.4.1 Theory of Shot Peening

The surfaces of almost all materials contain some degree of micro-cracking, tiny cracks, discontinuities or even tool marks that can be a source of failure. When a metal part is stressed and subjected to cyclic loading these micro-cracks enlarge and propagate through the part. At some point in time the part will fail. Normally, tensile stresses concentrate at the top or bottom of the crack during loading. However, the compressive skin created by shot peening tends to cancel out the tensile stresses and the cracks do not propagate, as shown in Figure 6.10.

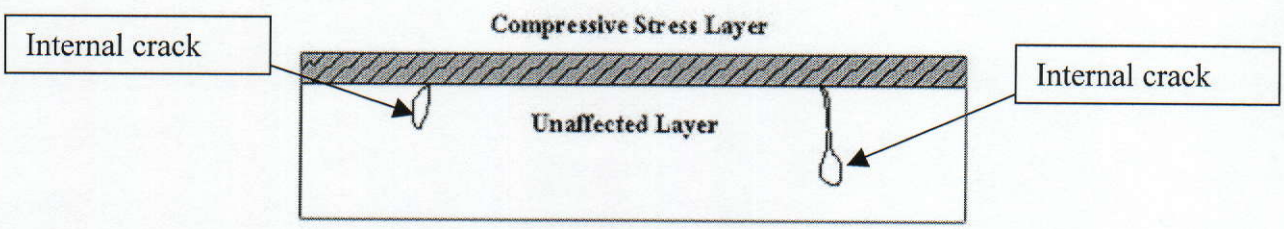

Figure 6.10 Shot Peened Metal Strip

Cyclic fatigue failures generally begin at surface defects or stress concentrations known as stress raisers. Examples of high stress areas are machine marks, scratches, sharp corners or holes, fillets, keyways, splines or other changes and interruptions in

the smooth surfaces of the metal. Peening improves fatigue life, strength, operation and corrosion resistance. Reliability of parts is enhanced as this treatment provides repeatedly uniform finishes, surface durability and wear resistance qualities. Peening can relieve all surface stresses and most internal stresses. Surface stresses resulting from ordinary machining operations may be transformed into hardwearing compressive stresses. To-date the Shot peening treatment is not used for improving physical properties of elastomers. It is hoped that this treatment will successfully diminish stress raisers that are on the surface introduced by the manufacturing process. Typical voids or surface defects on Natural Rubber (NR) and EPDM Rubber consist of 50μm to 100μm in diameter.

6.4.2 Material and Equipment

Again the EPDM used in the fatigue test was Buna EP G 5450, (having the chemical composition shown in Table 3.1, pp.54). Test specimens were cut to size using a punch die producing the following dimensions: width: 15mm, length: 80mm and thickness: 2mm.

The Shot Peening test rig was designed and built in Faculty of Engineering[3]. The main components of the machine are: Pneumatic Cylinder, Stepper Motor, Lead screw, Slide Assembly, PLC Controller, Shot Delivery Unit. The Machine is shown in the Figure 6.11, below.

[3] The Shot Peening test rig was designed and build by Mr. James Vahey

Machine Axes Specification:

1. X-axis movement is 30mm,
2. X axis speed is 0 to 2 m/sec,
3. Total Y-axis movement is 75mm,
4. Minimum Y-axis increment is 0.02mm.

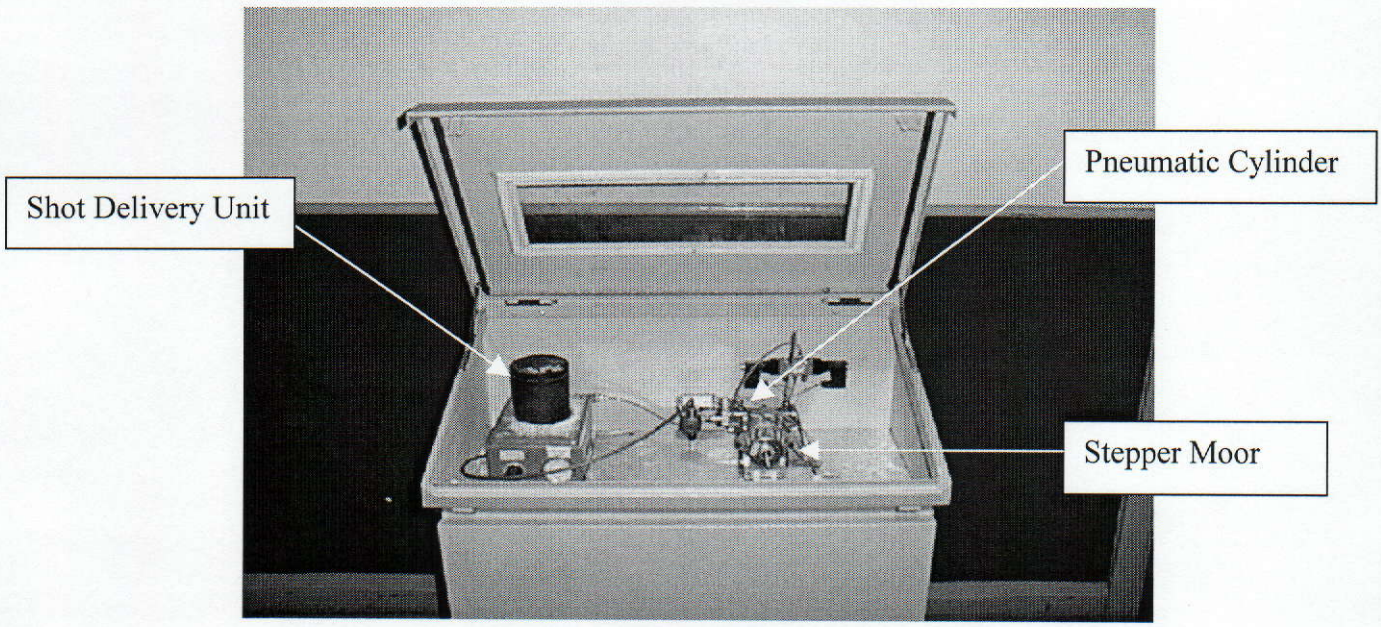

Figure 6.11 Shot Peening Test Rig

6.4.3 Shot Peening Process

Five EPDM rubber test specimens were shot peened. The Material used for the Shot Peening Process was Zirshot and the composition of this material is shown in Table 6.1, the Shot size was 300μm in diameter.

Zirconium (Z_rO_2)	67 %
Silicon (SiO2)	31 %
Other	2 %

Table 6.1 Shot Composition

The peening was carried out with an air pressure of 4 Bar, a nozzle diameter of 2mm giving 100% coverage with a distance from the nozzle to the work surface of 45mm, shown in Figure 6.12. A test specimen would be placed directly under the nozzle. Four passes were then made over each side of the specimen. A visible difference was noticed as observed in Figure 6.13 but the rubber did not show the same reaction to this treatment as the metal strip did. A Metal strip under this condition would arch up to 0.5 mm at the centre as shown in Figure 6.14, under the Almen Shot intensity test.

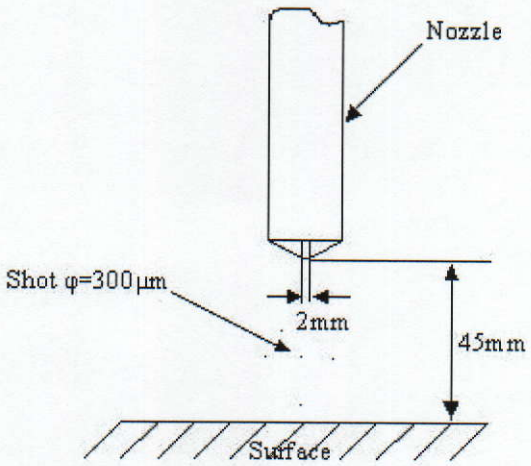

Figure 6.12 Shot Peening Process

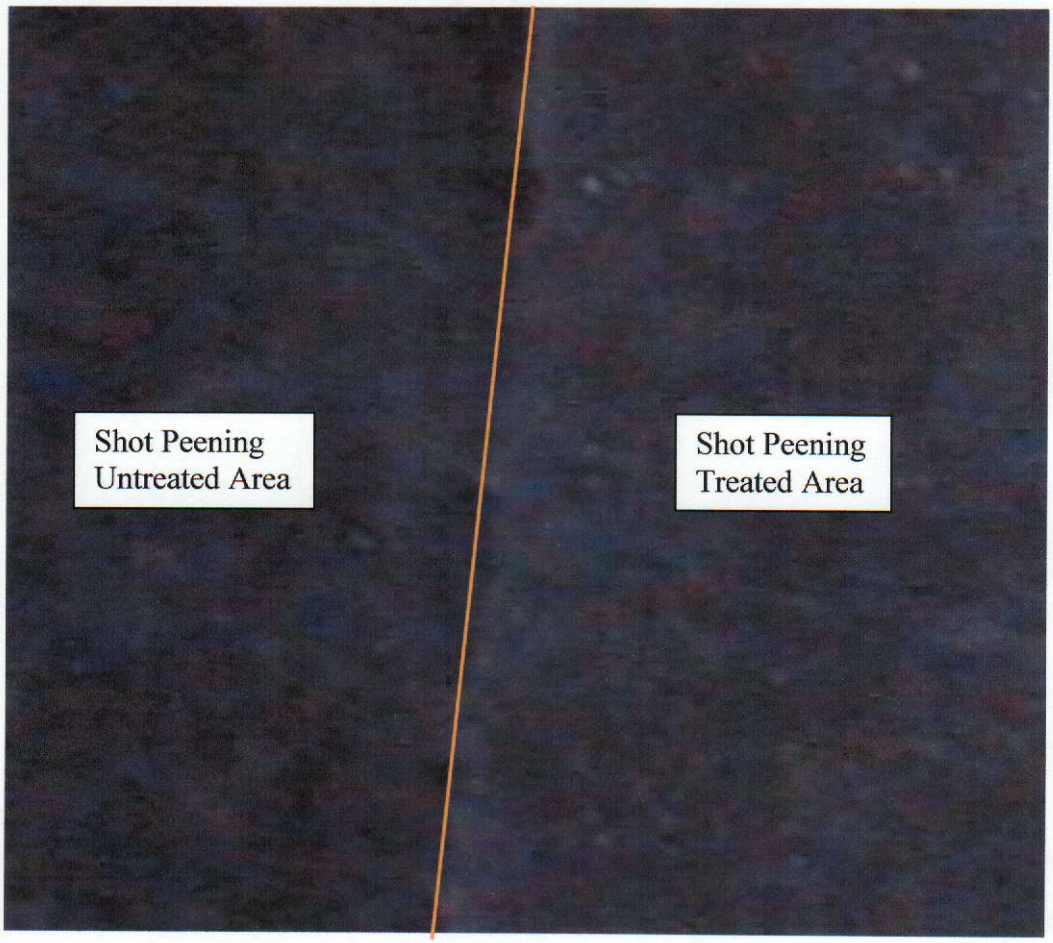

Figure 6.13 Difference between Shot Peen Treated EPDM Sample and Untreated EPDM Sample

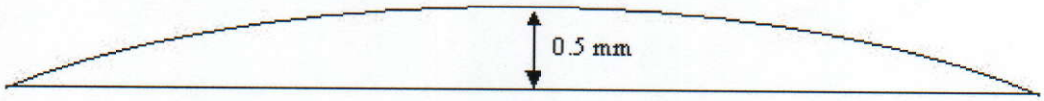

Figure 6.14 Arching of a Metal Strip after Shot Peening

6.4.4 Microscopic Analysis

Using the Micro XAM White Light Interferometer, the surface of Shot Peen treated EPDM rubber sample and untreated EPDM rubber samples were profiled. It is significant that the surface finish was seen to improve with the treatment, as shown in Table 6.2.

Average Surface Roughness R_a of Shot Peen treated EPDM rubber	Average Surface Roughness R_a of untreated EPDM rubber
0.49μm	0.75μm

Table 6.2 Average Surface Roughness R_a of Shot Peen Treated EPDM Rubber and Untreated EPDM Rubber

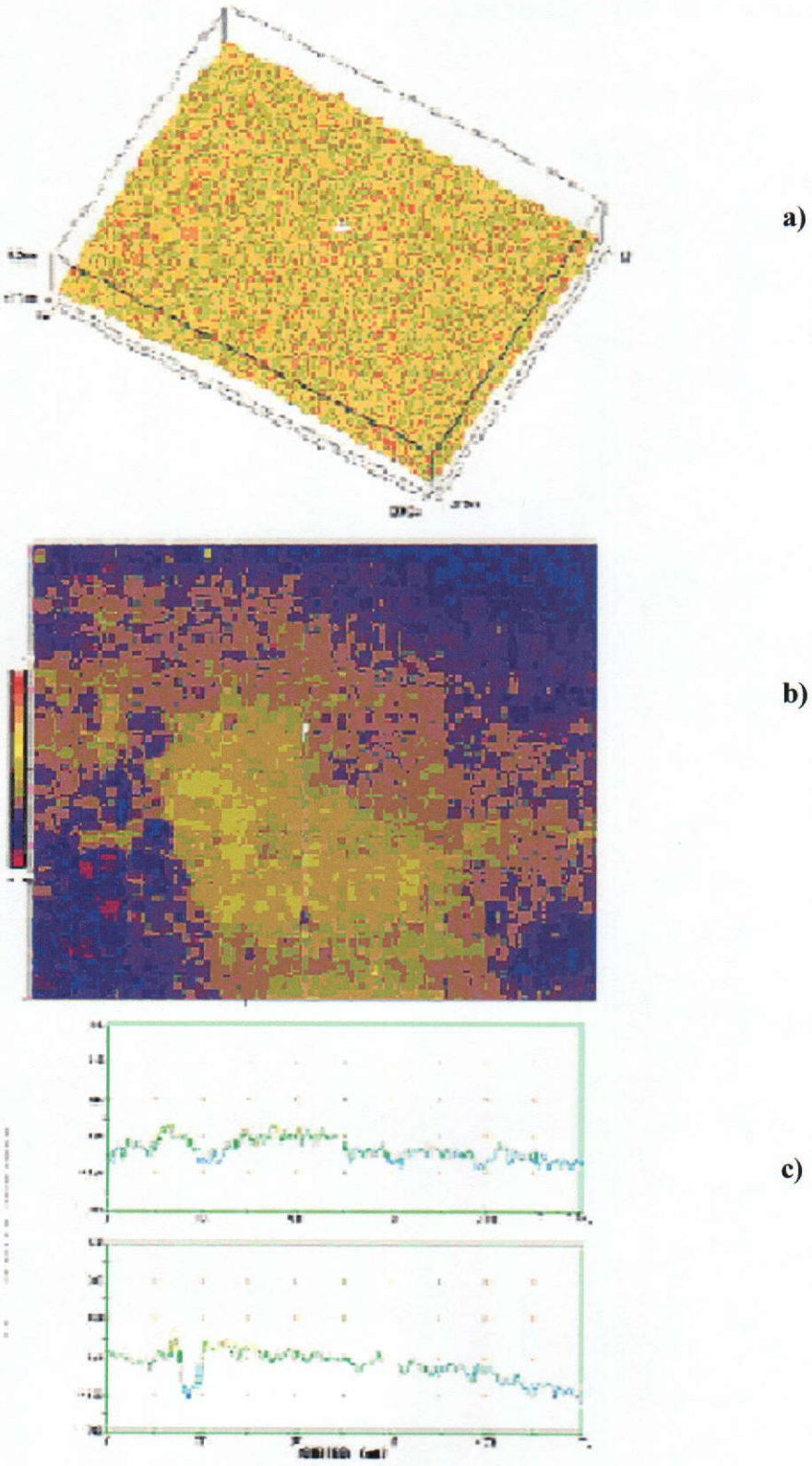

Figure 6.15 EPDM Rubber Surface profiled using MicroXAM 3D While Light Profiler a) 3D Surface Profile, b) 2D Image of the Surface 260.51µm X 197.27µm, Average Surface Roughness R_a= 0.49µm, c) X-Y Surface Profile of Shot Peen treated EPDM Rubber Sample

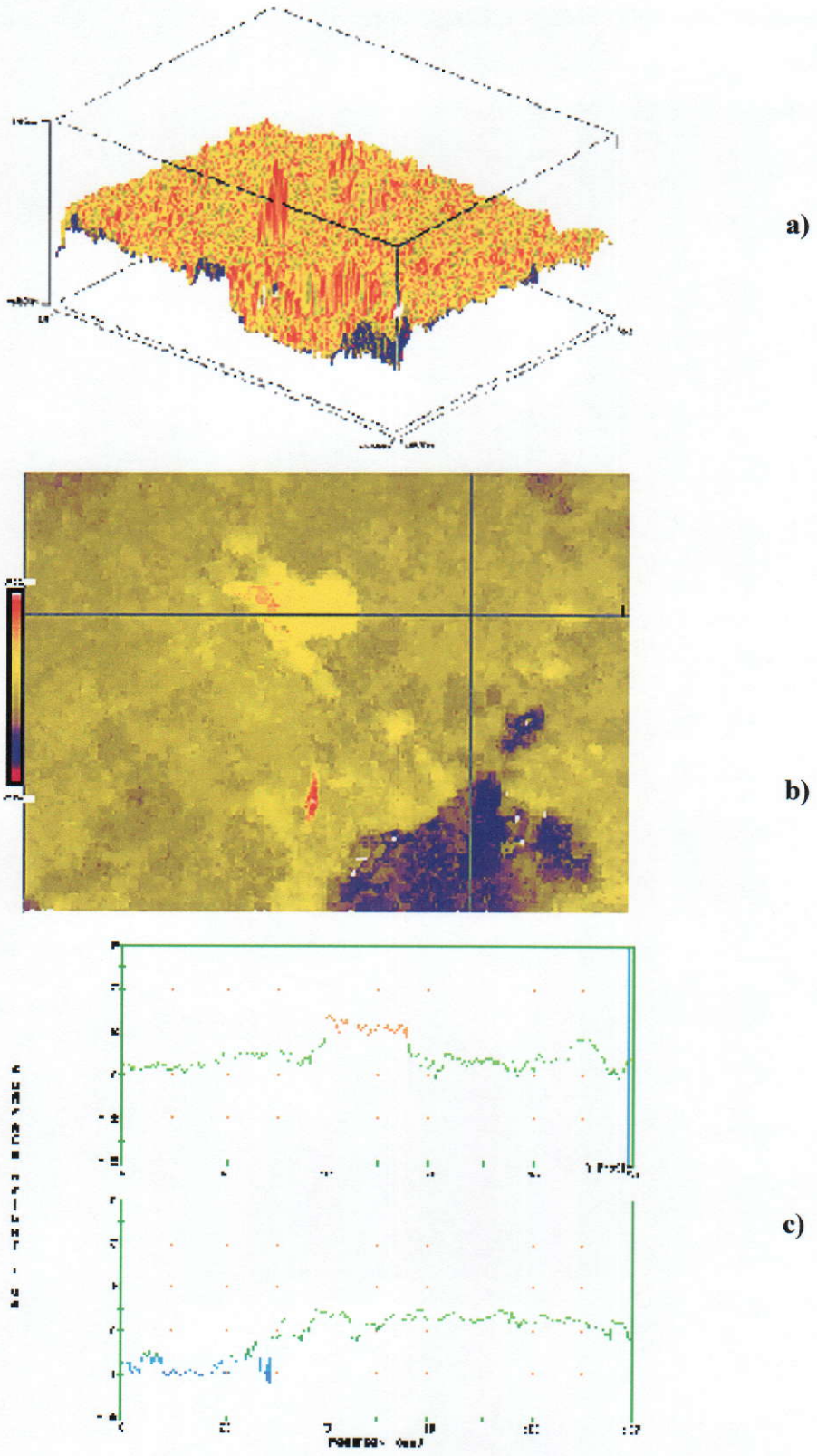

Figure 6.16 EPDM Rubber Surface profiled using MicroXAM 3D While Light Profiler a) 3D Surface Profile, b) 2D Image of the Surface 260.51µm X 197.27µm, Average Surface Roughness R_a= 0.75µm, c) X-Y Surface Profile of EPDM Rubber Sample

6.4.5 Tensile Test

The tensile machine used was a Lloyd LR 30K, with Nexygen 4.1 software the equipment can be seen in Figure 6.17. The crosshead speed was 500mm/min and the gauge length was 15mm.

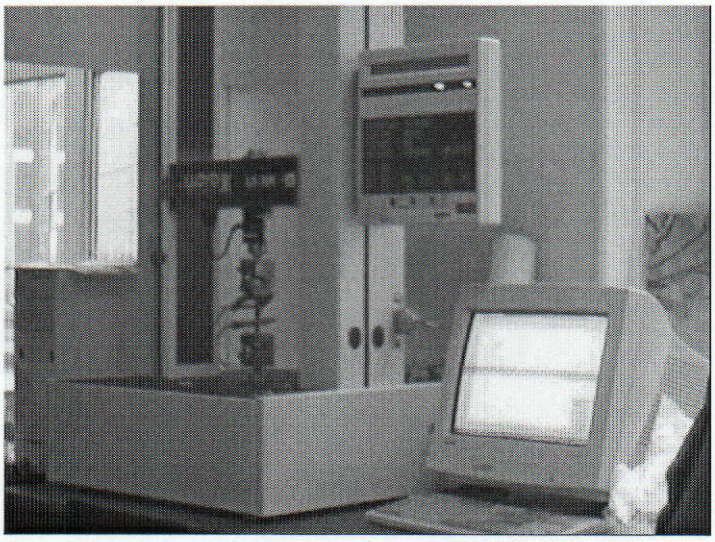

Figure 6.17 Lloyds LR30k Extensometer With Working Station

Shot peening, as discussed previously improves the fatigue properties of the metallic material. However fatigue test equipment was not available and therefore a tensile test was the only test that was possible to perform.

Each specimen was subjected to tensile load with zero minimum load. During the test tensile properties were recorded to evaluate the influence of the Shot peening treatment on the tensile strength of EPDM rubber.

Ten specimens were tested, 5 treated and five untreated. There was no difference in the tensile strength of specimens therefore surface finish does not appear to have any effect on tensile strength of EPDM rubber. Figure 6.18 show a plot of Stress vs

Strain for both the treated and untreated samples and it can be seen that there is no change in the tensile properties of EPDM Rubber.

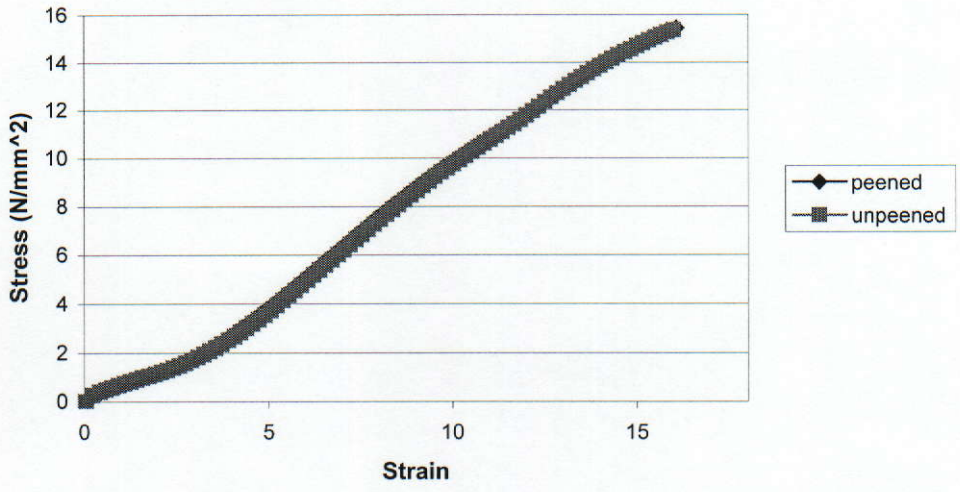

Figure 6.18 Stress vs Strain Curve of Shot Peening Treated EPDM Rubber and Untreated EPDM Rubber

As rubber is a self-recovery material, this treatment shows no significant improvements in the physical properties of rubber. However, the microscopic analysis showed improvements in surface roughness (R_a), as shown in Table 6.2. Further tests would be needed before this treatment could be completely rejected as a valid rubber material treatment. This treatment for rubber material should also be evaluated for: adhesion and wear resistance as well as fatigue strength.

Chapter 7

Non-Linear Finite Element Analysis of Rubber

7.1 Introduction

7.1.1 Using FEA to Model Large Reversible Deformations

Rubber's ability to withstand large strains makes it an ideal material for many applications. Those applications include: tyres, vibration insulators, seals hoses, belts, structural bearings, impact bumpers, medical devices, footwear, etc. Applications are subject to large static and time-dependent strains. Their long-term durability is therefore a critical issue. While many factors contribute to long-term durability, mechanical fatigue, the nucleation and the growth of cracks in the rubber, is often the primary consideration. The current research aim is to make lifetime predictions for rubber components to address the issue effectively and economically, engineers need to design models for mechanical fatigue early in the product development process. This need has been partially solved by the development of computer software called Non-linear Fatigue Element Analysis which is capable of predicting stress and strain histories [65-68].

One of the major aims of this project was to use FEA software, to model elastomeric crack propagation. It was hoped that it would be possible to model loading of rubber components and that the results gained would correlate with the results form the physical tests. The software chosen for FEA was MSC MARC Non-linear Finite Element software.

Finite element analysis of elastomers is complex for a number of reasons:

i) elastomers are subjected to large deformations and rotations when loaded and there are associated changes in boundary conditions,

ii) the material is assumed incompressible

iii) instabilities result from the material composition.

Even the experienced FE analyst cannot always predict the problems that may arise during testing. Some are due to the material composition, some due to the discretisation of the model and some due to a combination of both. Therefore it is very important all FEA results are considered carefully.

This chapter describes the application of MSC Marc FEA software.

7.1.2 Material Characterisation

How well do these material models work in FEA programs? One way of illustrating this is to model the test specimen used to generate the test data, as seen in Figure 7.1. This model used the loading conditions applied to obtain the stress-strain curve. The validity of results was checked using plausibility theories developed by Johannknecht *et al* [69], who have established plausibility criteria for a range of elastomeric material models.

The accuracy of FEA is largely dependent on the accurate modelling of the product's material properties and geometry. The properties of metals, which are most often subjected to FEA, can usually be modelled with linear equations.

Elastomers, however, have non-linear stress-strain characteristics for the relatively large deformations that they experience in normal service.

The Ogden and Mooney-Rivlin (see Chapter 2, pp.30) material models are often used to define the characteristics of elastomers. The Ogden model closely follows elastomeric material property responses in both tension and compression.

The question remains as to how we can use loading histories to estimate the life of the component. The following conditions must be observed to conduct a valid Finite Element stress analysis.

i) Equilibrium of forces.

Internal forces must be balanced with external loads.

ii) Compatibility of displacements.

Deformed elements must fit together.

iii) Laws of material behaviour.

Linear elasticity.

Later in this chapter the terminology and parameters necessary to understand and conduct valid FEA analysis are described.

7.1.3 Dumbbell Tensile Test Correlations

A ¼ of a dumbbell tensile test specimen was modelled, as shown in Figure 7.1. The lower edge of the model was fixed to simulate the upper grip in the test machine. The upper edge was fixed in the direction parallel to the edge. Also deflected in the Y direction to simulate the upper grip moving.

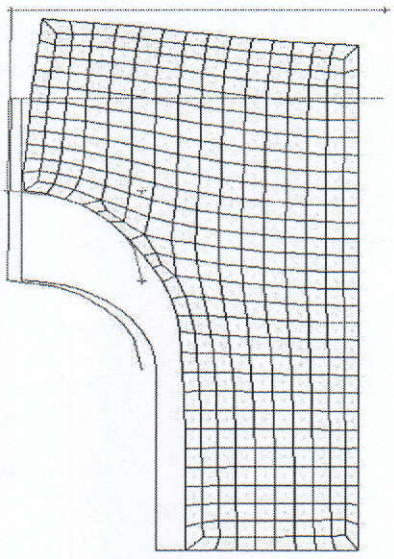

Figure 7.1 Dumbbell Test Specimen Modelled in MSC Marc FEA

7.1.4 Terminology

To understand FEA, several terms need to be defined and understood:

1. *Element*: The structure to be analysed is broken down into pieces called "elements ", which are usually quadrilaterals. When these elements are joined together they form a mesh that fully form the geometry of the component to be analysed.
2. *Node*: A "node" is a point at which the elements are joined. There is always a node at the corner of an element and some elements also have midside nodes which need to be specified.

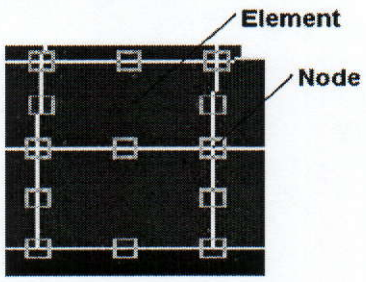

Figure 7.2 Mesh or Grid

3. DOF: Each has certain degrees of freedom (DOF). This means that the node is capable of moving in various directions, depending on the boundary conditions imposed on the node. These movements consist of displacements in three mutually perpendicular directions and rotation about these three axes for a total of six DOF.
4. Mesh or Grid: These two terms are used interchangeably and refer to joined elements that look like a "grid" or "mesh", as shown in Figure 7.4.
5. Boundary Conditions: The "boundary conditions" which describe the loading to be applied to the component, include deflections, pressures, forces, body forces, contacts, etc.

7.1.5 Types of FEA Model

Four types of FEA model can be constructed, depending on the component that needs to be analysed and the capabilities of the FEA program used.

The most common model is a two-dimensional (2D) cross section of the component with a rotational axis of symmetry this is also called an axisymmetric model. Other common models are plane strain and plane stress models. For a plane strain model it is assumed that out of plane displacement is constant over the entire model. A similar

model to the plane strain model is plane stress model. The plane stress model assumes out of plane stress to be constant over the entire model. The last model is a three-dimensional (3D) model. This model does not usually have a plane of symmetry or a continuous cross section. A 3D model is generally difficult to build and requires skill in interpreting the results.

7.1.6 Model Building

An accurate geometry can be achieved by using drawing packages like Auto-Cad or Rhino. The geometry can be transferred into the MSC MARC FEA software package. The initial step in solving a problem using FEA is to take the geometry of the component and break it down into an element mesh. Each node is located in a defined coordinate system and the nodes are connected to form the elements so a fine mesh can be modelled. Care must be taken to provide a sufficiently fine grid in areas with high strain gradients. These regions may be determined by experience, or by solving the FEA problem using an initial mesh to locate the high regions and refining the element mesh in these regions. They usually occur in discontinuities such as fillets and corners, and also in this case at the edge of the elastomer, near to the bond line.

7.1.7 Boundary Conditions

After the mesh is generated, the boundary conditions have to be applied. Applying the boundary conditions to elastomers is different than for metals, because of the elastomeric nature of the material.

The fixed boundary condition exists when the surface of the component is firmly fixed, attached to another component or to the ground. When the node is fixed, all of

the DOFs are set to equal zero and the node cannot move in any direction. Loading can be applied as a force or pressure. Forces are usually applied at nodes, while pressure is applied along a surface. In either case it is essential to consider the type of model being used and to specify the loading accordingly. A plane problem will usually require the loading to take into consideration the length and depth of the model. In an axisymmetric problem, the model cross section is assumed to be part of a 360^0 model. Therefore, the loading is specified per radian, per arc length, or force per unit area (pressure).

The loading can be applied as a deflection at the nodes or along the surface. If it is known how a surface moves, this is the simplest and most appropriate method of loading an elastomeric component. To apply a force or a pressure over a surface, it is necessary to know how the force or pressure is distributed.

7.1.8 Model Verification

After the mesh is generated it is important to verify:

1. that the component is correctly meshed,
2. that the nodes are joined correctly,
3. that the correct boundary conditions are applied at the correct locations,
4. that the correct material property is specified for each element.

7.1.9 Understanding Results

Stress contours, as determined by FEA, enable us to evaluate areas of low and high stress within a dumbbell or other elastomeric component. The areas with similar stresses are marked in FEA by the same colour. Each colour has a unique stress value

associated with it and is shown in the colour palette as shown in Figure 7.3. Positive stresses indicate regions of the specimen in tension and negative stresses depict compression.

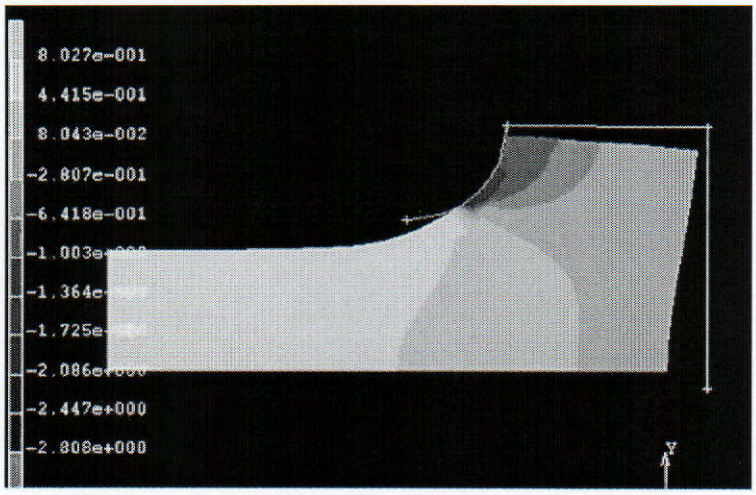

Figure 7.3 Nonlinear Finite Element Analysis of Rubber Dumbbell

Normally, data extracted from FEA solutions for steel or aluminium components are measurements of stress. This is because the stress level of a metal component can be readily compared with known failure theory stresses, yield stress or ultimate tensile stress. However a comparison and evaluation of FEA stress results from the analysis of elastomeric components can only be made if the specified elastomer material properties are characterised by strain energy function that represents the non-linear behaviour of the material.

7.2 Finite Element Axisymmetric Analysis

7.2.1 Modelling of EPDM Fatigue Test Axisymmetric Analyis

It is very important to appreciate the issue of accuracy when performing fatigue life calculations with Finite Element Analysis models. Small changes in load application,

load steps and boundary conditions as well as detailed modelling procedures such as mesh density, can have great influence on predicted stresses. Therefore, the FEA based calculations should only be undertaken when correlated against tests. In fact, even this is problematical because if the same test is carried out on two specimens, very different results can be obtained. Three underlying effects on fatigue life are:

i) Small changes in modelling practice can have considerable effects on fatigue life.

ii) Small changes in applied loading can cause substantial changes in fatigue life.

iii) In tests, components subjected to the same loading can experience substantial variations in fatigue life. So many tests are required nonetheless it is important to recognise that precise prediction of fatigue life is not feasible.

However there are underlying benefits of FEA based fatigue calculations, since ultimately expensive cycling testing of components is avoided.

Before any detailed practical work could be undertaken, the physical tests had to be conducted and evaluated. EPDM rubber dumbbell test specimens were coated in the laboratories of EI and brought to DIK for fatigue tests as described in detail in chapter 6, pp.98 & pp.103. After the tests were conducted, the results were analysed and the stress strain data of the first recorded cycle and the last recorded cycle were obtained. The model was created using the cycle by cycle method. Engineering stress / Engineering strain data was than calculated and the data was imported into the Curve fitting program in MSC MARC and its plausibility was investigated [69].

The two-term Ogden model was seen to provide a good fit as can be seen in Figure 7.4.

For this initial investigation, a model of the Dumbbell was created. In order to speed the analysis times only a quarter model was produced, with boundary conditions applied to he sample. Taking all factors into account, the standard run format summarised below was used and was adapted to all EPDM material models.

i) Grips separation 8.333 mm/s (500 mm/min),

ii) Full contribution of initial stress to stiffness,

iii) 50 incremental load steps,

iv) Analysis type: Axisymetric.

An indication of the quality of the various material models was given by comparing the FEA results with the test results. The comparison is shown in Table 7.1

Maximum Stress N/mm^2			
FEA			Test
A	B	C	D
3.624	2.138	3.674	2.853

Key: A) Three parameter Mooney- Rivlin, B) Yeoh, C) Two-term Ogden, D) Average from the test

Table 7.1 A Comparison of DLC Coated EPDM Rubber Maximum Stresses During the First Fatigue Cycle

Maximum Stress N/mm^2		
FEA		Test
A	B	C
1.358	2.538	2.78

Key: A) Yeoh, B) Two-term Ogden, C) Average from the test

Table 7.2 A Comparison of DLC Coated EPDM Rubber Maximum Stresses During the Last Fatigue Cycle

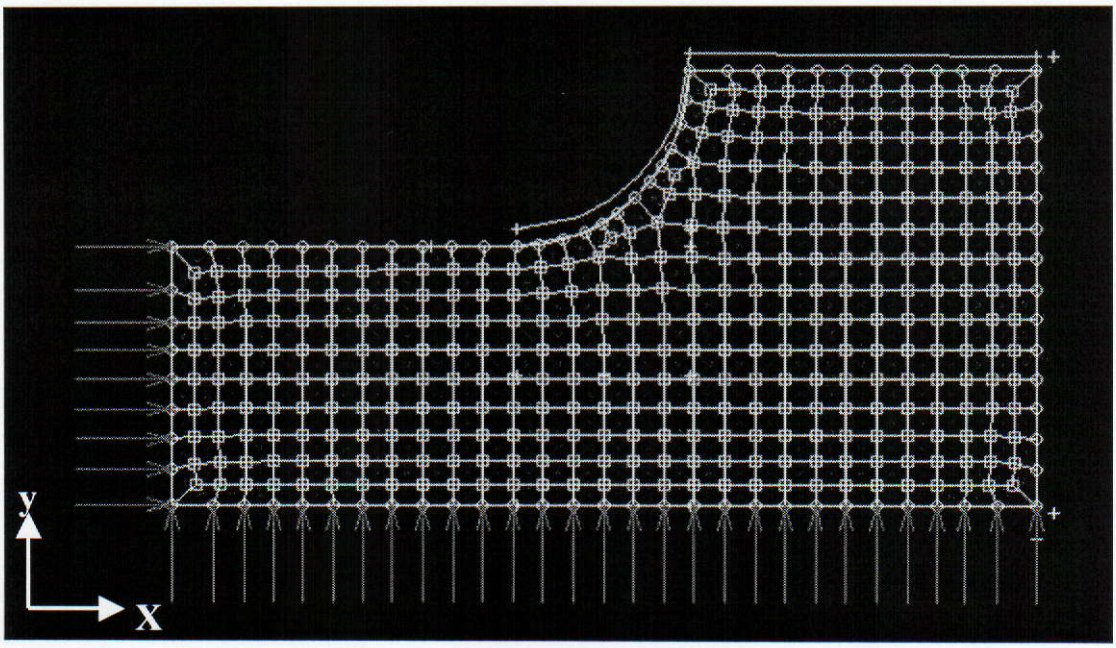

Figure 7.4 Standard FEA EPDM Rubber Mesh Including Boundary Conditions

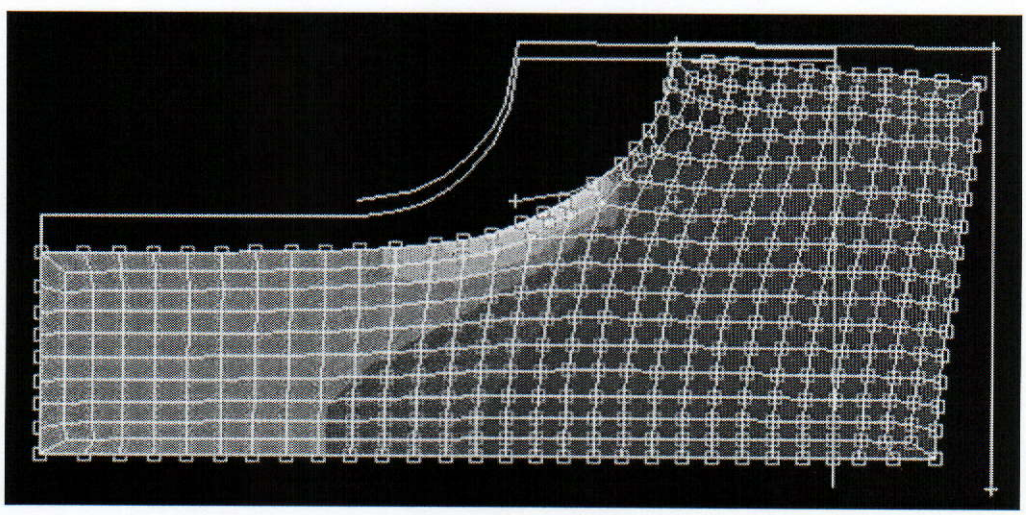

Figure 7.5 FEA of EPDM Rubber Axisymmetric Analysis showing Deformed Profile

From the results it can be seen that the axisymmetric FEA models produced reasonably accurate results when compared with the physical tests results, as can be seen in Tables 7.1-7.2. For the FE Analysis, the minimum loads were assumed to be zero, however the minimum loads in the fatigue tests differed from zero due to a tendency in the test process for the sample to go minimally into compression in each cycle. Abraham [70] highlighted that the fatigue life of elastomers, with or without preloading, can be predicted by measuring the dynamic stored energy or, for some non-strain crystallising rubbers, the dynamic total energy. The dynamic stored energy is given by the area below the hysteresis loop without considering the total energy of deformation in the cycle. This predictor is motivated by a consideration of applied stress and it works for both unfilled and filled EPDM and SBR with or without minimum loads in compression and tension. This new predictor allows for the simulation of the fatigue life of elastomeric components with higher precision.

7.2.2 Finite Element Analysis of SBR Axisymmetric Analysis of Stress at a Crack Tip

The second test was conducted to compare with an FEA plane strain model of EPDM rubber with a controlled crack. Dumbbell test specimens of SBR carbon black rubber with an initiated cut (slit) are used for this investigation. Uncut areas of specimens were now $A_1 = 99.35mm^2$ (3/4d) and $A_2 = 44.15\ mm^2$ (1/2d). Slits were made using a Lathe head-stock and a fine blade, which was mounted in to the tool holder of the Lathe. The slowest head rotational speed was used, 80RPM and the blade was fed in by hand. Each specimen was subjected to tensile stress with a minimum load of zero to failure. During the tests the load and extension properties were recorded. The

dimensions of the test specimens were the same as in the EPDM rubber fatigue test. The same model was used although different boundary conditions were applied. On the left hand side fixed displacement forces were not applied for the length of the initiated crack, as shown in Figure 7.6. No forces were applied at the crack in order that the properties of the crack could be simulated. Engineering stress / Engineering strain data from the tensile test were used to determine the best curve fit and hence the best material model. An indication of the quality of the various material models was given by comparing the FEA results between different plausible models. The comparison is shown in Table 7.3. For the SBR Carbon Black with a cross sectional area of 44.15 mm^2, the only plausible model was the one-term Ogden model. The one-term Ogden fit predicts that the stress at a tip of the crack is 23.91 N/mm^2 where the result from the uniaxial test nominal stress in section is 2.9 N/mm^2.

Maximum Stress N/mm^2		
FEA		Test
A	B	C
13.48	15.68	2.78

Key: A) Three parameter Mooney- Rivlin, B) Two-term Ogden, C) Nominal Stress in Section

Table 7.3 A Comparison of SBR Carbon Black with Initiated Crack with Cross Sectional Area of 99.35mm^2

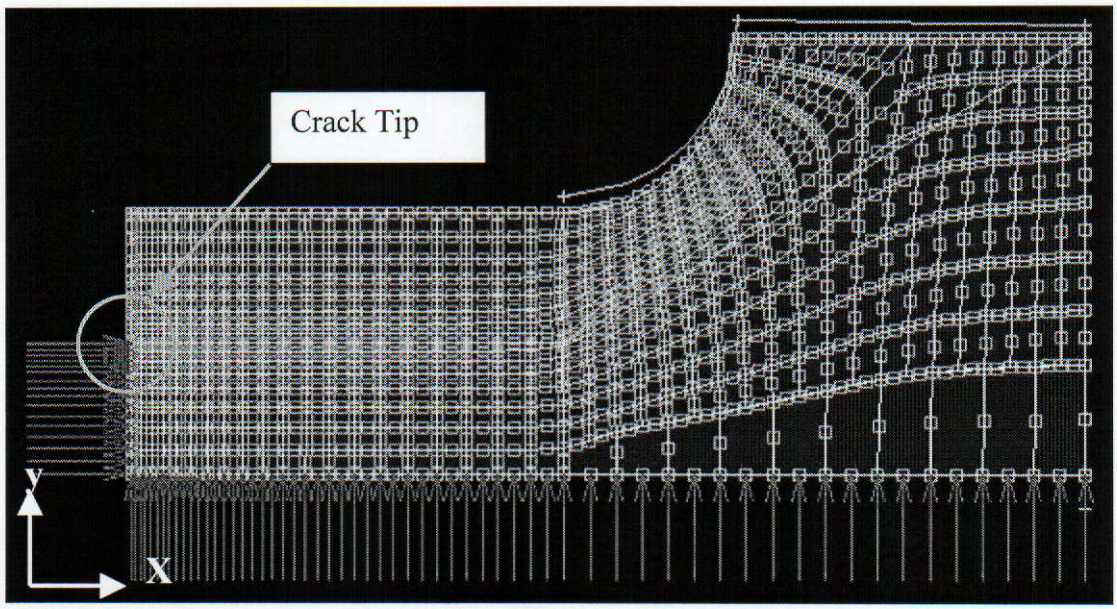

Figure 7.6 Standard FEA of EPDM Rubber with an Initiated Cut Mesh Including Boundary Conditions

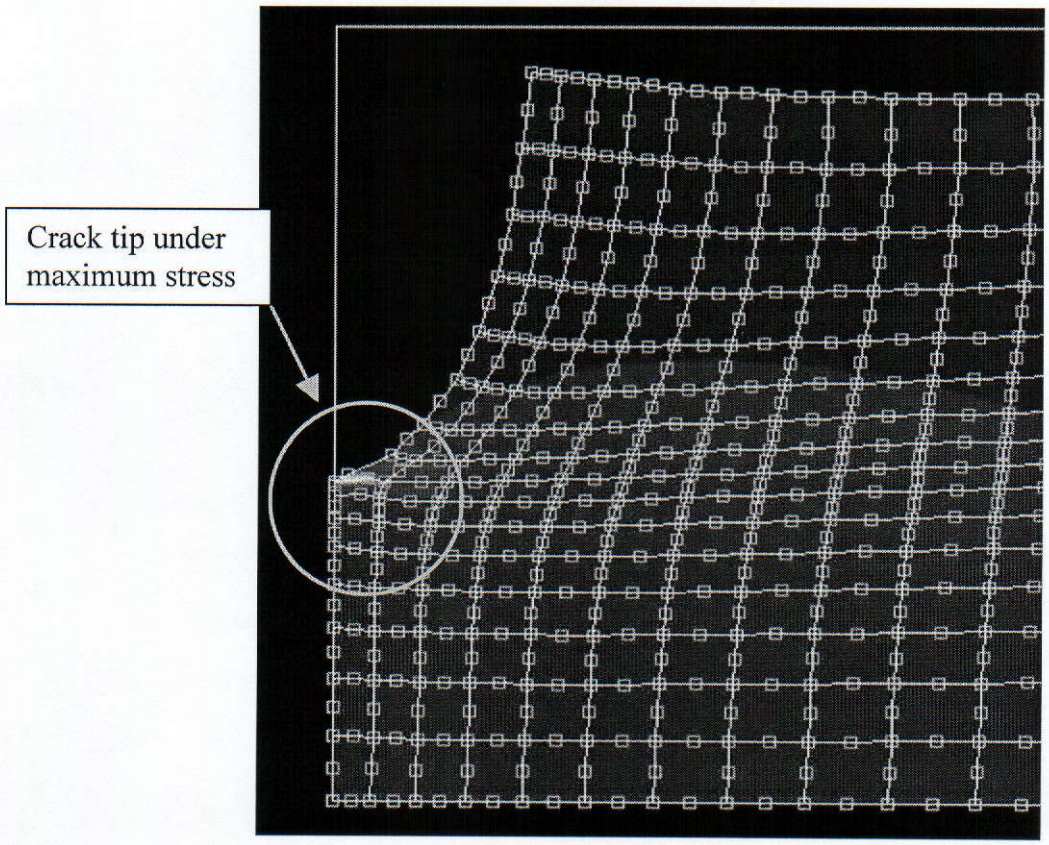

Figure 7.7 FEA of EPDM Rubber Axisymmetric Surface Crack showing Deformed Profile

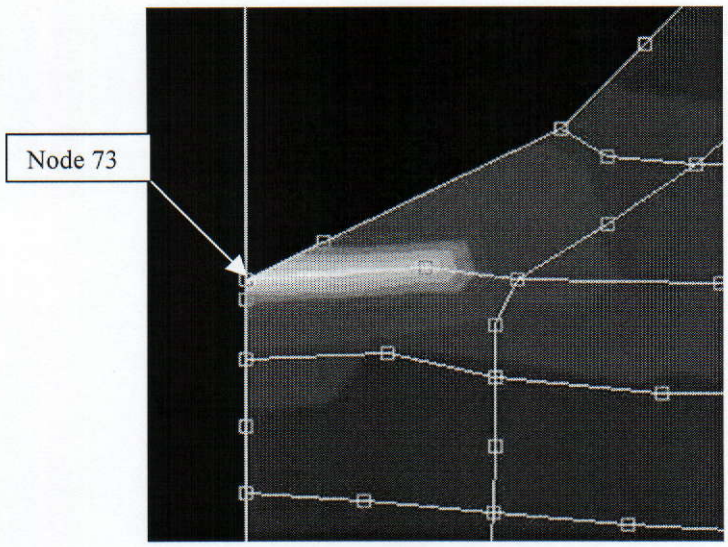

Figure 7.8 Adaptive Meshing in the Crack Vicinity

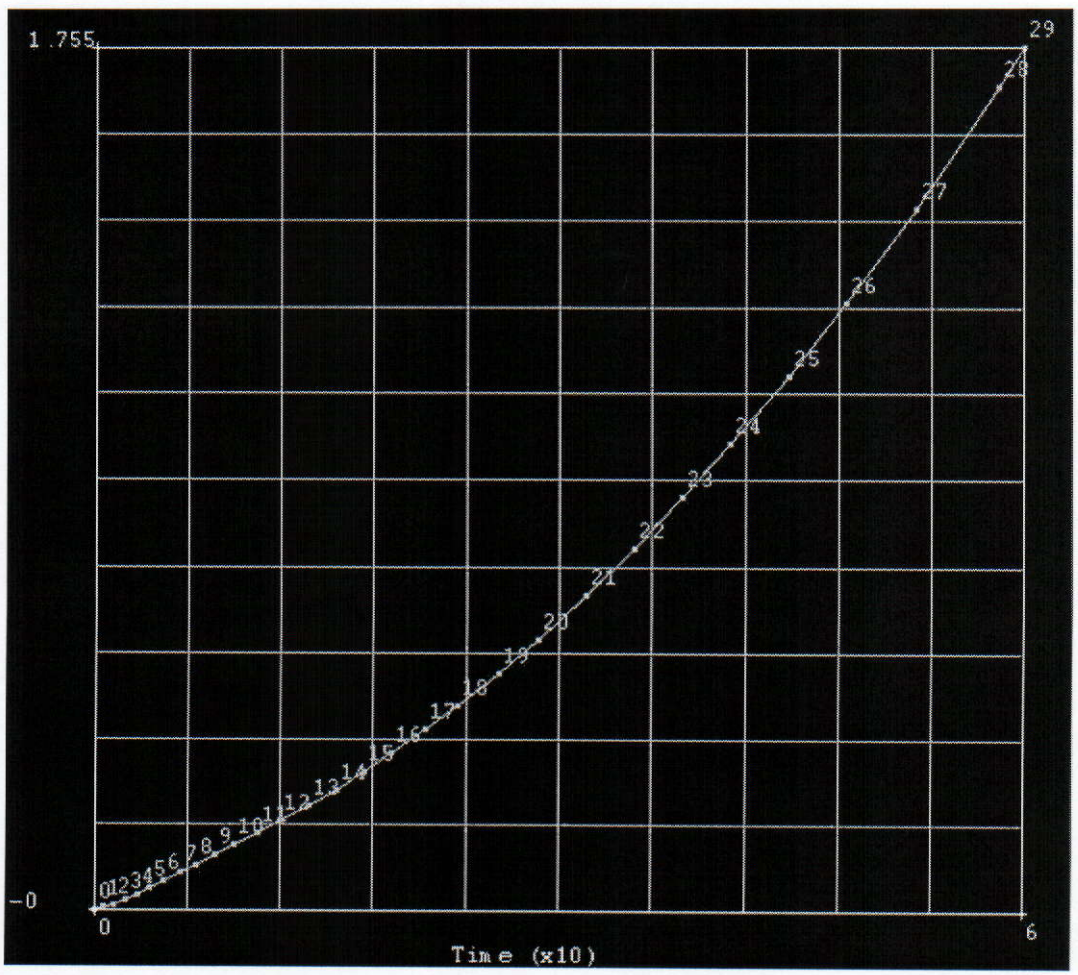

Figure 7.9 History Plot of Component 11 Cauchy Stress vs Time at Node 73

The Axisymmetric FEA model results of a controlled crack showed substantial difference between the nominal stress and the stress at the crack tip. This can be explained by Griffith's theory of crack propagation [32]. The relief of strain energy in a crack would be expected to be proportional to the square of the crack length, or crack depth. Therefore, a crack 2 mm deep releases four times the strain energy as a crack of 1 mm deep. The only drawback with the use of MSC MARC FEA modelling of crack behaviour during tensile tests, is that crack propagation through the model cannot be simulated. This is a problem when using FEA modelling of a crack, which should be taken into consideration in further research.

7.3 Finite Element Plain Strain Analysis

7.3.3 Finite Element Analysis of Plane Strain Surface Flaw

The third test is to model the stress in an EPDM surface flaw using a plane strain option in FEA. The first step in this analysis was to create a model of the surface flaw using the Rhino drawing package [71]. This was later imported into MSC Marc FEA software package, see Figure 7.10. A problem arose with the meshing because the software could not join two entities together. It would mesh them separately, as shown in Figure 7.11. As a result, an alternative approach was taken which involved modelling the simple plane strain model with a quarter of the 60 μm diameter flaw as shown in Figure 7.12.

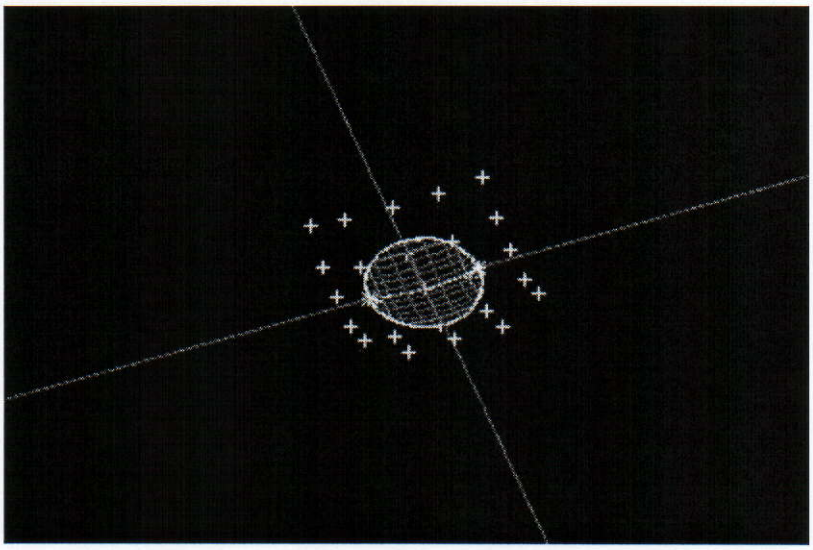

Figure 7.10 Geometries of Flaw of 60μm in Diameter

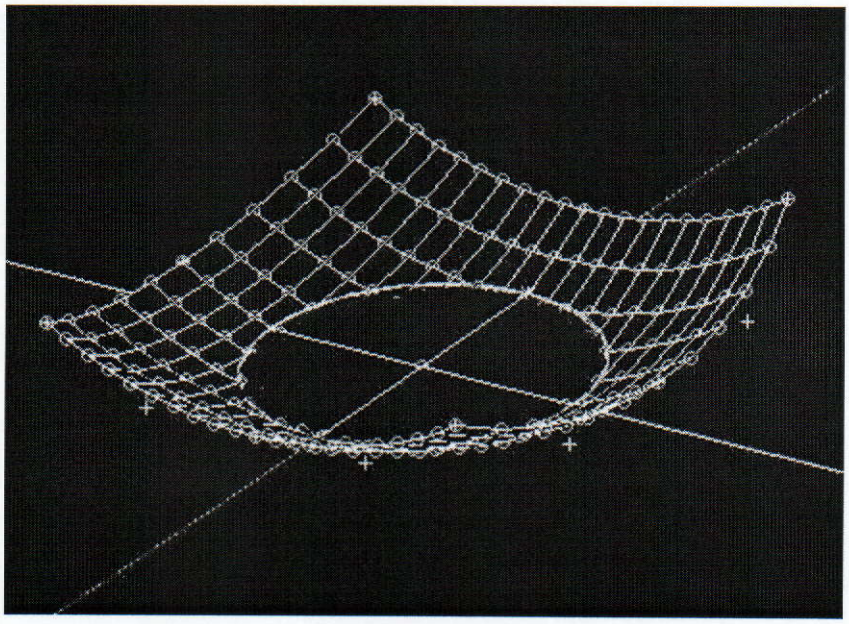

Figure 7.11 Flaw Mesh

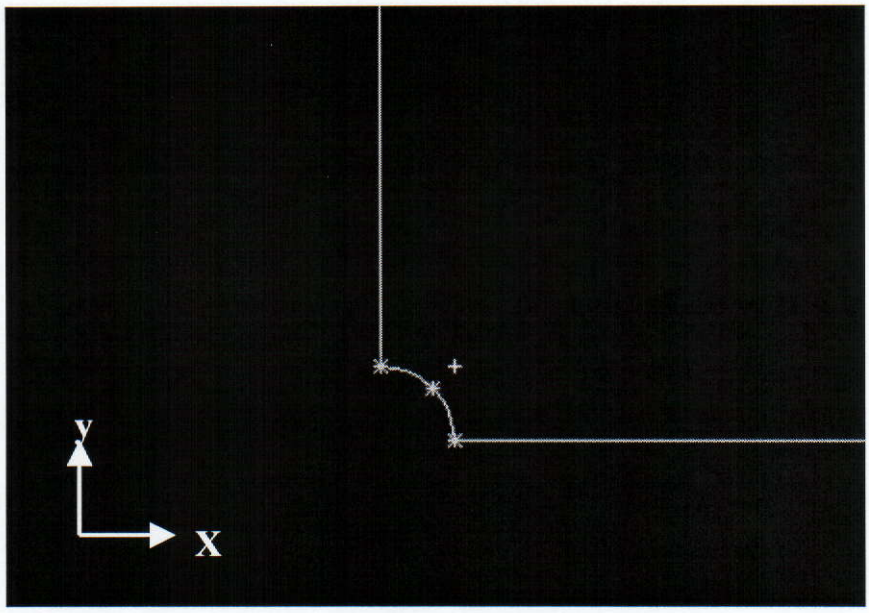

Figure 7.12 Standard Plane Strain EPDM Rubber with a ¼ of Flaw 60μm in Diameter

7.3.3.1 Modelling of EPDM flaw plane strain analysis

An attempt to determine the stresses at geometries of a small flaw was made. An alternative material model was used to represent the deformation of the EPDM rubber strip. The stress/strain data was determined from the uniaxial tensile test data previously conducted in DIT laboratories with the use of Lloyds LR30k extensometer. The uniaxial test separation speed was 500mm/min. Initially the Mooney-Rivlin 2 term, the Mooney-Rivlin 3 term and Yeoh models were applied. However after a plausibility check [69] they were considered unacceptable, the results are shown in Appendix B.3, pp.189. The Ogden 2-term model was a plausible curve fit, as shown in Figure 7.13 and the constants used in this material model were:

i) $\mu_1 = 0.347457\ N/mm^2$, $\alpha_1 = 2.32607$

ii) $\mu_2 = -0.212956 \times 10^{-5}\ N/mm^2$, $\alpha_2 = -4.53000$

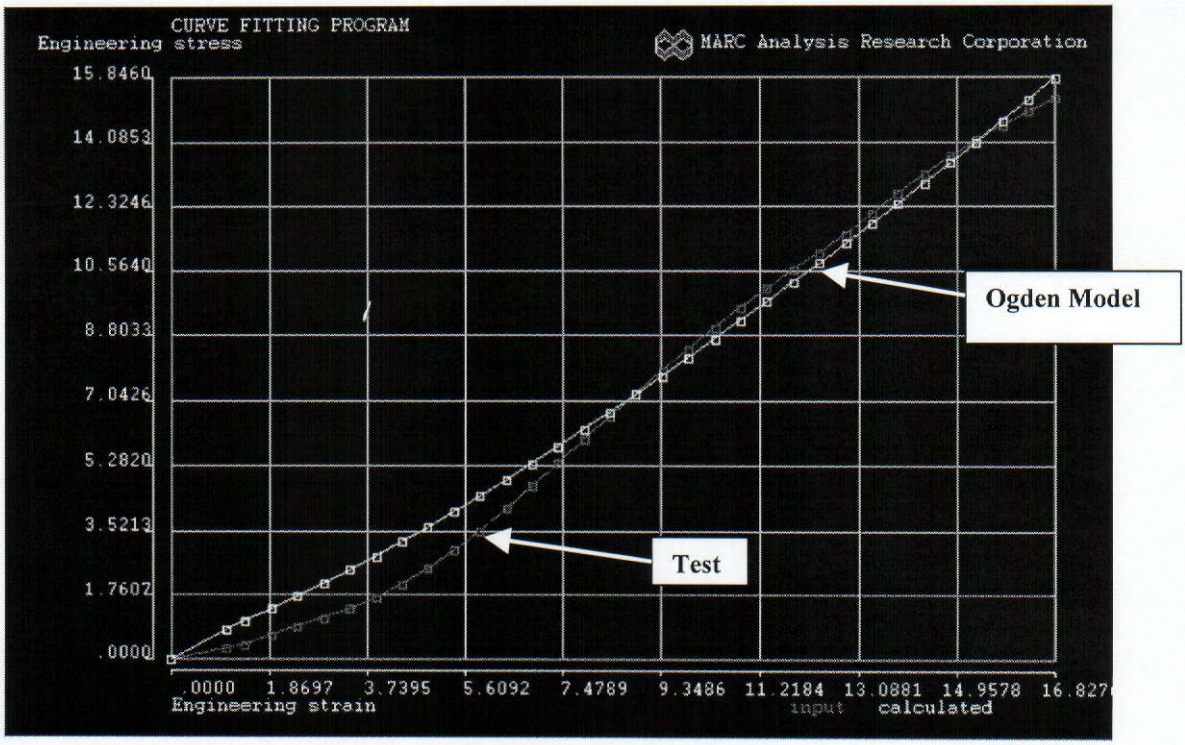

Figure 7.13 EPDM Rubber Ogden Model Curve Fit

The standard run format for the EPDM model containing a flaw was:

i) Grips separation 8.33 mm/s (500mm/min)

ii) Adaptive load steps criteria,

iii) Analysis type: Plan Strain.

The deformed shape of the flaw is shown in Figure 7.14. The model showed that maximum concentration of stress is at the root of the flaw in the model marked as node 2 with maximum stress of 4.11 N/mm^2, as shown in Figure 7.15. It should be taken into consideration that this is a quarter model and therefore the maximum stress for a full model is 16.44 N/mm^2, nominal stress of uniaxial test of EPDM rubber was 15.4 N/mm^2, which appears to be a very accurate result. Using these two results, stress concentration at the flaw was calculated k_t = 1.067, whereas stress

concentration test result showed that k_t = 1.83 when the rubber is pre-stretched to three times its gauge length, as shown in Table 5.10, pp. 90.

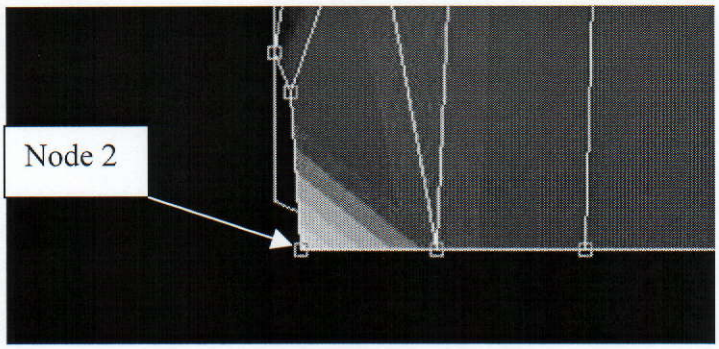

Figure 7.14 Deformed Shape of Flaw

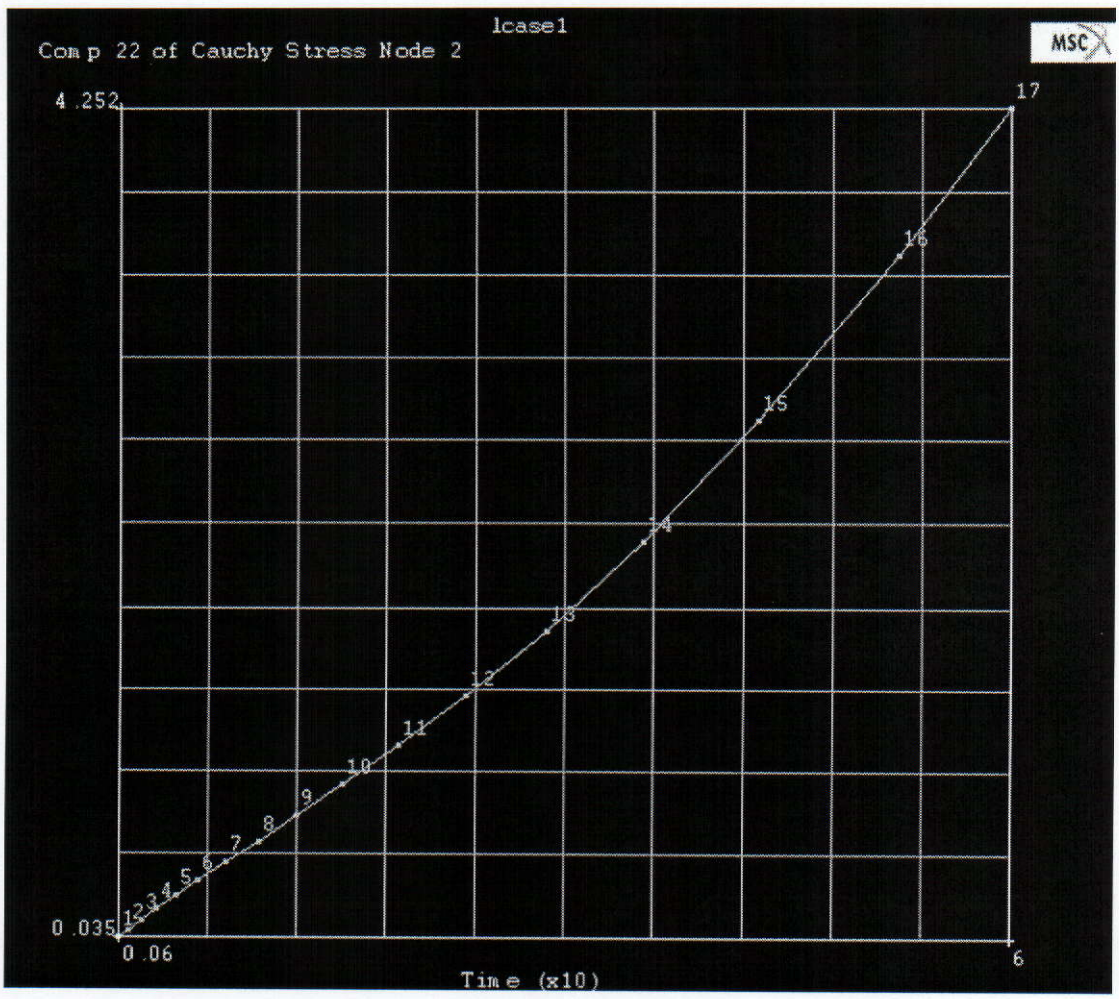

Figure 7.15 History Plot of Component 22 Cauchy Stress vs Time at Node 2

With the FE Plane Strain model of a flaw in EPDM rubber it was possible to accurately simulate the Uniaxial tensile test. The Ogden formula can be considered to give a reasonably accurate model of the test. In the future, further emphasis should be given to the creation of appropriate material models.

Chapter 8

Discussions

In strain crystallising rubbers (NR) under cyclic loading, a crystalline region develops at the crack tip and crystallinity remains intact for repeated load applications where the loads are not fully removed which consequently inhibit crack growth. Fatigue life increases in this situation. However, non-crystallising rubbers (EPDM) are not subject to this phenomenon. Many Experts in rubber technology believe that increasing the minimum stress will not improve the fatigue life of non-strain crystallising rubbers. Abraham's work [3-6] proved otherwise. Abraham ascertained that an increase in the minimum stress applied to non-strain crystallising rubbers resulted in substantial improvements in fatigue life. Therefore the central research question in this project is: *"Whether the improvement of surface finish and reduction of the stress concentration at surface defects produced by a manufacturing process of a rubber component relate to the improved fatigue life of the rubber component when subjected to pre-loading?"*

The following were the methods used to profile the rubber surface:

First of all the Taylor-Hobson Tallysurf was used to profile the surface of the Natural Rubber (NR). The surface of EPDM is very soft and, during the Talysurf testing, the probe scraped the surface of the EPDM. Therefore the results obtained using the Talysurf were not reliable. On the basis of this research finding, it is recommended that non-contact surface methods, such as 'white-light interferometry', be employed for testing EPDM rubber.

Accordingly, different non-contact methods were used to represent the profile of the surface of EPDM rubber. They were:

i) the Olympus BX60M System Microscope

ii) the Olympus BX60M System Microscope in combination with the Omnimet Archive Digital Imaging System (86-4000)

ii) White Light Interferometry (WLI)

iv) Electronic Speckle Pattern Interferometry (ESPI).

The Olympus BX60M System Microscope was used in combination with the Omnimet Archive Digital Imaging System this method had shown good results. However there was one draw back to this method which was that a special test rig for pre-stressing rubber had to be designed and incorporated into its systems as was the case with WLI.

The White Light Interferometry gave a complete profile of the rubber surface, as shown in Figures 5.3, 5.6 and 5.7. However this technique is limited as it has a small field of view (260.51μm x197.27μm).

The ESPI method has previously shown positive results in measuring the crack propagation and delamination of metals [8]. However, due to its high sensitivity to background noise, it was not possible to obtain accurate readings using this method for rubber. The ESPI system was not able to focus on the small defects in the rubber surface, eg. a surface flaw of 60μm in diameter. Unfortunately, it must be concluded that this method is not a suitable method for measuring surface displacement or the surface finish of rubber.

The White Light Interferometer produced the best results for measuring the surface roughness and profiling the geometries of surface defects. In this research, it was hoped that the ultrasonic technique could be used to measure surface roughness and detect any defects that occur on the body of rubber specimen or on the surface of the rubber specimen during the vulcanisation process. The advantage of this method is that defects inside the specimen could be detected [48-50]. Unfortunately this method was not tested because the equipment was not available for the project and a whole system would have to be built. However, as this method showed promise, a proposed Non-contact Ultrasonic Analysis System was outlined for a future research project in Figure 4.19.

The loaded NR and EPDM rubber components that were produced by conventional modelling methods contain surface defects that increase the stress and contribute to fatigue failure. The surface finish of NR and EPDM rubber improves with increases in tensile strain. In fatigue, higher stress levels in the pre-stressed (pre-strained) material are partially compensated for by such improvements in surface finish.
The tests show that stress concentration diminishes with strain, as can be seen from Tables 5.7-5.11. Irrespective of the notch sensitivity of the material, dynamic stress concentration (k_f) will diminish with a reduction in static stress concentration (k_t). Again, higher mean stress in a fatigue cycle is in a part redressed by lower stress concentration.

Rubber Surface treatments for the improvement of the physical properties of rubber were also investigated. This investigation included the use of Diamond Like Carbon

Coating for coating EPDM rubber samples and Sol-gel coating and Shot peening technology were also used.

The test results showed that any of these coatings or treatments are not suitable for the improvement of the fatigue life of rubber materials. It is possible that the high temperatures required in the coating procedure altered the properties of the material. Sol-gel technology offers the possibility of controlling the thickness of the coating, but the coating material did not give desired reaction with the parent material. On the other hand, more brittle diamond like carbon coatings gave a better reaction, but the thickness and dispersion of the coating material over the surface was poor. It is recommended that further physical fatigue tests on the DLC coated samples be conducted as, to date, only one set of results has been obtained and only one procedure used.

EPDM rubber did not show any change in its tensile properties after being submitted to a Shot Peening treatment. As rubber is a self-recovery material, this treatment shows no significant improvements in physical properties. The Microscopic analysis showed improvements in surface roughness (R_a), as shown in Table 6.2 and it may be that improved surface finish will load to higher fatigue lives. Further tests would be required before this treatment could be accepted or rejected as a valid rubber material treatment. This treatment for rubber material should also be tested for adhesion and wear resistance as well as fatigue resistance.

The FEA fatigue results showed reasonably accurate values of the maximum stress in the component when compared with other test results, as depicted in Tables 7.1-7.2. The tables show that the fatigue test results slightly differ from the FEA results. Abraham highlighted that the fatigue life of elastomers, with or without preloading,

can be predicted by relating life to dynamic stored energy or in some cases dynamic total energy criterion [70].

This predictor is physically motivated and it works for both unfilled and filled EPDM and SBR with minimum loads in compression, tension and zero. It also is applicable to tests with amplitude variations. This new predictor allows the simulation of the fatigue life of elastomeric components with higher precision. This is important because, in service, minimum loads often differ from zero.

The Axisymmetric FEA of stress at the crack tip predicted high stress as this is explained by the Griffith theory of crack propagation [32]. The relief of strain energy in a crack would be expected to be proportional to the square of the crack length, or crack depth. Therefore a crack of 2 mm deep releases four times as much strain energy as a crack of 1 mm deep. The Axisymmetric FEA is a good method for modelling the behaviour of a controlled crack.

Modelling the behaviour of a flaw in the EPDM rubber using a plane strain option in FE also showed very good results. Likewise, the tests showed that the Ogden formula can be considered to give a reasonably accurate representation of the test.

In future research, an emphasis should be placed on the creation of appropriate plausible material models.

Chapter 9

Conclusions and Recommendations for Future Work

The initial objectives of the research were:

i) to assess surface finish measurements and to investigate the changes in stress concentration in preloaded rubber samples using White Light Interferometry,

ii) to consider other non-contact methods of observing changes in stress concentration in preloaded samples through use of: i) the Electronic Speckle Pattern Interferometry (ESPI) method, ii) the Ultrasonic method,

iii) to examine whether coatings or other surface treatments can play a part in diminishing the surface flaws produced in the manufacturing process using i) Diamond Like Carbon Coating (DLC), ii) Sol-gel Coating Technology and iii) Surface Peening treatments,

iv) to use MSC MARC Non-linear Finite Element software to model: i) fatigue behaviour of DLC coated EPDM rubber, ii)EPDM rubber elastomeric crack propagation, iii) flaw behaviour in EPDM rubber,

v) to advise on design standards for pre loaded rubber components and to establish criteria for selecting elastomers that will minimise the likelyhood of fatigue failures in the light of Abraham's research and of this study.

9.1 Conclusions

White Light Interferometery is the best metrology method considered for measuring surface roughness and profiling the geometries of surface defects in rubber materials.

This research has shown that the tensile loading of elastomers reduces the severity of defects produced during the manufacturing process. Surface defects, such as flaws of approximately 60 μm in diameter and 5 μm in depth are considered as a sharp edge cut. If a tensile load "smoothes out" stress concentration, it could be argued that stress cycles become less injurious. The higher mean stress in a fatigue cycle is in a part redressed by lower stress concentration. Abraham's ascertation that the fatigue life in preloaded elastomers is related to the available dynamic strain energy is supported by this research. It is at the same time reasonable to conclude that crack propagation in non-strain crystallising rubbers is partially inhibited in preloaded elastomers due to improvements in the Surface Roughness and reduction in stress concentration.

From the results shown in Figures 6.5-6.9, it can be concluded that DLC and also Sol-gel coating are not suitable for the treatment of rubber materials. The procedures do not improve the physical properties of the rubber material and are not economically viable. It is clear that coating treatments on rubber materials do not have the same effect on fatigue properties as for metals. Without further testing and considering other processes, which would require additional funding and the availability of equipment, these conclusions can only be considered preliminary.

Improvement in surface finish of an elastomer can be represented by a formula having the form

$$R_{as} = R_{ao} (1 - Cl_n \lambda)$$

Where:

R_{as} = surface finish at stretch ratio λ (μm)

R_{ao} = surface finish of unstrained rubber (μm)

C = a material dependent constant (no units).

The shot peening treatment, using the metrology method, showed an improvement in surface roughness (R_a), as can be seen in Table 6.2. It might be possible to establish whether a correlation between measured surface finish and fatigue life exists. This treatment for rubber material should also be tested for adhesion and wear resistance as well as fatigue properties.

During the fatigue test of EPDM rubber DLC, coated and uncoated, the stiffness of the material and loss factor (tan δ) decreased, as shown in Figure 6.6. The test showed that tested rubber samples failed when the complex modulus E* attained the value approximately 76% of the initial complex modulus, as shown in Figure 6.9. The loss in the modulus could be used as a predictor of failure of a rubber component. When the value of the complex modulus and value of the material stiffness is known, it is possible for the maintenance to exchange elastomeric component prior to its failure.

FE Axisymmetric and Plane Strain Analysis are efficient and economically viable methods for predicting the properties of a rubber specimen. For the Fatigue FEA, Abraham's prediction method would allow the simulation of the fatigue life of

elastomeric components with higher precision. This is important because in service minimum loads often differ from zero.

In using FE Axisymmetric and Plane Strain Analysis of stress in rubber models, future emphasis should be placed on creating appropriate plausible material models.

9.2 Recommendations for Future Work

1. An Elastomeric Fatigue Testing Machine must be available for any future work to be performed,

2. A test rig that in combination with WLI will be able to perform a profiling of the surface roughness and the geometries of the flaws in elastomers should be designed and built,

3. It should be established whether the correlation between measured surface finish and fatigue life exists after shot peening rubber surface treatment,

4. Abraham's prediction method, of the dynamic stored energy or the dynamic total energy for some types of non-crystallising rubbers should be incorporated into non-linear Finite Element Analysis software,

5. Crack propagation from fluids in multi-axial fatigue should be investigated using the bubble inflation method, under development by Murphy *et al.* [72].

However many of the findings are found to be positive, additional research is required to draw firm conclusions. These are preliminary findings.

Master research problems are found to be: time, finance, equipment and support.

It was necessary to link with different institutions to enable research to progress at all. The first and main challenge throughout the project was to obtain testing equipment and test material. This represented the biggest challenge throughout. The creation of links with different institutions partially solved the problem. The Deutsches Institut für Kautschuktechnologie (DIK) was of great help to the project by providing the testing material and allowing the use of its fatigue testing equipment and the equipment for the rubber vulcanisation process. However throughout the project, securing material and equipment was a constant difficulty. At various stages, testing was limited to available equipment and material.

Regrettably these problems limited the scope and depth of the research.

All of the different results and findings of this research project should be noted as design recommendations to increase the service life of the rubber products.

References

1. A. N. Gent, P.B. Lindley, A. G. Thomas, " Cut Growth and Fatigue of Rubbers Part 1: The Relationship Between Cut Growth and Fatigue", Journal of Applied Science, volume 8; 1964: pp. 455
2. R.S. Rivlin, A. G. Thomas, "Rupture of Rubber. I. Characteristic Energy of Tearing", Journal of Polymer Science, Volume 10, No. 3; 1953, pp291
3. F. Abraham, T. Alshuth, S. Jerrams, "Ermüdungsbeständigkeit von Elastomeren - Einfluss der Spannungsamplitude und der Unterspannung", KGK Kautschuk Gummi Kunststoffe, Nr. 12/2001, volume 54; 2001: pp643
4. F. Abraham, T. Alshuth and S. Jerrams, "The Dependence on Mean Stress and Stress Amplitude of the Fatigue Life of EPDM Elastomers", Plastics, Rubber and Composites, Vol. 30, No. 9; 2001: pp. 421
5. F. Abraham, T. Alshuth, S. Jerrams, "Ermüdungsbeständigkeit von Elastomeren - Einfluss der Spannungsamplitude und der Unterspannung Teil 2", KGK Kautschuk Gummi Kunststoffe, Nr. 12/2002, 55; 2002: pp 674
6. T. Alshuth, F. Abraham, S. Jerrams, "Parameter Dependence of the Fatigue Properties of Elastomer Products", Rubber Chemistry and Technology, No.4, Vol. 75; 2002: pp. 635
7. S. Jerrams, A. Tabaković, "The Influence of Fatigue Properties of NR", Paper for Birmingham Elastomer Symposium, June 2001
8. E. Mihaylova, "Application of ESPI and Moirė Interferometry to detection of crack and delaminations", Paper for Dublin Institute of Technology International Conference of Material Tribology MT2002
9. M. C. Bhardway, I. Neeson, L. Vandervale, "Ultrasonic analysis of plastics and composites by non-contact analyser the NCA 1000"

10 R. Johannknecht, S. Jerrams, G. Clauss, "The uncertainity of implementing Curve-fitting Procedure in FE Software" in D. Boast, V. A. Coveney, Finite Element Analysis of Elastomers; 1999: pp.141

11 D.L. Herz Jr., "Introduction" in A.N. Gent, Engineering with Rubber – How to Design Rubber Components; 2000, pp.2

12 A.N. Gent, "Elasticity" in A.N. Gent, Engineering with Rubber – How to Design Rubber Components; 2000, pp.37-70

13 A. Stevenson, R. Campion, "Durability" in A.N. Gent, Engineering with Rubber – How to Design Rubber Components; 2000, pp.177-222

14 P.B. Lindley, "Engineering Design with Natural Rubber" in K.N.G.Fuller, A.H. Muhr, N R Technical Bulletin, The Malaysian Rubber Producers – Research Association, 1992, pp.16

15 P.B. Lindley, "Engineering Design with Natural Rubber" in K.N.G.Fuller, A.H. Muhr, N R Technical Bulletin, The Malaysian Rubber Producers – Research Association, 1992, pp.5

16 S.J. Jerrams, "Notes from Non-linear Material Work Shop", Dublin Institute of Technology; 09 October 2002

17 A.N. Gent, K.W. Scott "Dynamic Mechanical Properties" in A.N. Gent, Engineering with Rubber – How to Design Rubber Components; 2000, pp.74-78

18 A. Stevenson, R. Campion, "Durability" in A.N. Gent, Engineering with Rubber – How to Design Rubber Components; 2000, pp.180-184

19 R.H. Finney, "Finite Element Analysis" in A.N. Gent, Engineering with Rubber – How to Design Rubber Components; 2000, pp.265-273

20 R. Browm, "Physical Testing of Rubber", Chapnan &Hall, Third edition; 1996, pp. 98-105

21 J.S. Dick, "Vulcanizate Physical Properties, Preformance Characteristics and Testing" in J.S. Dick, Rubber Technology – Compounding and Testing for Performance; 2001, pp.47-48

22 J.L. Brass, "Introduction to Rubber", Maclaren and Sons LTD. London; 1968, pp.47-48

23 Trelour, R.L.G., "The physics of rubber elasticity", Clarendon Press, 3rd edition; 1975, pp.6-8

24 O. Kramer, S. Hvidt, D.F. John, "Dynnamic Mechanical Properties", Science and Technology of Rubber, 1994; 2nd edition, pp. 222-225

25 W.V. Mars, A. Fatemi, "Aliterature Survey on fatigue analysis approaches for rubber", International Jurnal of Fatigue, 2001; 24: pp949-961

26 T. Alshuth, F. Abraham and S.J. Jerrams, "Parameter Dependence and Prediction of Fatigue Properties of Elastomer Products" Presented at a meeting of the Rubber Division, American Chemical Society, October 2001, Cleveland, Ohio, USA

27 M.D. Ellul, "Mechannichal Fatigue" in A.N. Gent, Engineering with Rubber – How to Design Rubber Components; 2000, pp.144

28 U. Eisele, S. Kelbach, H.W. Engels, "The Tear Analyser – A New Tool for Quantitative Measurements of the Dynamic Crack Growth of Elastomers", Kautschuk + Gummi Kunstoffe 45, Jahrgang. Nr. 12/92, pp1064 – 1068

29 Kelbh, St., "Predictiv Testing of Elastomers", presented at the conference: "Bruchmechanik und Lebensdauer von Elastomeren", DIK, Hannover, March 2002

30 R. W. Hertzberg, J.A. Manson,"Fatigue of Engineering plastics", 1980, pp. 1-4

31 C.E. Inglis, "Stress in Plate due to the presence of Cracks and Sharp Corners", Transactions of the Institute of Naval Architects,1913; 5: pp219-241

32 Griffith, A.A., "The phenomena of rupture and flow in solids ", Philosophical Transaction of the Royal Society of London, Series A, 1920; 221: pp163-198

33 R.S. Rivlin, A.G. Thomas, "Rupture of Rubber I Characteristic Energy of Tearing", Journal of Polymer Science; 1953, pp. 291-318

34 R.S. Rivlin, A.G. Thomas, "Rupture of Rubber II The Strain Concentration at an Inclusion", Journal of Polymer Science; 1955, pp. 177-188

35 R.S. Rivlin, A.G. Thomas, "Rupture of Rubber. V. Cut growth in Natural Rubber Vulcanisates", Journal of Polymer Science 1958; 31: pp. 467-480

36 G.J. Lake, "Fatigue and fracture of Elastomers", Rubber Chemistry and Technology, 1995; 68: pp. 435 - 460

37 A.H. Muhr, "Properties of rubber Compounds for Engineering Applications", Reprint from of Natural Rubber Research, 1992; 7: pp14-36

38 G.Clauβ, "Lebendauer und Ermüdung von Elastomer", DIK Fortbildungs seminar, Hannover 8-9 July, 1999

39 G.R. Hamed, "Materials and Compounds" in A.N. Gent, Engineering with Rubber – How to Design Rubber Components; 2000, pp.30-31

40 ISO 4661: Part 1, 1993, Preparation of Samples and Test Pieces, Physical Tests

41 L. Smith, L. Henessy, "Engineering Technology", The Educational Company Ireland, 1996

42 B. Bowe, "Development and Optimisation of Optical Interferometric Techniques for Surface Metrology", Unpublished DPhil Thesis done in Dublin Institute of Technology but submitted to Trinity College Dublin, June 1999

43 http://www.tcd.ie/CMA/html/new_view_100.html, 14/03/2002

44 http://phase-shift.com/microxam.shtml, 22/10/2002

45 Manual for Omnimet Archive Digital Imaging System

46 J.N. Butters, J.A. Leendertz, Journal of Measurement and Control; 1971, pp.344-350

47 J. Gryzagoiridis, "Fundamentals of Holographic Interferometry, Electron Speckle Pattern Interferometry (ESPI) and Shearography"

48 Mahesh C. Bhardway, I. Neeson, L. Vandervalk, "Ultrasonic analysis of plastics, rubber and composites by non contact analyser the NCA 1000", Aircraft Engineering and Aerospace Technology International Jurnal, Volume 7, Number 1, 1999, pp39-41

49 K. Jeongguk, P. K. Liaw, "The Nondestructive Evaluation of Advanced Ceramics and Ceramic-Matrix Composites", JOM, Volume 50, No. 11, pp1-14

50 S. I. Rokhlin, J. Y. Kim, "In situ ultrasonic monitoring of surface fatigue crack initiation and growth from surface cavity", International Journal of Fatigue, Volume 25, 2003, pp.41-49

51 K.H. Schwalbe, "Bruchmechanik metallischer Werkstoffe", Carl Hanser Verlag , 1980

52 J.W. Bergmann, R. Heidenreich, H. Bügler, W. Oberparleiter, "IABG" Bericht B-TF-2355, 1988

53 A. N. Gent, "Strength of Elastomers", Science and Technology of Rubber, Second edition, Academic Press Inc.,1994, pp 474-475

54 http://www.brunel.ac.uk/faculty/tech/systems/groups/dlcc/, 19/10/2001

55 M. Atik, M.A. Aegerter, Journal of Non-Crystallising solids, 1992, pp.813-815.

56 A. Kawashima et al, Journal of Material science, 1994; 43, pp.854-859

57 M. Affatigato, D. Osborne, R.F. Haglund, Journal of Non-Crystallising Solids, 1995; 181, pp.27-38

58 W. Beier, Older, Material Research Society Symposium, Pittsburg, 1990; 180, pp.467-472.

59 S.R. Holmes-Farley, L.C. Yanyo, Journal of Adhesion Science Technology, 1991; 5, pp.131-151

60 B. Enright, "Research and development of the Sol-Gel Coating Process", Unpublished Final Year Thesis, Dublin Institute of Technology, June 2000

61 http//www.mts.com/menusys.asp?datasource=0&nodelD=1064, 22/05/2003

62 R. Seldėn, "Fracture Mechanics Analysis of Rubber Fatigue – a review", Progress in Rubber and Plastic Technology, Volume 11, No. 1, The Institute of Matrials/ RAPRA, 1995

63 L. Mullins, "Rubber Chemistry and Technology", 1969; 42, pp339.

64 F. Abraham, T. Alshuth, S. J. Jerrams, "The dependence on Minimum Stress and Stress Amplitude of the Fatigue Life of Non Strain Crystallising Elastomers" The International Rubber Conference (IRC2001), Birmingham (2001), Bruchmechanik und Lebensdauer von Elastomeren, Hannover, Germany (2002)

65 D.W. Nicholson, N.W. Nelson, "Finite-element analysis in design with rubber", Rubber Chemistry and Technology, 1990; 63, pp368-406

66 "Nonlinear finiete element analysis of elastomers", MSC Software Corporation, www.mscsoftware.com

67 K. N. Morman, T.Y. Pan, "Application of finite element analysis in the design of automotive elastomeric components", Rubber Chemistry and Technology, 1988; 61: pp.503-533

68 R.F. Finney, "Finite Element Analysis"; pp.239-277

69 R Johannknecht, S Jerrams and G Clauss "The uncertainty of Implementing Curve-Fitting Procedures in Finite Element Software" in D. Boast, V. A. Coveney, Finite Element Analysis of Elastomers, Professional Engineering Publishing, 1999; pp.141-151

70 F. Abraham, "The Influence of Minimum Stress on the Fatigue Life of Non-Crystallising Elastomers", PHD dissertation, School of Engineering, Coventry University, 2003

71 http://www.rhino3d.com, 23/02/2002

72 N. Murphy, C. Spratt, R. Johnnknecht, S. Jerrams, " Investigation of Large Cyclical Equi-Biaxial Stresses and Strains in Thin Elastomeric Sheets by Bubble Inflation", Paper for Dublin Institute of Technology International Conference of Material Tribology MT2002

Bibliography

Jean Le Bras "Introduction to Rubber" Maclaren and Sons LTD London, (1968)

R.P. Brown "Physical Testing of Rubber", 2nd Edition Elsevier (1986)

N.P. Cheremisinoff "Elastomer Technology Handbook" CRC Press, (1993)

B.W. Cherry "Polymer Surfaces" Cambridge University Press, (1981)

A.B. Dayvey and A.R. Payene "Rubber in Engineering Practice" Meclaren, (1964)

A.N. Gent (Editor) "Engineering with Rubber- How to Design Rubber Components" Hanser, (2001)

R.W. Ogden "Non-linear Elastic Deformations" Ellis Horwood, (1984)

R.L.G. Treolar "The Physiscs of Rubber Elasticity" 3rd Edition Clerdon Press (1975)

E.M. James, E. Burak, R.E. Frederick (Editor) "Science and Technology of Rubber" 2nd Edition, Academic Press, (1994)

Indian Rubber Institute "Rubber Engineering" Tata McGraw-Hill, (1998)

D. Boast, V.A. Coveney (Editiors) "Finite Element Analysis of Elastomers" Professional Engineering Publishing, (1999)

A. Dorfman, A. Muhr (Editors) "Constitutive Models for rubber" A.A. Balkema, (1999)

D. Besdo, R.H. Schuster, J. Ihlemann (Editors) "Constructive Models for Rubber II" A.A. Balkema, (2001)

John S. Dick (Editor) "Rubber Technology – Compounding and Testing for Performance" Hanser, (2001)

Glossary

Adhesion	The sticking together of the surface parts
Adsorption	The taking up of molecules from the surface of one substance to the surface of another
Anisotropy	Having properties that are different in all directions in a material at a point
Butadiene	Diolefin that polymerises to form rubber-like substances
CCD Camera	Charged-coupled device camera. In this text, a camera that is connected to a computer system to digitise information from the images produces
Carbon-black	An amorphous form of finely divided carbon
Cauchy stress	True stress (Force/ deformed area)
Conditioning	Taking a test specimen through a number of stress cycles to remove stress softening
Copolymer	A polymer that comprises chains made up of two or more chemically different repeating units
DLC Coating	Diamond Like Carbon Coating
Elastic Deformation	When the stress is removed, the material returns to the dimension it had before the load was applied
Engineering Stress	The ratio of the force to the initial area
Entropy	A measure of disorder. Rubber has its greatest molecular disorder in the unstrained state
EPDM	Ethylene Propylene Diene Polymer

ESPI	The Electronic Speckle Pattern Interferometry
Fatigue	Fatigue is a reduction of strength as a result of cyclic stressing over a period of time
FEA	Finite Element Analysis
IRHD	International Rubber Hardness Degree. A standard system for measuring the hardness of rubber
Invariant	Non-varying quantity irrespective of the Cartesian axis system chosen
Interferometry	The branch of science devoted to the study and measurement of the interaction of waves
Isochoric	Volume retaining, incompressible
Isotropic	Properties of a material that are the same in all directions in a material at a point
Monomer	The single unit that with others joined chemically end to end makes up a chain
NR	Natural Rubber
Plane Strain	Strain system with zero strain in one direction
SBR	Styrene Butadiene Polymer
Sol-gel Coating	Deposition of a thin film or coating
Shot Peening	Bombarding a surface with a small particles
Strain	A change in dimensions, or deformation elongation, ΔL as a result of a tensile or compressive stress
Strain Crystallising	The property of a material to form crystals with an associated change in size

Stress	Force divided by area
Stretch Ratio	Ratio of deformed to original length (i.e. $1+\varepsilon$)
TEOS	Tetraoxidsilicate. Sol-gel coating material
True Stress	Force divided by deformed area
Van der Waal's forces	Relatively weak forces between atoms that are not the result of chemical bond formation
Vulcanisation	The process of forming cross-links between long chain molecules by chemical reaction, achieved by heating rubber in the presence of sulphur and / or other agents

APPENDIX A

Design Drawings

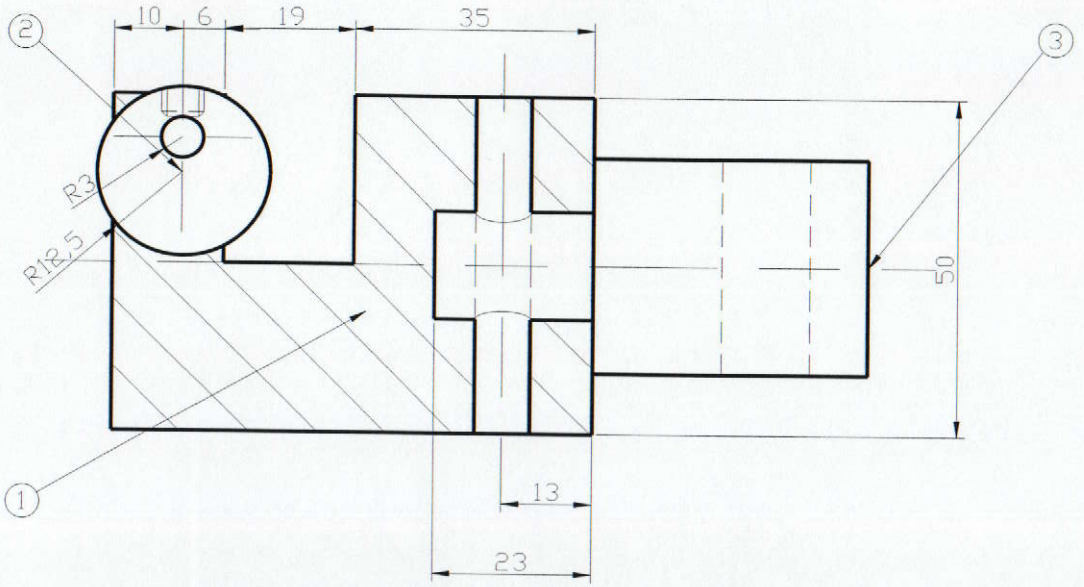

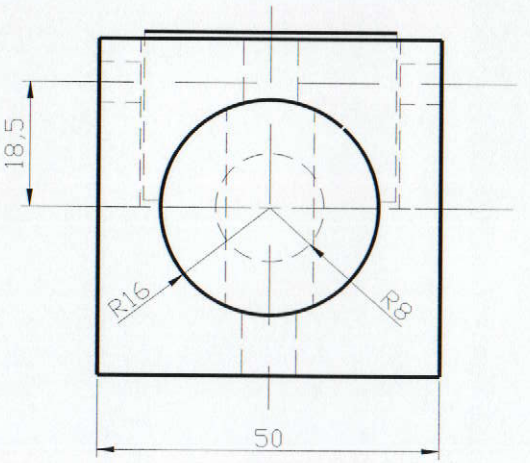

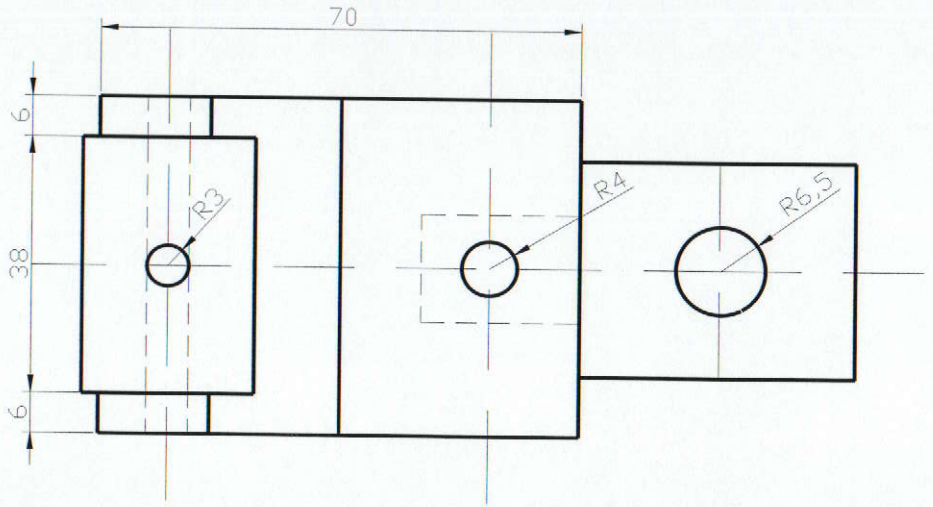

Number	Name of Component		
1	Main Body of the Clamp		
2	Grip		
3	Instron Machine Extension		
Date	Name	Signature	Projection
10/02	Amir Tabakovic		

Elastomeric Clamp	Drawing Number: 1	Scale 1:1

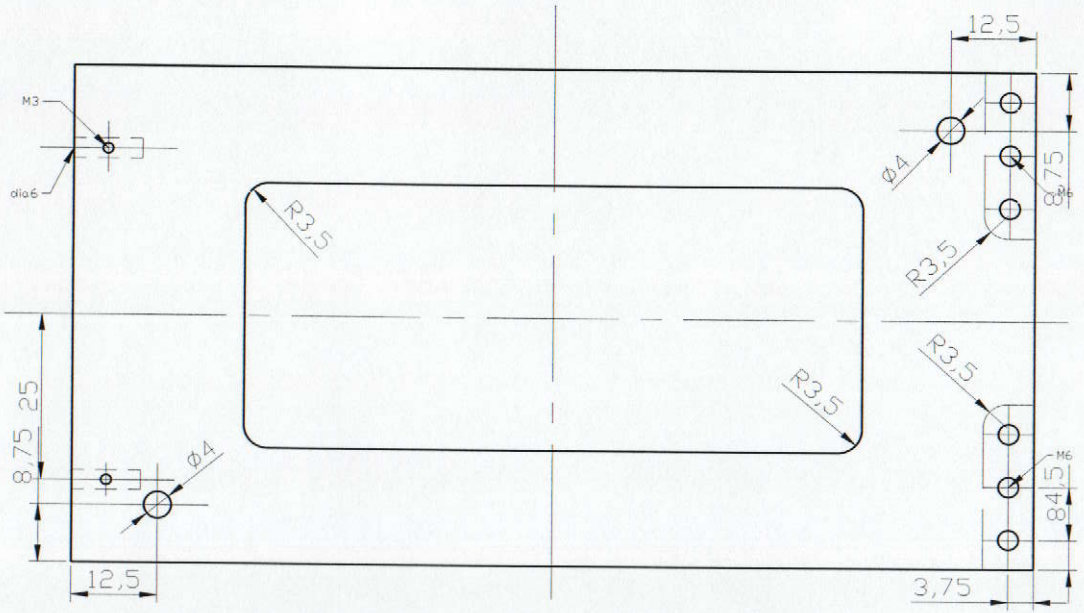

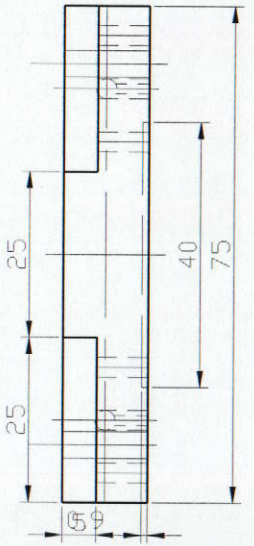

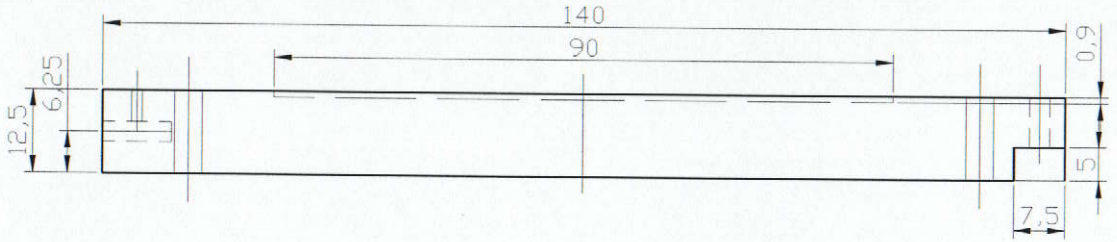

Date	Name	Signature	Projection
12/02	Amir Tabakovic		

Compression Mould Bottom	Drawing Number: 2.1	Scale 1:2

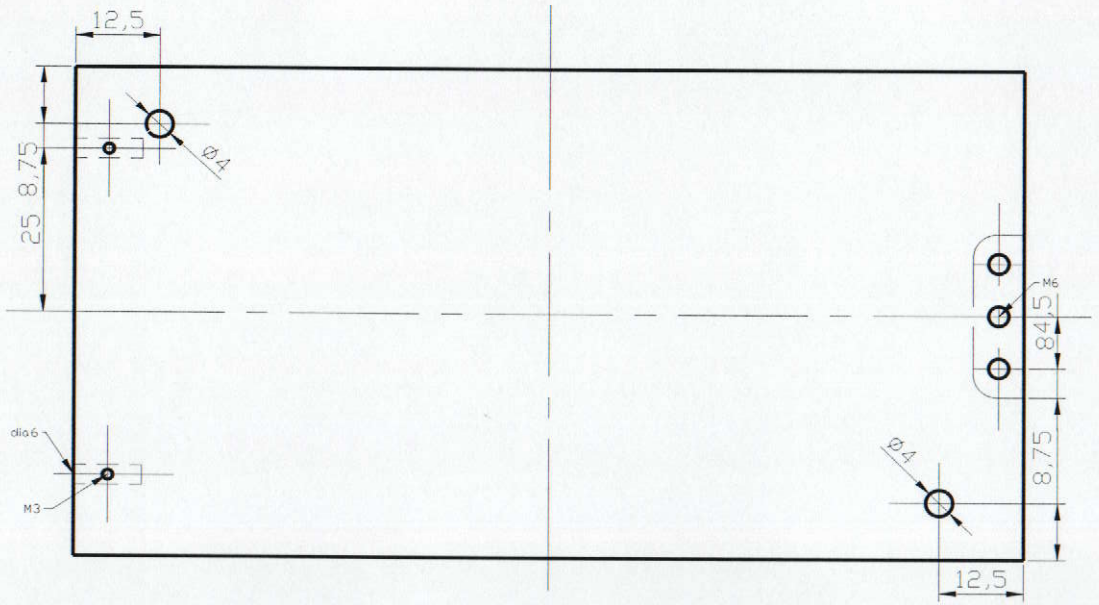

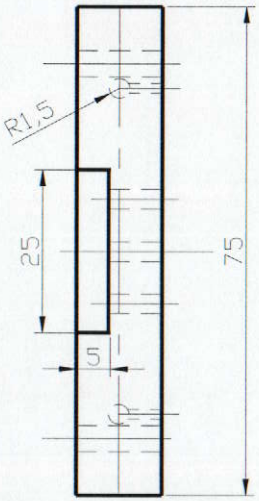

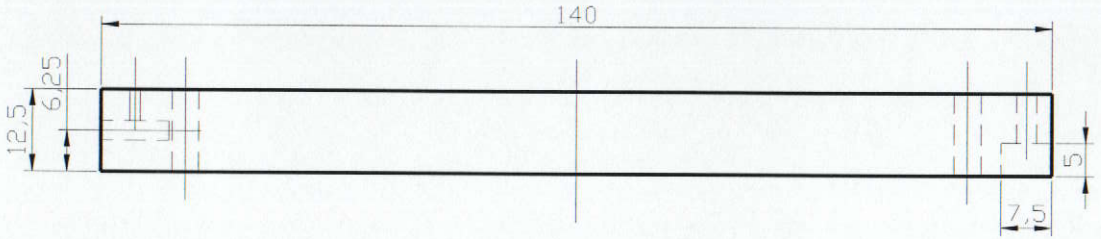

Date	Name	Signature	Projection
12/02	Amir Tabakovic		

Compression Mould Top	Drawing Number: 2.2	Scale 1:2

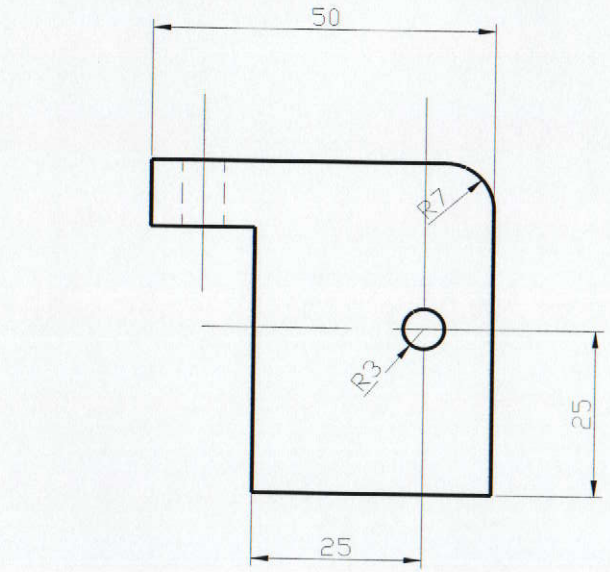

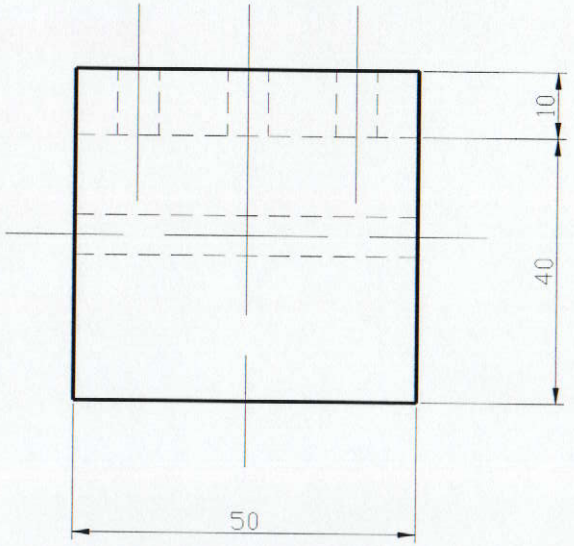

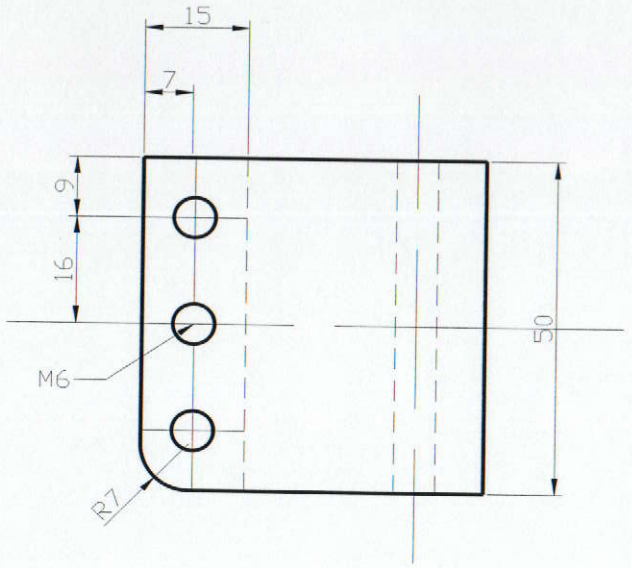

Date	Name	Signature	Projection
12/02	Amir Tabakovic		

Compression Mould Bottom Mould Left Hinge	Drawing Number: 2.3	Scale 1:1

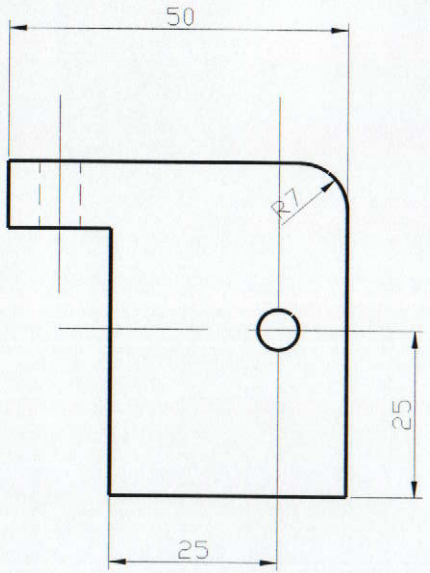

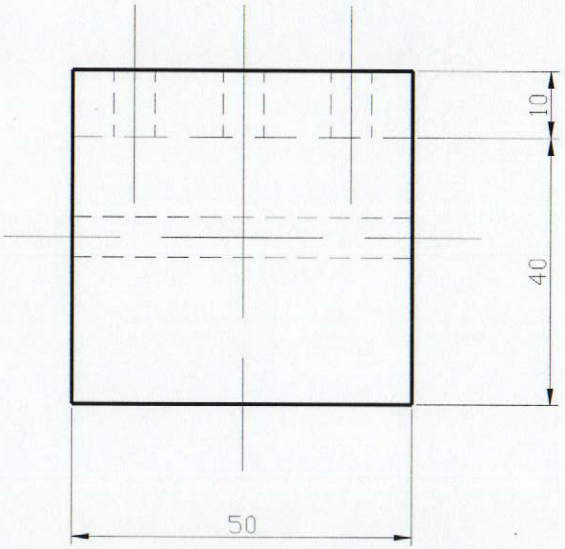

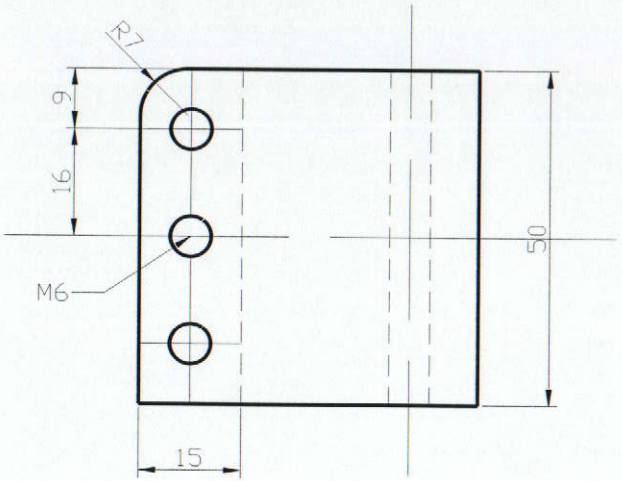

Date	Name	Signature	Projection
12/02	Amir Tabakovic		

Compression Mould Bottom Mould Right Hinge	Drawing Number: 2.4	Scale 1:1

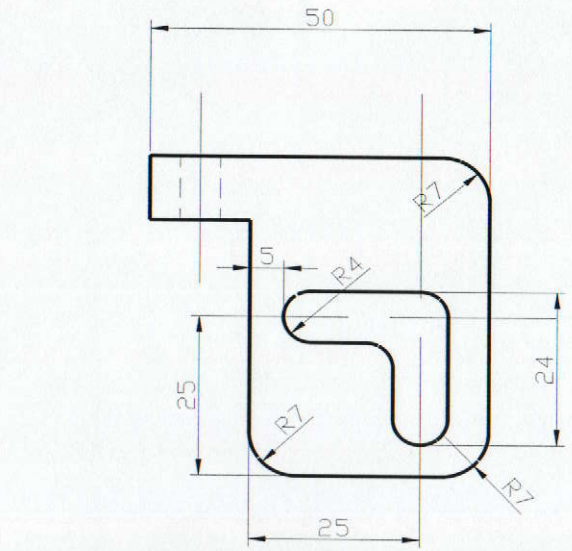

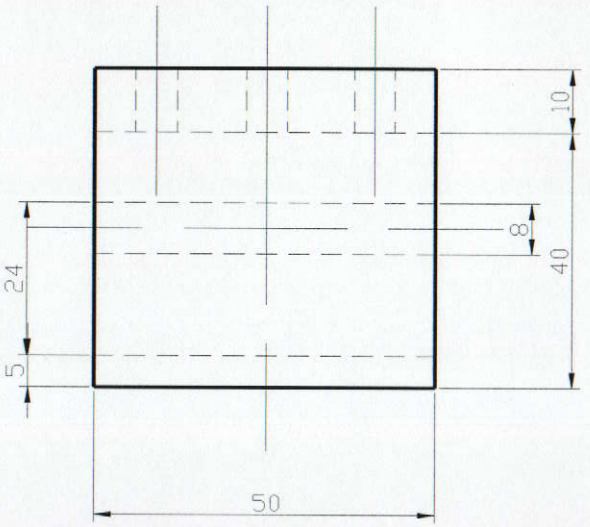

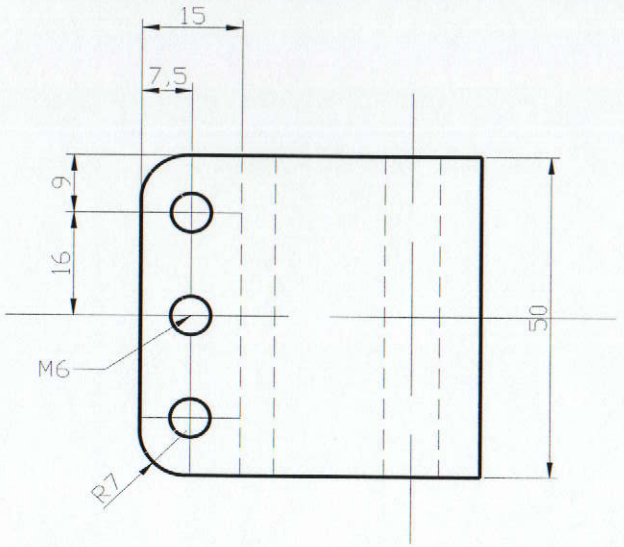

Date	Name	Signature	Projection
12/02	Amir Tabakovic		

Compression Mould Top Mould Hinge	Drawing Number: 2.5	Scale 1:1

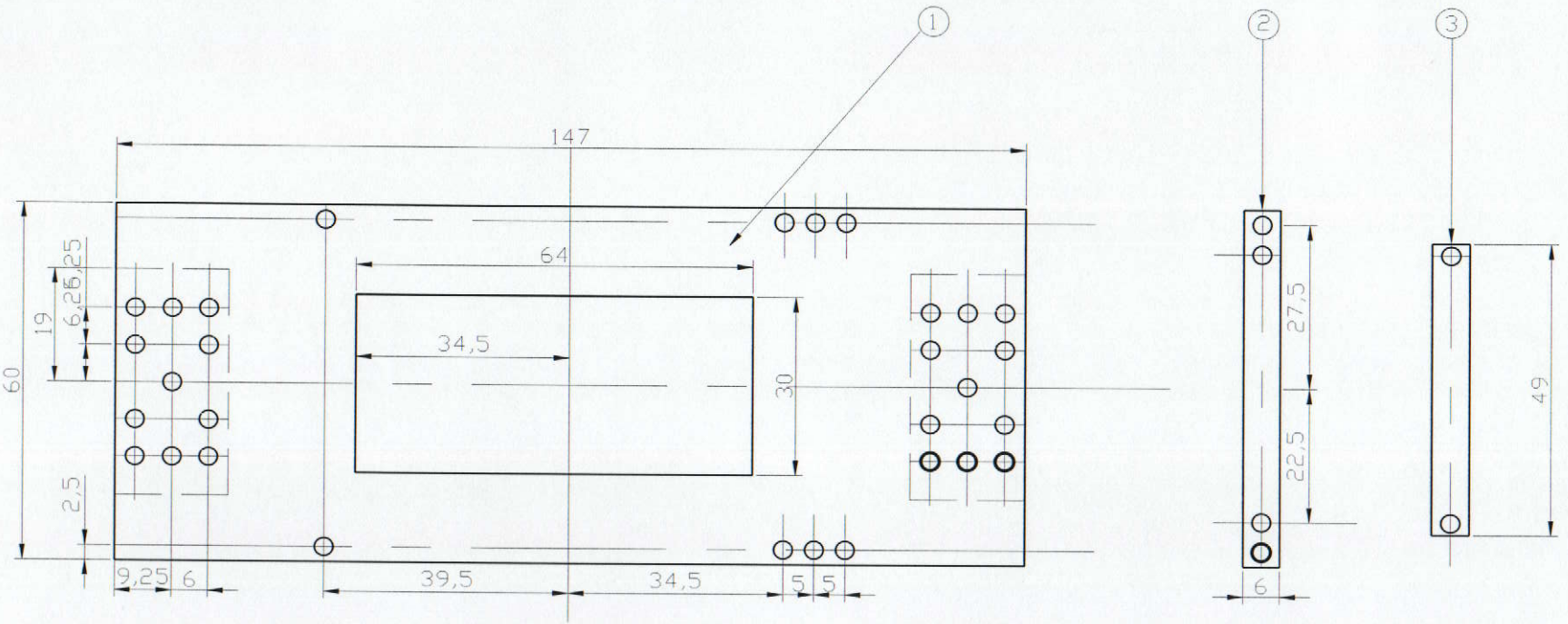

Number	Name of Component		
1	Test Sample Holder		
2	Grip 1		
3	Grip 2		
Date	Name	Signature	Projection
10/02	Amir Tabakovic		

ESPI In-plane Test Rig	Drawing Number: 3	Scale 1:2

APPENDIX B

Plausibility Models

1. DLC Coated EPDM Rubber Plausibility Models

1.1 Curve-fitting Results of DLC Coated EPDM Rubber, First Recorded Cycle

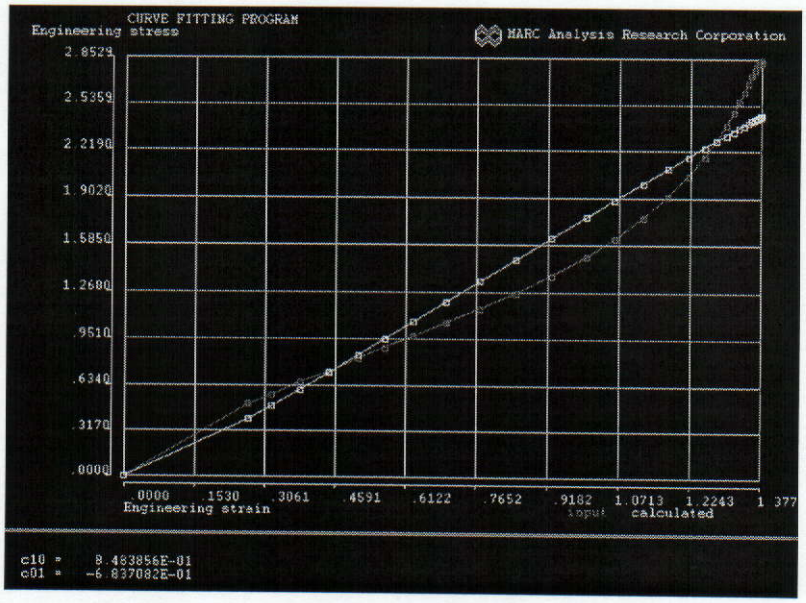

Figure B.1 DLC Coated EPDM Rubber 2 term Mooney-Rivlin Curve-fit Model of First Recorded Cycle

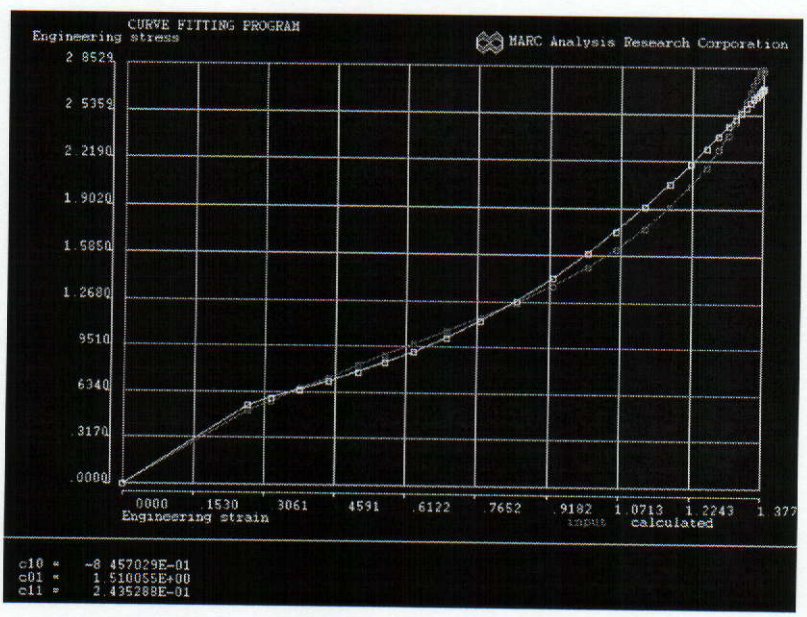

Figure B.2 DLC Coated EPDM Rubber 3 term Mooney-Rivlin Curve-fit Model of First Recorded Cycle

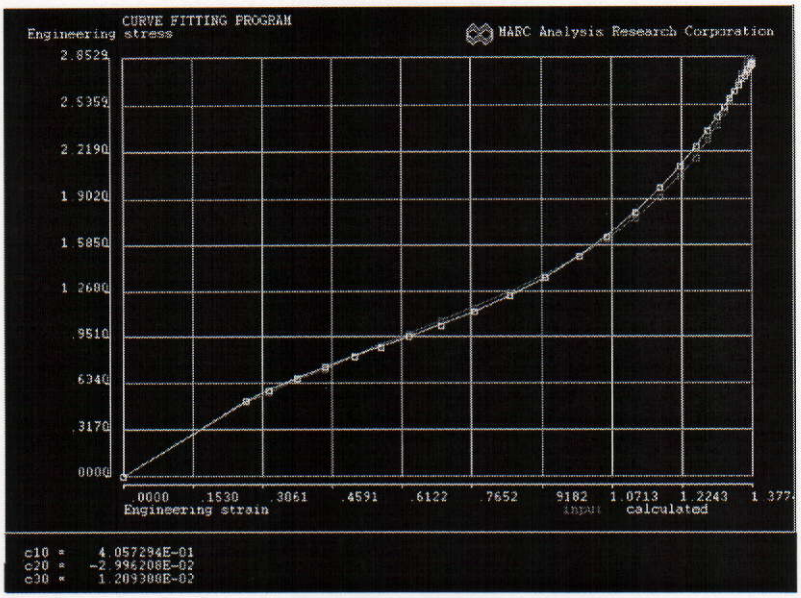

Figure B.3 DLC Coated EPDM Rubber Yeoh Curve-fit Model of First Recorded Cycle

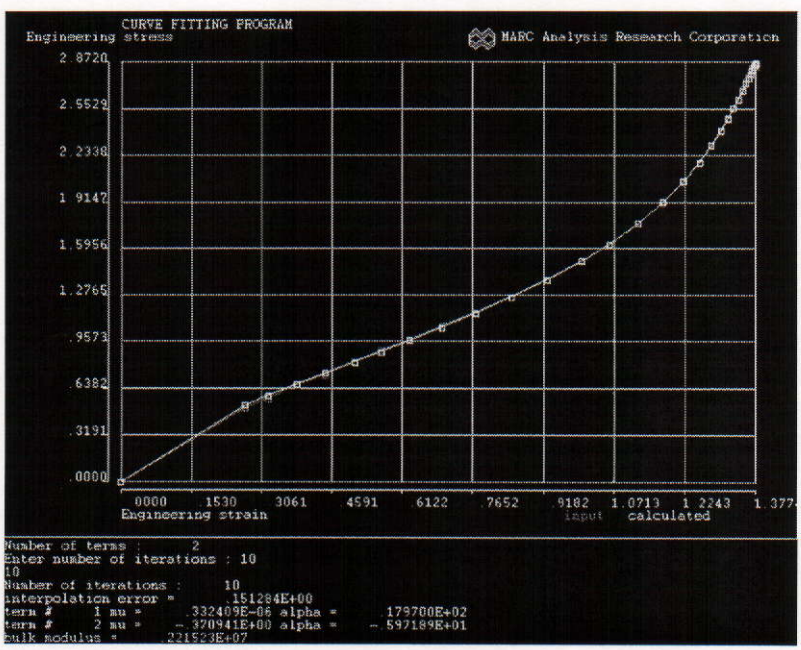

Figure B.4 DLC Coated EPDM Rubber Ogden 2 term Curve-fit Model of First Recorded Cycle

Mooney Rivlin 2 term model:

C_{10}	0.8483856 N/mm^2
C_{01}	-0.6837082 N/mm^2

Mooney 3 term model:

C_{10}	-0.8457029 N/mm^2
C_{01}	1.510055 N/mm^2
C_{11}	0.2345288 N/mm^2

Yeoh model:

C_{10}	0.4057294 N/mm^2
C_{20}	-0.02996208 N/mm^2
C_{30}	0.0109388 N/mm^2

Ogden 2 term model:

μ_1	0.332409E-06 N/mm^2	α_1	17.97
μ_2	-0.370941 N/mm^2	α_2	-5.97189

Table B.1 Plausibility Models for DLC Coated EPDM Rubber for First Recorded Fatigue Cycle

Using the plausibility theory [10] three Curve-fit models are valid for modelling plane strain analysis of stress at the crack tip. Ogden 2 term model, Mooney Rivlin 3 term model and Yeoh model.

1.2 Curve-fitting Results of DLC Coated EPDM Rubber, Last Recorded Cycle

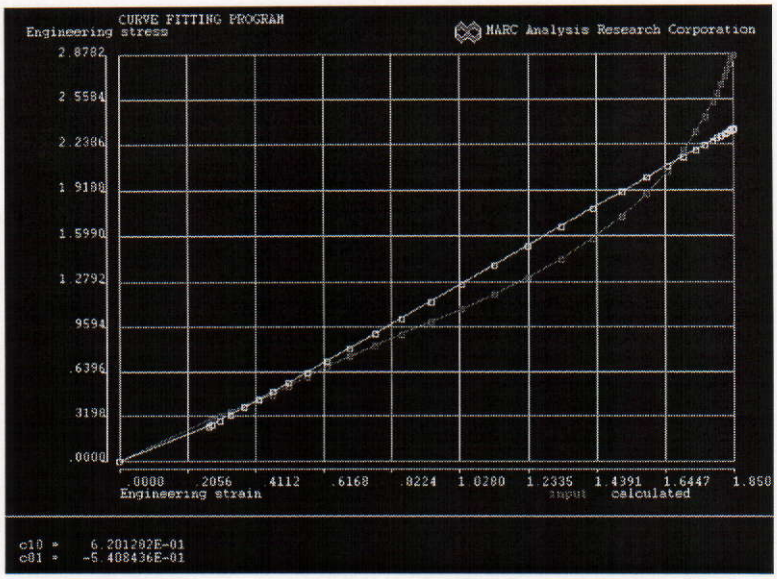

Figure B.5 DLC Coated EPDM Rubber Mooney Rivlin 2 term Curve-fit Model of Last Recorded Cycle

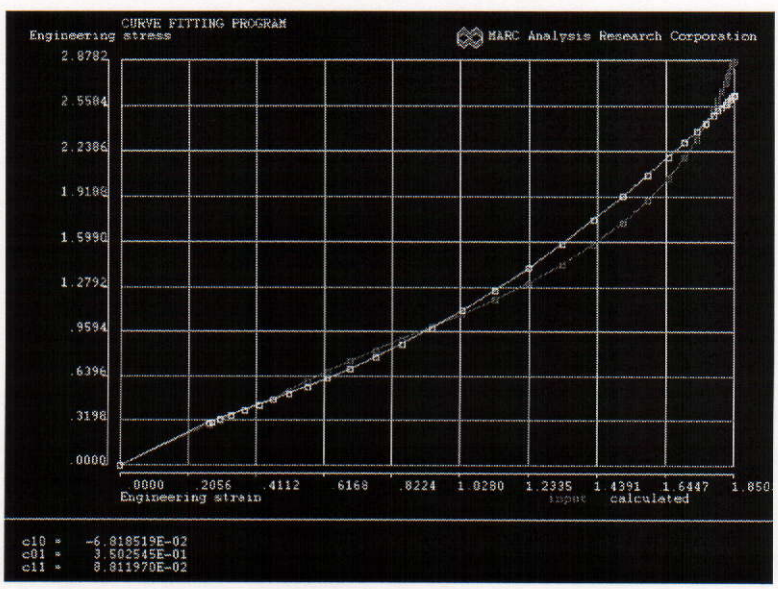

Figure B.6 DLC Coated EPDM Rubber Mooney Rivlin 3 term Curve-fit Model of Last Recorded Cycle

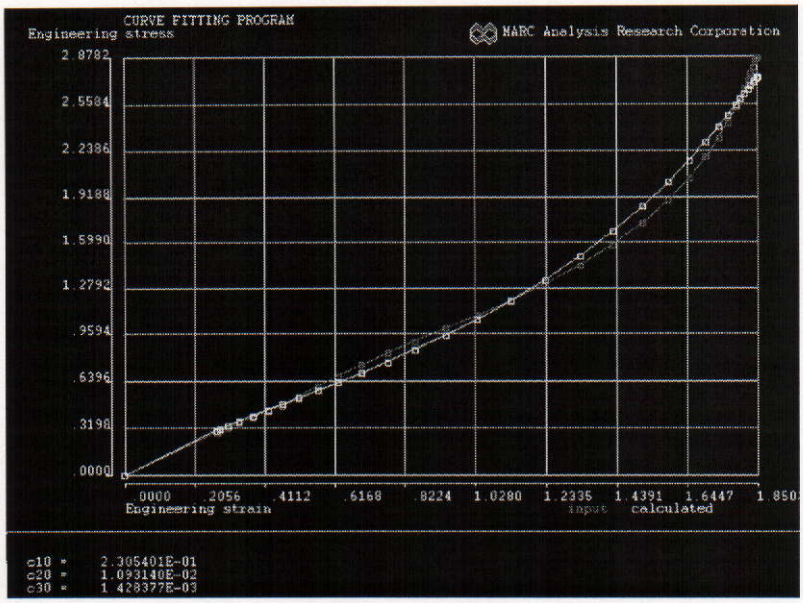

Figure B.7 DLC Coated EPDM Rubber Yeoh Curve-fit Model of Last Recorded Cycle

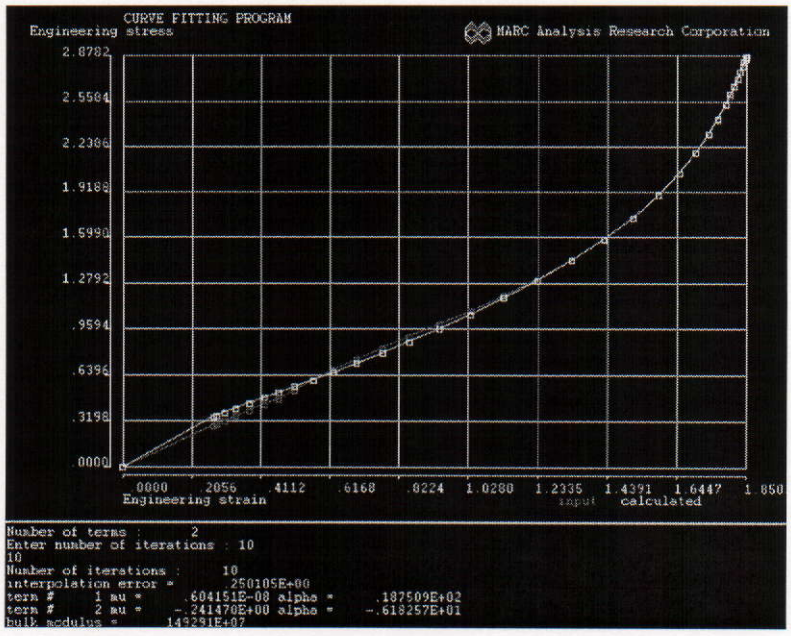

Figure B.8 DLC Coated EPDM Rubber Ogden 2 term Curve-fit Model of Last Recorded Cycle

Mooney Rivlin 2 term model:

C_{10}	0.6201282 N/mm^2
C_{01}	-0.5408436 N/mm^2

Mooney 3 term model:

C_{10}	-0.06818519 N/mm^2
C_{01}	0.3502545 N/mm^2
C_{11}	0.08811970 N/mm^2

Yeoh model:

C_{10}	0.2305401 N/mm^2
C_{20}	0.01093140 N/mm^2
C_{30}	0.001428377 N/mm^2

Ogden 2 term model:

μ_1	0.604151E-08 N/mm^2	α_1	18.7509
μ_2	-0.241470 N/mm^2	α_2	-6.18257

Table B.2 Plausibility Models for DLC Coated EPDM Rubber for Last Recorded Fatigue Cycle

Using the plausibility theory two Curve-fit models are valid for modelling plane strain analysis of coated EPDM last fatigue cycle. They are: the Ogden 2 term model and the Yeoh model.

2. SBR Carbon Black and SBR Silicon with an Initiated Cut, Plausibility Models

2.1 Curve-fitting Results of SBR Carbon Black Rubber with Initiated Cut

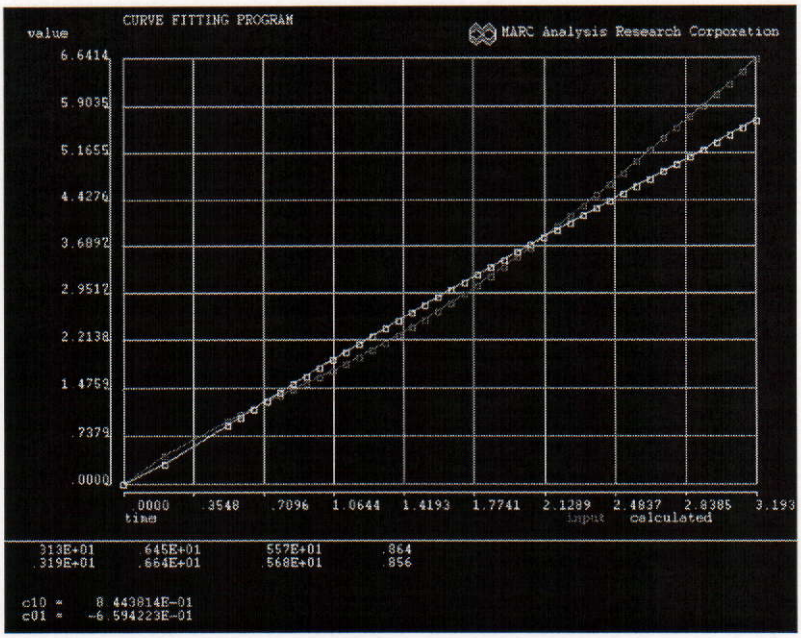

Figure B.9 SBR Carbon Black Rubber of Cross Sectional Area 99.35 mm^2 2 term Mooney-Rivlin Curve-fit Model

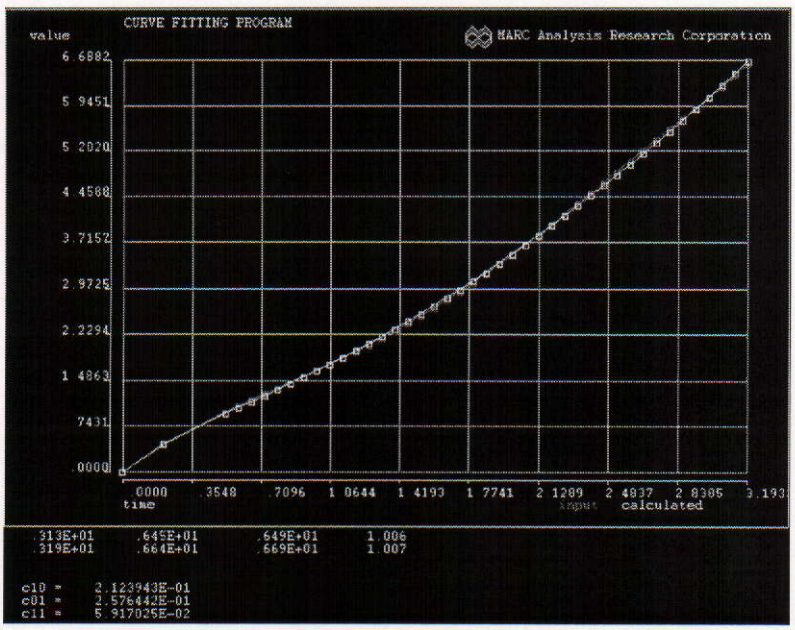

Figure B.10 SBR Carbon Black Rubber of Cross Sectional Area 99.35 mm^2 3 term Mooney-Rivlin Curve-fit Model

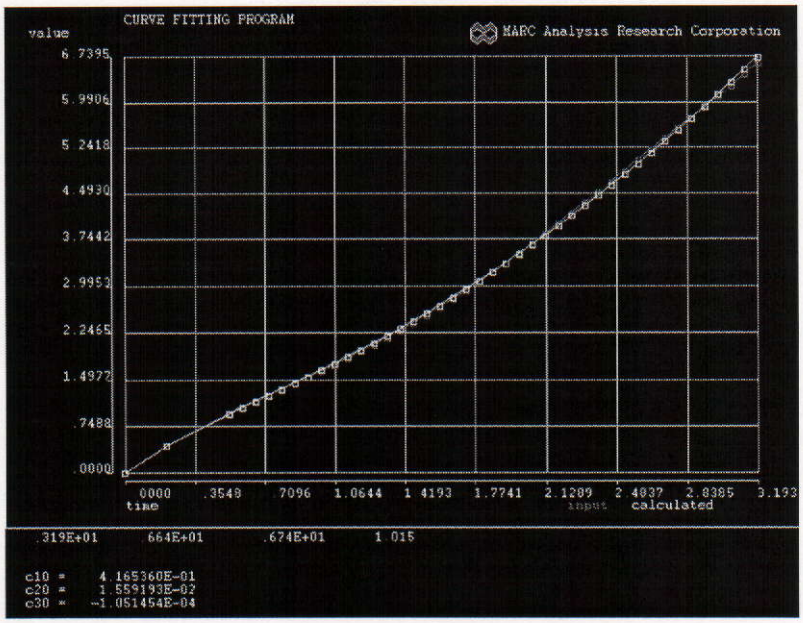

Figure B.11 SBR Carbon Black Rubber of Cross Sectional Area 99.35 mm^2 Yeoh Curve-fit Model

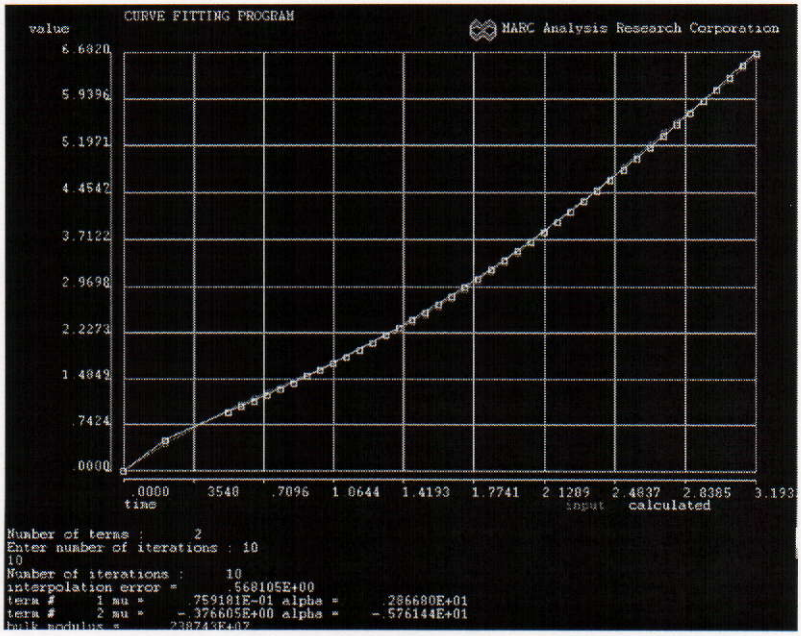

Figure B.12 SBR Carbon Black Rubber of Cross Sectional Area 99.35 mm^2 Ogden 2term Curve-fit model

Mooney Rivlin 2 term model:

C_{10}	0.8443814 N/mm^2
C_{01}	-0.6594223 N/mm^2

Mooney 3 term model:

C_{10}	0.2123943 N/mm^2
C_{01}	0.2576442 N/mm^2
C_{11}	0.05917025 N/mm^2

Yeoh model:

C_{10}	0.4165360 N/mm^2
C_{20}	0.01559193 N/mm^2
C_{30}	-1.051454E04 N/mm^2

Ogden 2 term model:

μ_1	0.0759181 N/mm^2	α_1	2.8668
μ_2	-0.376605 N/mm^2	α_2	-5.76144

Table B.3 Plausibility Models for SBR Rubber Carbon Black Filled, with Cross Sectional Area 99.35 mm^2

Using the plausibility theory [10] two Curve-fit models are valid for modelling plane strain analysis of stress at the crack tip. Ogden 2 term fit and Mooney Rivlin 2 term fit.

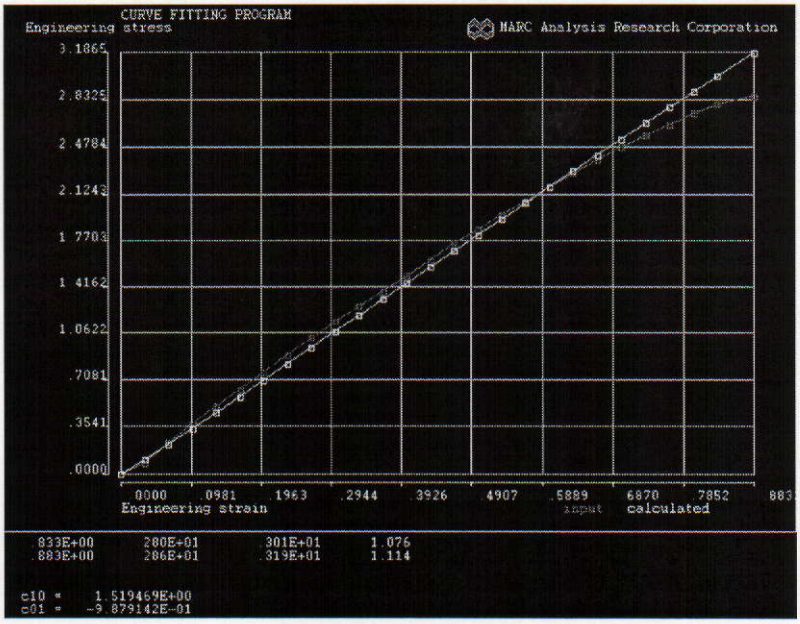

Figure B.13 SBR Carbon Black Rubber of Cross Sectional Area 44.15 mm^2 Mooney Rivlin 2 term Curve-fit Model

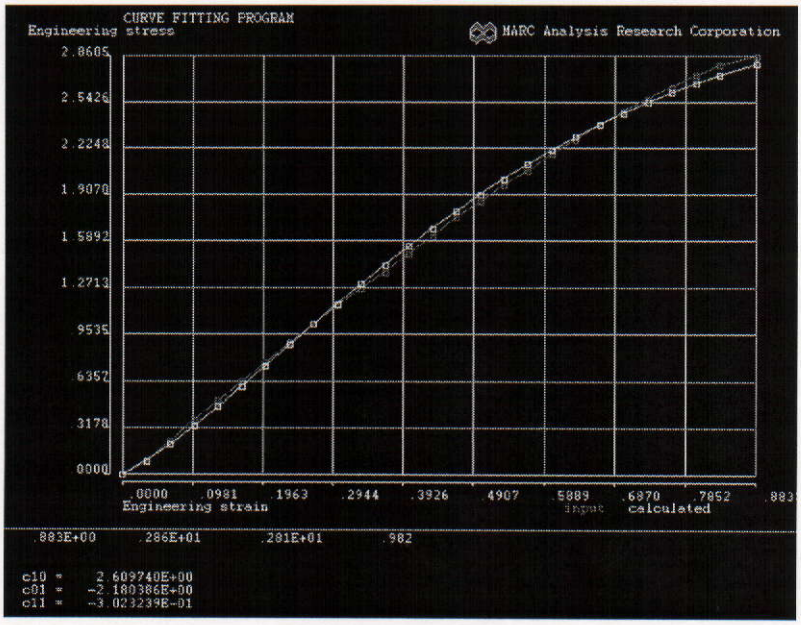

Figure B.14 SBR Carbon Black rubber of Cross Sectional Area 44.15 mm^2 Mooney Rivlin 3 term Curve-fit Model

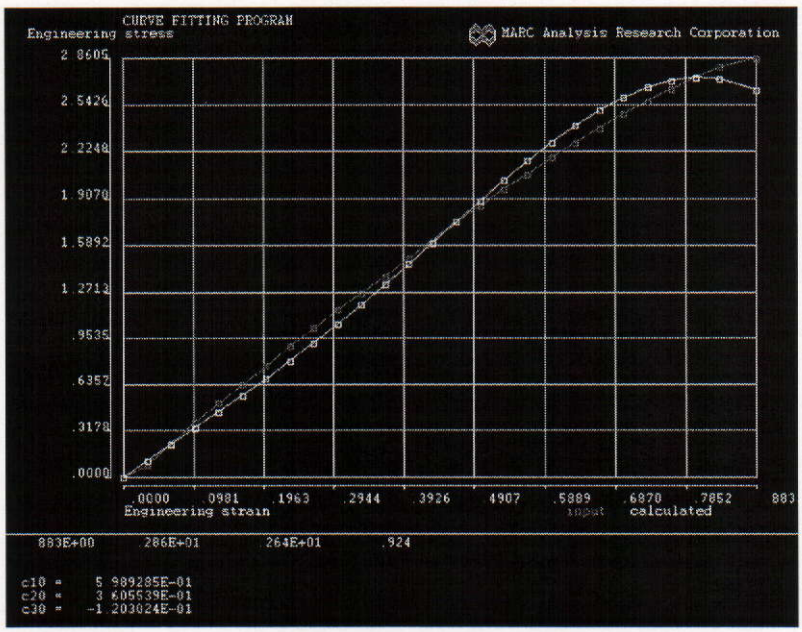

Figure B.15 SBR Carbon Black Rubber of Cross Sectional Area 44.15 mm^2 Yeoh Curve-fit Model

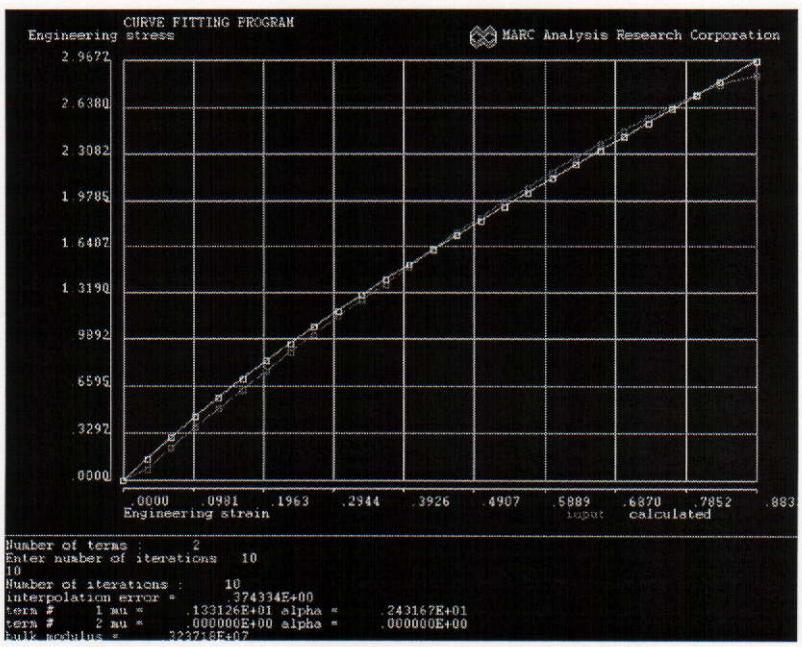

Figure B.16 SBR Carbon Black Rubber of Cross Sectional Area 44.15 mm^2 Ogden 2 term Curve-fit Model

Mooney Rivlin 2 term model:

C_{10}	1.519469 N/mm^2
C_{01}	-0.9879142 N/mm^2

Mooney 3 term model:

C_{10}	2.60974 N/mm^2
C_{01}	-2.180306 N/mm^2
C_{11}	-0.3023239 N/mm^2

Yeoh model:

C_{10}	0.5989285 N/mm^2
C_{20}	0.3605539 N/mm^2
C_{30}	-0.1203024 N/mm^2

Ogden 2 term model:

μ_1	1.33126 N/mm^2	α_1	2.43167
μ_2	0 N/mm^2	α_2	0

Table B.4 Plausibility Models for SBR Rubber Carbon Black filled with Cross Sectional Area 44.15 mm^2

Using the plausibility theory one Curve-fit model is valid for modelling plane strain analysis of stress at the crack tip. Ogden 2 term fit. Second term is zero therefore it was treated as one term Ogden model.

2.2 Curve-fitting Results of SBR Silicon Rubber with Initiated Cut

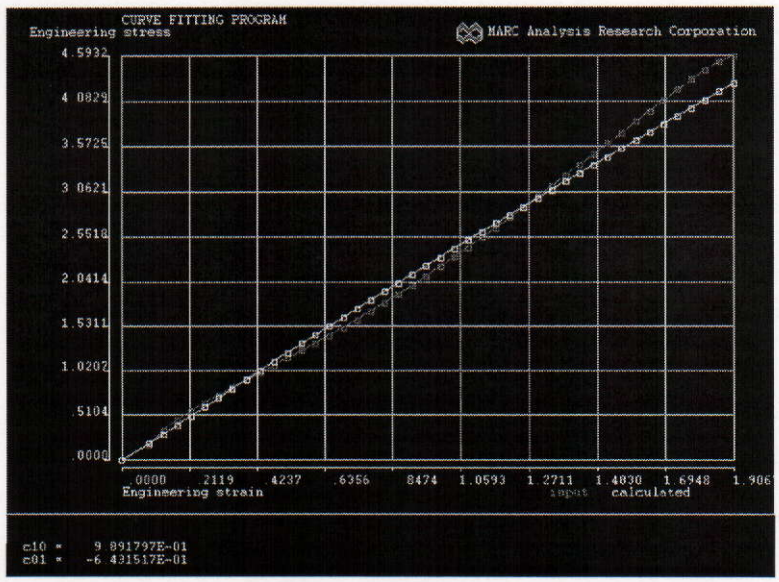

Figure B.17 SBR Silicon Rubber of Cross Sectional Area 99.35 mm^2 2 term Mooney-Rivlin Curve-fit Model

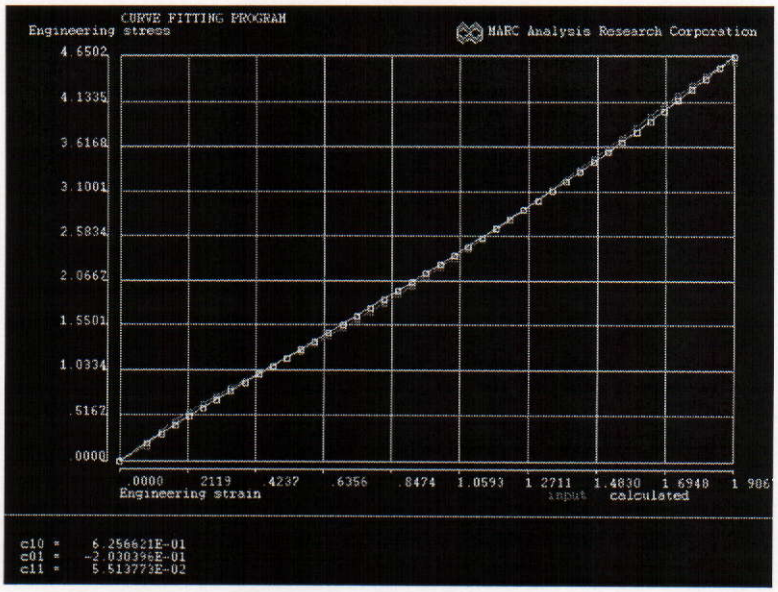

Figure B.18 SBR Silicon Rubber of Cross Sectional Area 99.35 mm^2 3 term Mooney-Rivlin Curve-fit Model

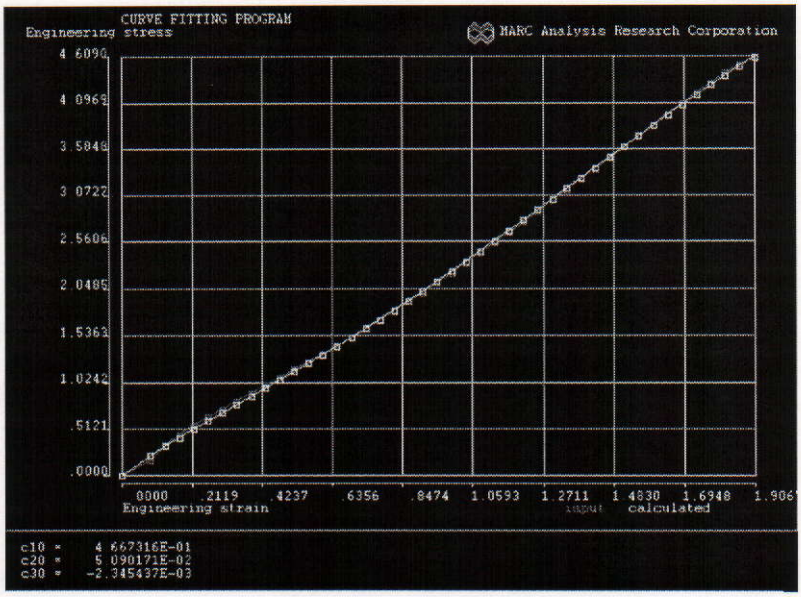

Figure B.19 SBR Silicon Rubber of Cross Sectional Area 99.35 mm^2 Yeoh Curve-fit Model

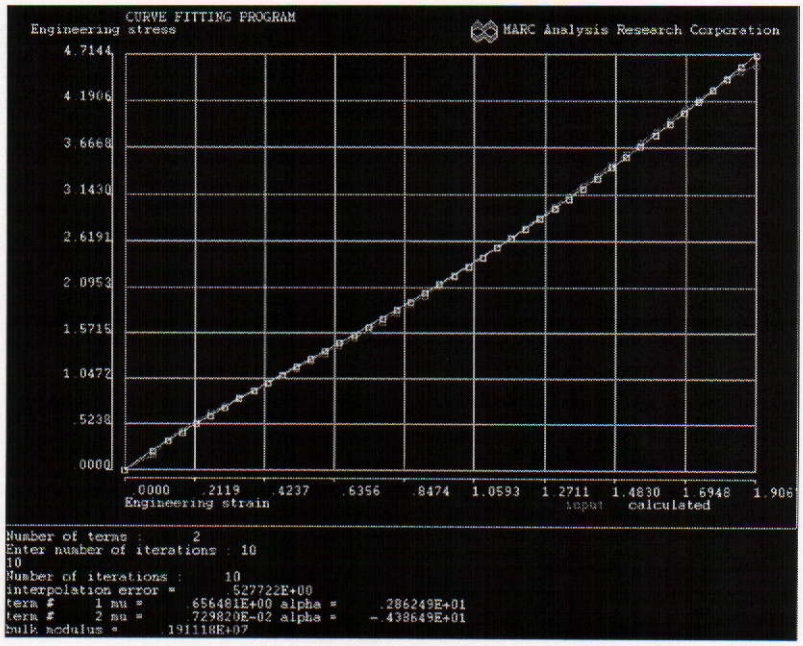

Figure B.20 SBR Silicon Rubber of Cross Sectional Area 99.35 mm^2 Ogden 2term Curve-fit Model

Mooney Rivlin 2 term model:

C_{10}	0.989179 N/mm^2
C_{01}	-0.643151 N/mm^2

Mooney 3 term model:

C_{10}	0.6256621 N/mm^2
C_{01}	-0.2030396 N/mm^2
C_{11}	0.05151377 N/mm^2

Yeoh model:

C_{10}	0.4667316 N/mm^2
C_{20}	0.5090171 N/mm^2
C_{30}	-0.002345437 N/mm^2

Ogden 2 term model:

μ_1	0.656481 N/mm^2	α_1	2.86249
μ_2	0.00729820 N/mm^2	α_2	-4.38649

Table B.5 Plausibility Models for SBR Rubber Silicon Filled with Cross Sectional Area 99.35 mm^2

Using the plausibility theory [10] none of the Curve-fit models is valid for modelling plane strain analysis of stress at the crack tip.

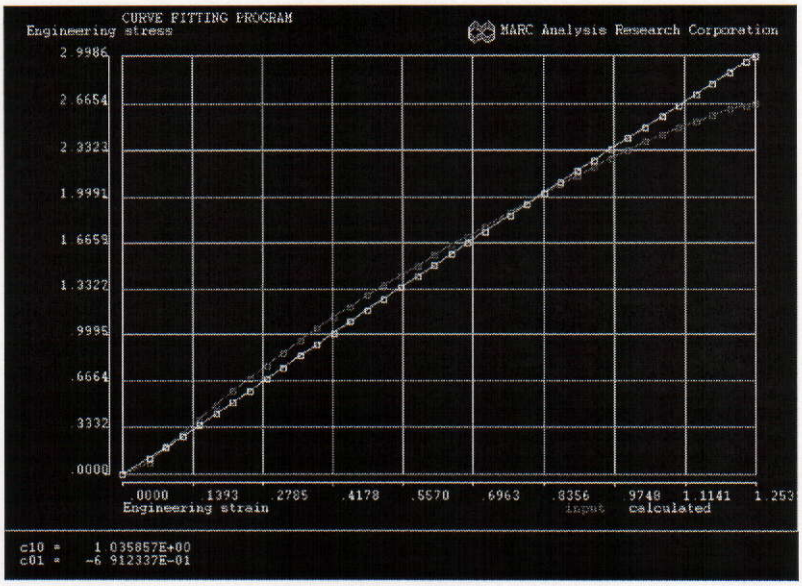

Figure B.21 SBR Silicon Rubber of Cross Sectional Area 44.15 mm^2 Mooney Rivlin 2 term Curve-fit Model

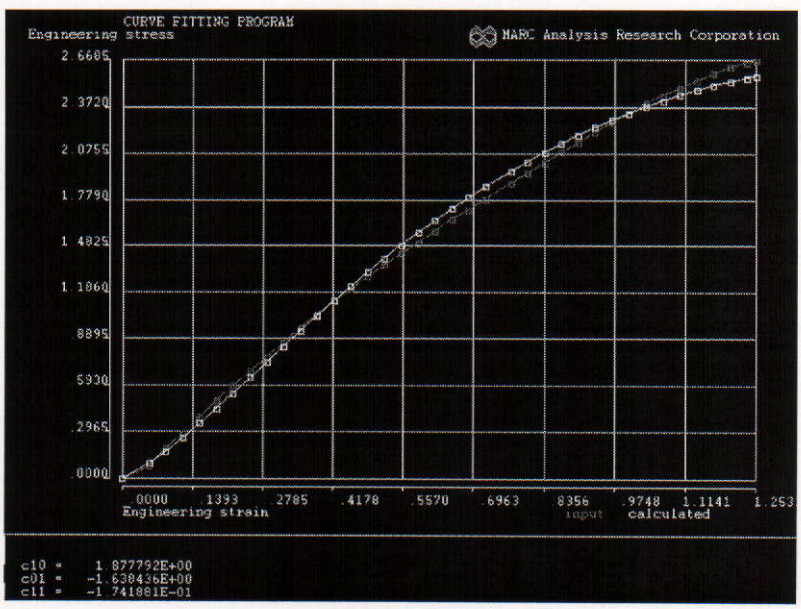

Figure B.22 SBR Silicon Rubber of Cross Sectional Area 44.15 mm^2 Mooney Rivlin 3 term Curve-fit Model

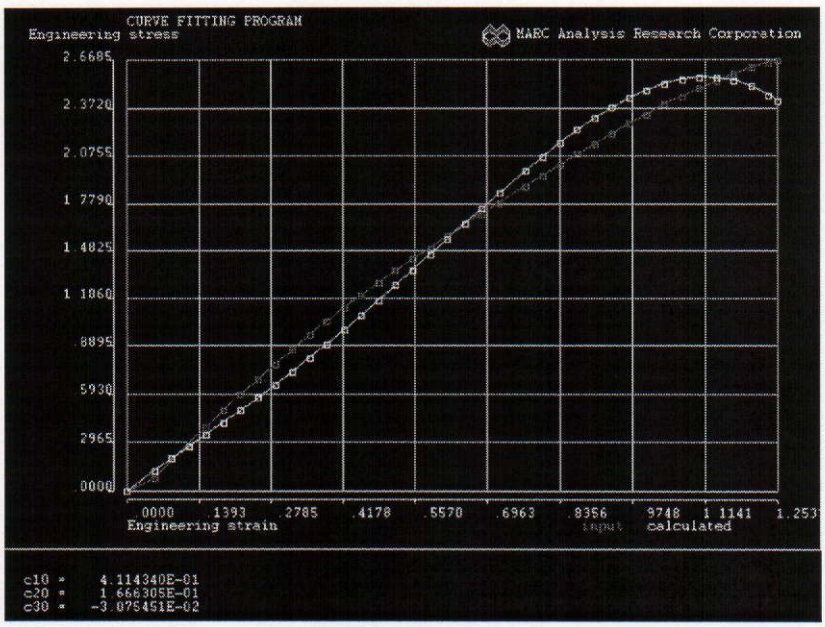

Figure B.23 SBR Silicon Rubber of Cross Sectional Area 44.15 mm^2 Yeoh Curve-fit Model

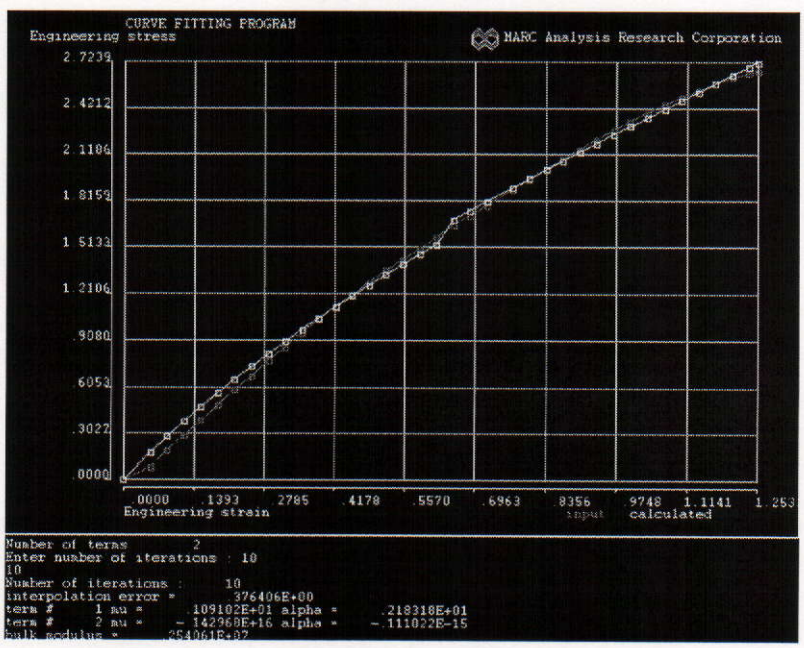

Figure B.24 SBR Silicon Rubber of Cross Sectional Area 44.15 mm^2 Ogden 2 term Curve-fit Model

Mooney Rivlin 2 term model:

C_{10}	1.035857 N/mm^2
C_{01}	-0.6912337 N/mm^2

Mooney 3 term model:

C_{10}	1.877792 N/mm^2
C_{01}	-1.638436 N/mm^2
C_{11}	-0.1741881 N/mm^2

Yeoh model:

C_{10}	0.411434 N/mm^2
C_{20}	0.166305 N/mm^2
C_{30}	-0.03075451 N/mm^2

Ogden 2 term model:

μ_1	1.09102 N/mm^2	α_1	2.1831
μ_2	-0.142968E+16 N/mm^2	α_2	-0.111022E-15

Table B.6 Plausibility Models for SBR Rubber Silicon filled with Cross Sectional Area 44.15 mm^2

Using the plausibility theory none of the Curve-fit models is valid for modelling plane strain analysis of stress at the crack tip. Even that Ogden 2 term model show plausible constants model was not able to run in the MSC Marc FEA software plain strain analysis.

3. EPDM Rubber Plausibility Models

3.1 Curve-fitting Results of EPDM Rubber

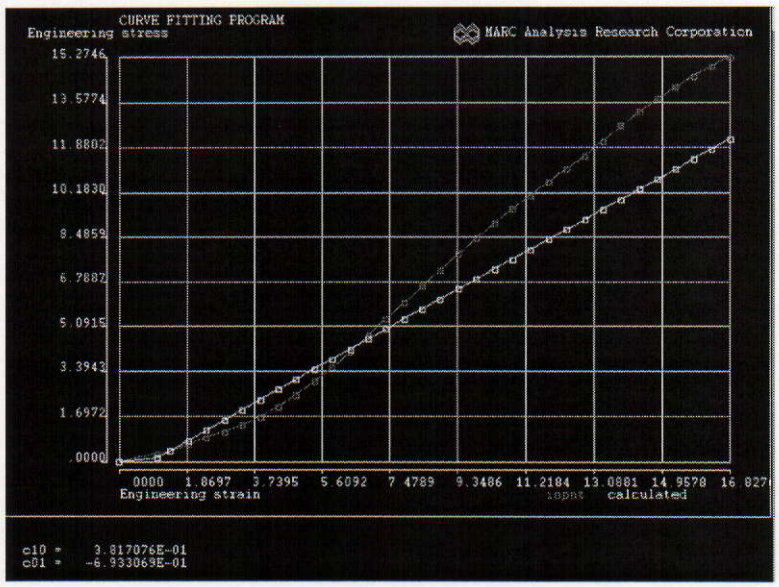

Figure B.25 EPDM Rubber 2 term Mooney-Rivlin Curve-fit Model

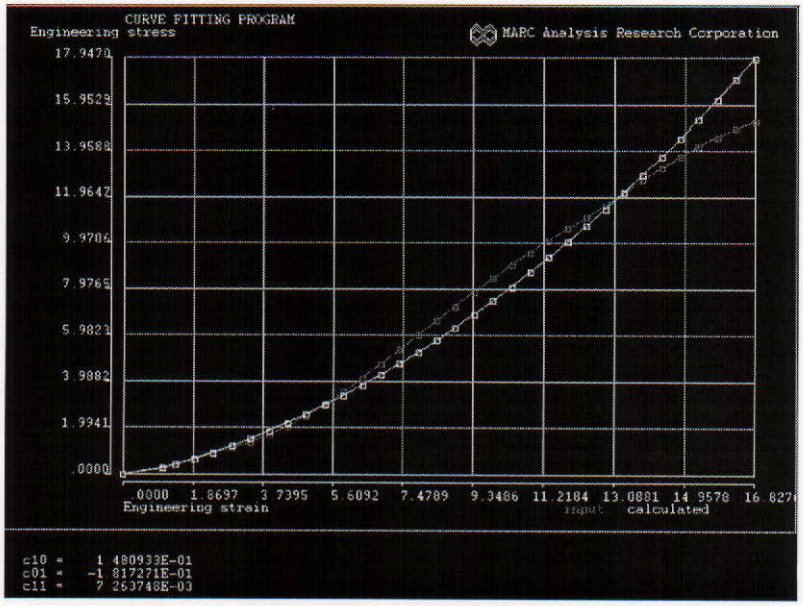

Figure B.26 EPDM Rubber 3 term Mooney-Rivlin Curve-fit Model

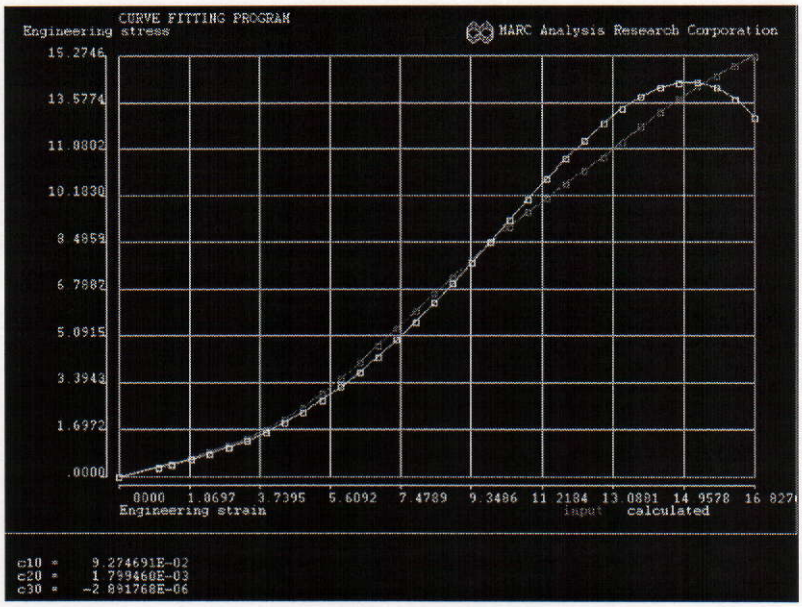

Figure B.27 EPDM Rubber Yeoh Curve-fit Model

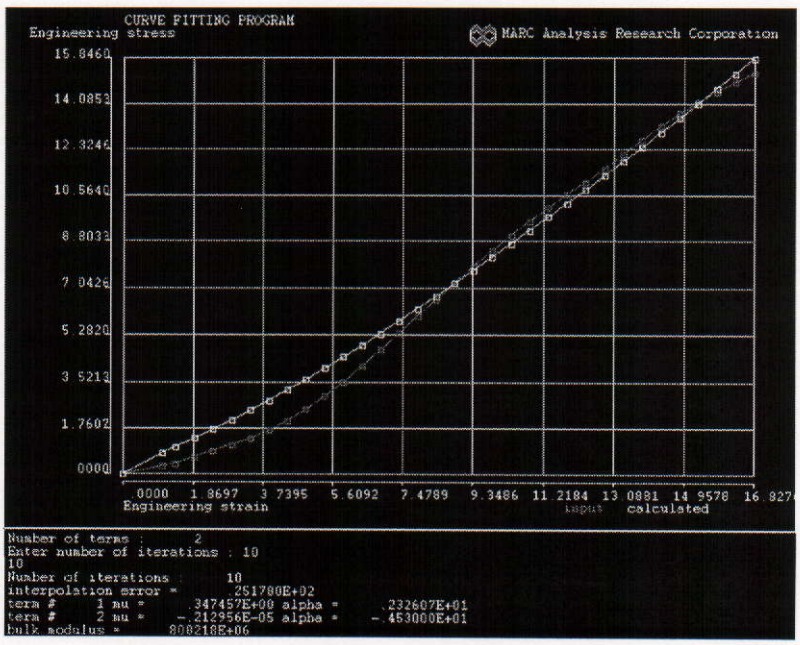

Figure B.28 EPDM Rubber Ogden 2 term Curve-fit Model

Mooney Rivlin 2 term model:

C_{10}	0.3817076 N/mm^2
C_{01}	-0.6933069 N/mm^2

Mooney 3 term model:

C_{10}	0.1480933 N/mm^2
C_{01}	-0.1817271 N/mm^2
C_{11}	0.007263748 N/mm^2

Yeoh model:

C_{10}	0.09274691 N/mm^2
C_{20}	0.001799460 N/mm^2
C_{30}	-2.891768E-06 N/mm^2

Ogden 2 term model:

μ_1	0.347457 N/mm^2	α_1	2.32607
μ_2	-0.212956E-0.5 N/mm^2	α_2	-4.53

Table B.7 Plausibility Models for EPDM Carbon Black Filled Rubber

Using the plausibility theory [10] one Curve-fit model is valid for modelling plane strain analysis of surface flaw. Ogden 2 term fit.

APPENDIX C

Papers

1. IRC 2001 Paper

The Influence of Mean Stress on the Fatigue Properties of Natural Rubber

S. Jerrams and Amir Tabaković, Dublin, (Ireland)

Fatigue, Strain Crystallisation, Surface flaws, Stress Concentration

As with other physical properties, rubber behaves very differently from conventional solids when it is subjected to cyclical loading. Previous research has suggested that strain crystallising filled rubbers exhibit higher fatigue resistance if pre-loads are not fully removed when components are stressed in service. This behaviour is attributed to crystallites inhibiting crack growth when loads are not completely relaxed. However, improved fatigue resistance in pre-loaded non strain crystallising filled rubbers has also been observed and alternative explanations for greater fatigue resistance require consideration. Fatigue resistance in filled rubbers is largely dependent on the energy available to propagate a crack, but the influence of stress concentration is undetermined in elastomeric fatigue. This paper describes an investigation into the change in surface flaws when filled Natural Rubber (NR) is pre-loaded. In metal fatigue, a stress concentration is virtually unaltered by cyclic loading. Rubber undergoes large reversible strains and it is argued that rubber components have less severe surface flaws when preloaded than in a stress free state.

1. Introduction

The design of a dynamically loaded rubber component must conform to different criteria than those for a metal component when subjected to fatigue. For instance, if the tensile cycles incurred by an elastomeric part are strain (displacement) controlled, the designer will choose the 'softer' of two appropriate compounds. However, if the cycles are stress (load) controlled, the harder material will be selected[1]. This choice is based on the amount of strain energy available to propagate a crack in each cycle, as shown in Figure 1. For a repeated displacement, the area under the load/displacement curve is smaller for the less rigid rubber (Fig 1a), but for a repeated load application the opposite is true (Fig 1b). In fatigue, metal components

experience micro-strains and such considerations are irrelevant. Also, the reduction in fatigue life in metals when tensile mean stresses are increased has been comprehensively researched and explained[2,3], but strain crystallising rubbers exhibit greater fatigue resistance if tensile mean stresses are increased, providing the stress is not fully relaxed between loading cycles[4,5,6]. Hence improved fatigue properties can be achieved by pre-loading Natural Rubber (NR) components. The increase is attributed to crystallites inhibiting crack growth at the crack tip in a component under load. If the load in the rubber is not fully removed then the crystalline region at the crack tip does not melt and the crack cannot propagate in subsequent load applications[7]. However, increased fatigue resistance, associated with higher tensile mean stress in the absence of full load relaxation, has also been observed in non strain crystallising rubbers[8,9]. The predominant reason for this increase in fatigue strength is again related to the 'dynamic' strain energy available to propagate a crack, but the influence of changes in stress concentration in elastomeric fatigue is unresearched. In metal fatigue, the geometry of notches and flaws are barely changed by repeated strain cycles, but rubber undergoes large reversible strains. Fatigue cracks in rubber are thought to emanate from naturally occurring surface defects of 40μm $\pm$ 20μm across[10]. These flaws occur in rubber components irrespective of the production process.

This text describes dimensional changes in flaws on the surfaces of elastomers, pre-loaded in tension and considers if a reduction in stress concentration in preloaded rubbers can partially explain improved fatigue properties. The rubber compound used in the physical test was a carbon filled, sulphur cured NR, produced in nine hardness values between 38 IRHD and 75 IRHD. Fatigue resistance in a component can be increased by introducing an improved surface finish at the predicted point of failure, so a superficial insight into elastomeric fatigue properties can be gained by comparing surface finishes in rubber in the strained and unstrained state. Initially, surface finishes of samples, both strain free and strained, for each rubber hardness were measured. Thereafter, microscopy was used to compare the geometry and stress concentration of individual surface flaws at different levels of strain

2. Surface finish of strained natural rubber

The surface finish of each of the hardness values was measured using a Taylor Hobson, Talysurf surface measurement machine with a Sutronic probe. The samples

were measured twice in the unstrained state and twice at 100% and 200% strain (stretch ratios of $\lambda = 2$ and $\lambda = 3$ respectively) based on a gauge length of 10 mm applied to test specimens of 2 mm nominal thickness and 19 mm wide. The gauge length and stretch ratios have no relevance to pre-strains in specific components, but allow comparisons to be made between each rubber hardness. After calibrating the analyser using a specimen of known surface finish, readings were taken over a traversing length of 8 mm and the mean value of surface finish R_a[11] obtained. R_a is the arithmetical average value of all absolute distances (y) of the roughness profile (R) from the centreline of the asperities within the measuring length (l_m) and is expressed mathematically by Eqn. 1. The traversing direction for the measurements

$$R_a = \frac{1}{l_m} \int_{x=0}^{x=l_m} |y| dx \qquad (1)$$

where R_a = Surface finish (μm)

l_m = measuring length

y = absolute distance from centreline of asperities

$$R_{a_S} = R_{a_0}(1 - 0.35 l_n \lambda) \qquad (2)$$

where R_{a_S} = surface finish at stretch ratio λ (μm)

R_{a_0} = surface finish of the unstrained rubber (μm)

was at 45^0 to the direction of stretch and consequently also inclined relative to the plane and normal of the tooling marks imparted by the die used to produce the rubber samples. Since the values of surface finish in the unstrained samples did not show an ascending or descending tendency with rubber hardness, quoting absolute values for surface finish is irrelevant. However, it is significant that surface finish was seen to improve in each of the eighteen tests on the rubber stretched to $\lambda = 2$ and further improved in the the eighteen tests on the rubber stretched to $\lambda = 3$. Surface finishes at intermediate stretch ratios ($\lambda = 1.5$ and $\lambda = 2.5$) were determined in a small number of tests to corroborate the test outcomes. The mean changes in surface finish with increased strain are shown as percentages in Figure 2 and Eqn 2 gives an approximate relationship between tensile strain and surface finish.

3. Microscopic analysis of surface flaws.

Microscopic analyses of surface flaws in NR were made with an Olympus BX60M System Microscope incorporating a universal infinity system (UIS infinity-corrected optical system). Magnified images of the rubber were captured using a video printer. Only one stress raiser is depicted in the text, but it typifies the change in geometry in strained surface voids in NR. Figure 3 shows a flaw in a 38 IRHD NR under increasing strain. Figure 3a shows a strain-free surface void; figure 3b, the void at 100% strain applied to a gauge length of 10 mm ($\lambda = 2$) which wholly encloses the flaw and figure 3c at 200% strain ($\lambda = 3$). It is evident from the sequence that the flaw is a void in the material surface, since the bottom of the depression comes into focus, as the depression becomes shallower with increased stretching of the rubber. Initially the void is approximately circular and 80 μm across. If the material is considered to behave like a linear elastic solid and comply with the simple expression for stress concentration given by Inglis[12] (Eqn 3), then the static stress concentration k_t reduces with strain as shown in table 1. For these large elastic deformations it is more appropriate to use Inglis's equation in its general form for enclosed flaws (Eqn 4). The revised stress concentrations are given in table 2 and they show similar improvements.

4. Discussion

Loaded NR components, produced by conventional moulding methods, contain surface defects acting as stress raisers that contribute to fatigue failures. The surface finish of NR improves with increases in tensile strain. In fatigue, higher stress levels in the pre-stressed (pre-strained) material are partially compensated for by these improvements in surface finish. Microscopically, naturally occurring surface defects, particularly voids, undergo large changes in geometry when rubber is loaded in tension. Stress concentration diminishes as strain increases and, irrespective of the notch sensitivity of the material, dynamic stress concentration (k_f) will diminish with reductions in static stress concentration (k_t). Again, higher mean stress in a fatigue cycle is in part redressed by lower stress concentration.

Further research, using reflected light interference microscopy or some other non-contact method, is required to study the three-dimensional changes in surface flaws in strained rubber. These changes will be correlated to measurements of fatigue resistance obtained from Wöhler tests on the same samples. Tests on both strain

crystallising and non strain crystallising rubbers are necessary to determine the separate contribution made to elastomeric fatigue properties by dynamic strain energy, stress concentration and crystallinity.

5. References

1 M. D. Ellul, (Gent A.N. Editor), *Chapter 6, "Mechanical Fatigue", Engineering with Rubber. How to Design Rubber Components* pp147-148, Hanser (1992).

2 K.-H. Schwalbe, *Bruchmechanik metallischer Werkstoffe*, Carl Hanser Verlag (1980).

3 J.W. Bergmann, R. Heidenreich, H. Bügler, W. Oberparleiter, *IABG-Bericht* B-TF-2355 (1988).

4 G. J. Lake and P. B. Lindley, *Journal of Applied Polymer Science 10*, p 343 (1966)

5 A. N. Gent, "Strength of elastomers" *Science and Technology of Rubber 2nd Ed.* Academic Press Inc., pp 474-475 (1994)

6 N. Andre, G. Cailletaud and R. Piques, "Haigh diagram for fatigue crack initiation prediction of natural rubber components". *KGK Kautschuk gummi Kunststoffe 52* Jahrgang, Nr 2/99 (1999).

7 A. N. Gent, "Strength of elastomers" *Science and Technology of Rubber 2nd Ed.* Academic Press Inc., p490 (1994)

8 F. Abraham, T. Alshuth and S Jerrams "Dependence of fatigue life of elastomers on stress amplitude and prestress", Kautschuck-Herbst-Kolloquium 2000 ~ Wissenschaftliche Fachtagung, Hannover, Germany, (2000)

9 F. Abraham and S. Jerrams, "The Dependence on Mean Stress and Stress Amplitude of the Fatigue Life of Elastomers" The International Rubber Conference (IRC2001) Birmingham (2001)

10 A. N. Gent, "Strength of elastomers" *Science and Technology of Rubber 2nd Ed.* Academic Press Inc., p474 (1994)

11 F. T. Farago "Handbook of Dimensional Measurement", 2nd Ed., Chapter 15, p390. Industrial Press Inc. (1982)

12 C.E. Inglis, *Trans. Inst. Naval Architects,* London, 55, p219 (1913)

Acknowledgment

The authors wish to thank Frank Abraham of the Deutschen Institut für Kautschuktechnologie e.V. and Coventry University, for providing the impetus for research into stress concentration in elastomers.

The Authors

Dr. Steve Jerrams is Senior Research Fellow at the Dublin Institute of Technology (DIT) and manages post graduate research in the field of mechanical engineering. He specialises in research into non-linear stress analysis and strain energy.

Amir Tabaković is a Mechanical Engineering student at the Dublin Institute of Technology about to begin postgraduate research into elastomeric material behaviour.

Correspondence

Dr Steve Jerrams,
Senior Research Fellow,
Faculty of Engineering,
Room 143,
Dublin Institute of Technology,
Bolton St.,
Dublin 1, Ireland
Phone: 00 353 (0)1 4023764
Fax: 00 353 (0)1 4023999
Email: stephen.jerrams@dit.ie

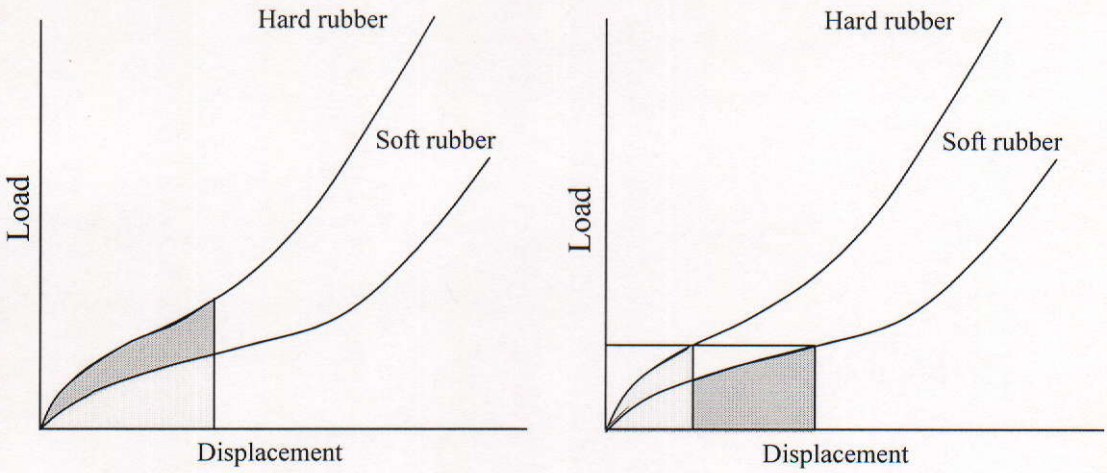

Figure 1. **Available strain energy for crack propagation in elastomeric fatigue**

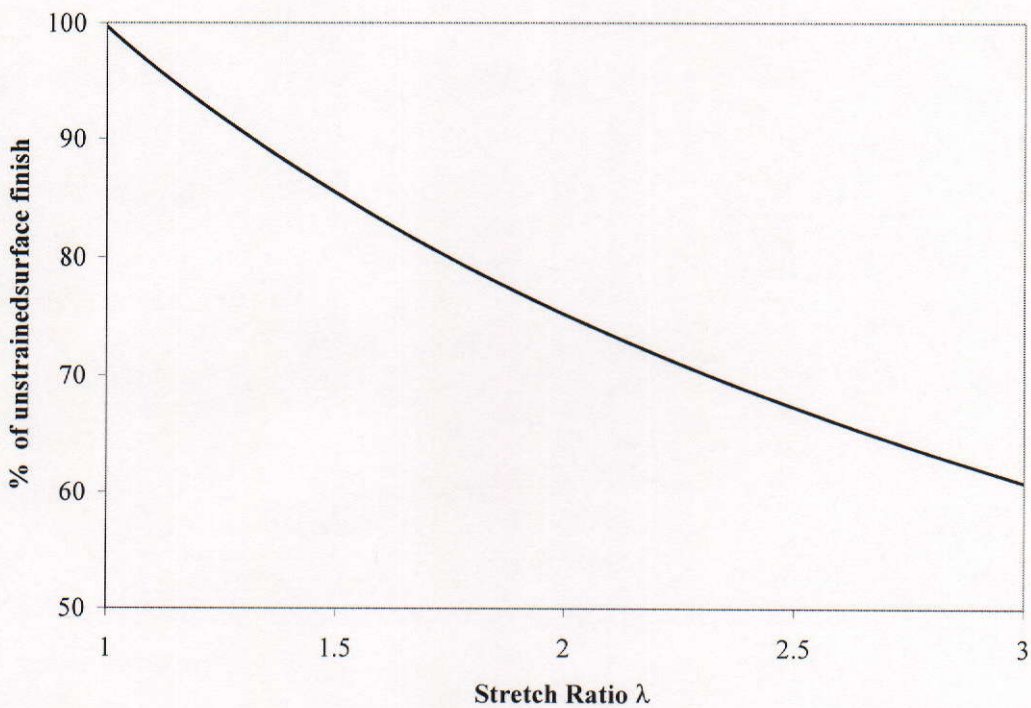

Figure 2. **Improvement in surface finish of NR subjected to tensile strain**

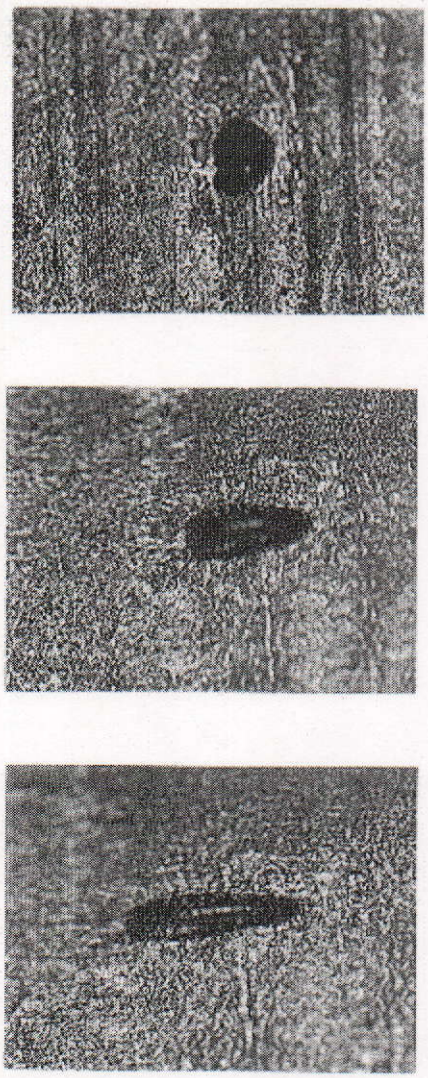

a) unstrained

b) $\lambda = 2$

c) $\lambda = 3$

Figure 3. **A surface flaw in a 38 IRHD NR subjected to uniaxial tensile strain**

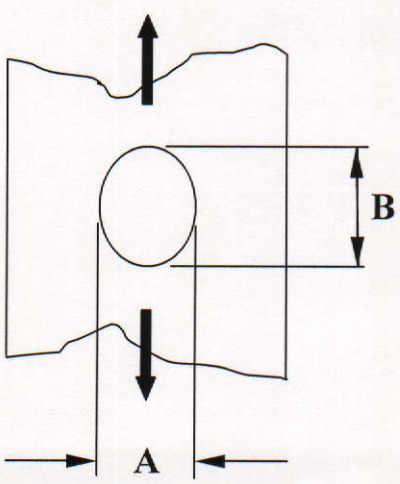

λ	k_t
1	2.6
2	1.79
3	1.46

$$k_t = 1 + \frac{2A}{B} \qquad (3)$$

Table 1. Change in stress concentration with tensile strain in NR samples (Eqn 3)

$$k_t = \frac{\sigma_t}{\sigma} = 1 + 2(0.5l/r)^{0.5} \qquad (4)$$

σ_t = stress at the tip of a sharp flaw, σ = nominal tensile stress, l = depth of edge flaw, r = radius of the tip in the unstressed state.

λ	k_t
1	2.80
2	1.85
3	1.38

Table 2. Change in stress concentration with tensile strain in NR samples (Eqn 4)

2. MT 2002 Paper

Surface Flaws in Elastomers and the use of Surface Treatments

Mr. Amir Tabaković, Dr. Steve Jerrams, Dr. Brian Bowe

Dublin Institute of Technology, Bolton Street, Dublin 1, Ireland.

Mr. Frank Abraham

Deutsches Institut für Kautschuktechnologie, Hannover, Germany.

Abstract

As with other physical properties, rubber behaves differently from conventional solids when subjected to cyclical loading. Previous research has suggested that strain crystallising filled rubbers exhibit higher fatigue resistance if pre-loads are not fully removed when components are stressed in service. However, improved fatigue resistance in pre-loaded non strain crystallising filled rubbers has also been observed and alternative explanations for greater fatigue resistance require consideration. Fatigue resistance in filled rubbers is largely dependent on the energy available to propagate a crack, but the influence of the stress concentration is undetermined in elastomeric fatigue. In metals fatigue, a stress concentration is virtually unaltered by cyclic loading. Rubber undergoes large reversible strains and it is argued that rubber components have less severe surface flaws when preloaded than in a stress free state. In fatigue, higher stress levels in the pre-stressed (pre-strained) material are thought to be partially compensated for by improvements in surface finish. It is expected that the size of flaws introduced during the manufacturing process, irrespective of whether the part is made by compression, injection or transfer moulding, can induce early failure of the specimen when it is under load. The fundamental question posed is 'can surface treatments influence fatigue resistance?' Reducing the size of a flaw has the potential to reduce concentration under load and thereby improve resistance. This paper describes an investigation of improvements in the surface characteristics and fatigue life of EPDM rubber dumbbell specimens using different coating technologies.

1. Introduction

The design of dynamically loaded rubber components must confirm to different criteria than those for metal components when subjected to fatigue. For instance, if the tensile cycles incurred by an elastomeric part are strain (displacement) controlled, the designer will choose the "softer" of two appropriate compounds. However, if the cycles are stress (load) controlled, the harder material will be selected[1]. This choice is based on the amount of strain energy available to propagate a crack in each cycle, as shown in figure1. For repeated displacement, the area under the load/displacement curve is smaller for less rigid rubber (Figure 1a), but for repeated load application the

opposite is true (Figure 1b). In fatigue, metal components experience micro strains and such conditions are irrelevant. Also, the reduction in fatigue life in metals when tensile mean stresses are increased has been comprehensively researched and explained[2,3], but strain crystallising rubbers exhibit greater fatigue resistance if tensile mean stresses are increased, providing the stress is not fully relaxed between loading cycles[4,5,6]. Hence improved fatigue properties can be achieved by pre-loading Natural Rubber (NR) components. The increase is attributed to crystallites inhibiting crack growth at the crack tip in a component under load. If the load is not fully removed then the crystalline region at the crack tip does not melt and the crack cannot propagate in subsequent load applications[7].

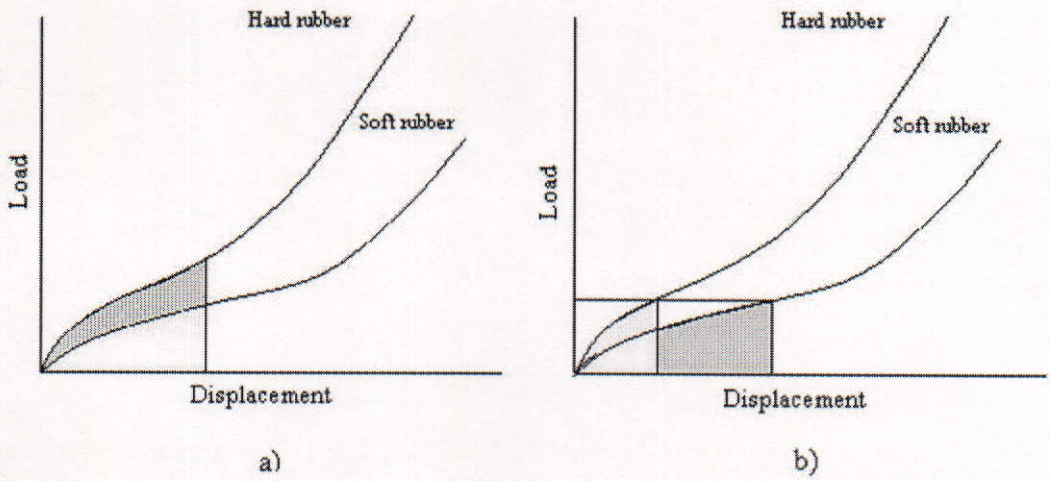

Figure 1. Available strain energy for crack propagation in elastomeric fatigue

Fatigue behaviour in strain crystallising and non-strain crystallising rubbers are considered to be dissimilar. However, increased fatigue resistance, associated with higher tensile mean stress, in the absence of full load relaxation, has also been observed in carbon black filled non strain crystallising rubbers by Abraham *et al*[8]. The predominant reason for this increase in fatigue strength is related to the dynamic strain energy available to propagate a crack, but the influence of changes in stress concentration in elastromeric fatigue is unresearched. In metal fatigue, the geometry of notches and flaws are barely changed by repeated strain cycles, but rubber

undergoes large reversible strains. Fatigue cracks in rubber are thought to emanate from naturally occurring surface defects of 40μm ± 20μm across[9].

Dimensional changes in flaws on the surfaces of elastomers were observed by Jerrams and Tabaković[10]. These flaws occur in rubber components irrespective of the production process.

This text describes surface treatments methods applied to elastomers and considers whether surface treatments can improve fatigue life. Different types of surface treatments are considered. To date rubber samples have been surface coated using Diamond Like Carbon coating (DLC). However, further surface treatments will be evaluated during the course of the research.

2. Material and Methods

Filled EPDM rubber is the material used in this research project. The EPDM contains 110 phr medium active carbon black and 70 phr softener oil. The tests used dumbbell test specimens of 25mm free length and 15mm diameter as shown in figure 2. This test specimen allows uniaxial testing under dynamic loading in tension and compression.

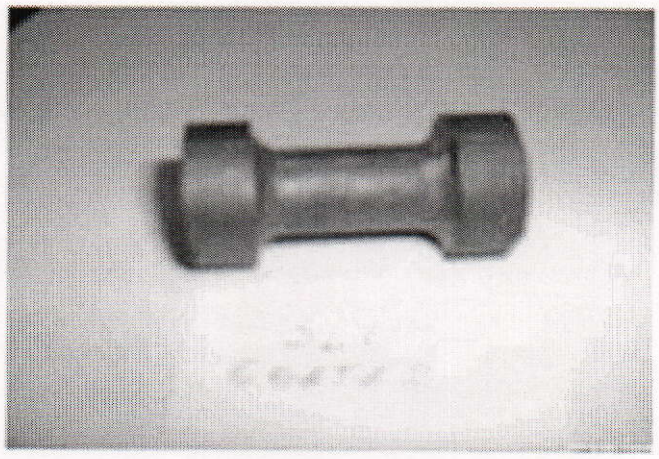

Figure 2. A dumbbell test specimen

2.1 Surface Treatments (Coatings)

The use of Diamond-like Carbon Coating (DLC) films results in two major problems in this application:

i) high internal compressive stresses leading to poor adhesion properties

ii) variation in friction coefficient (μ) that is dependent on the ambient relative humidity[11].

This research is concerned with the low adhesion properties of DLC. Carbon is a very versatile element. In graphite, carbon atoms bond strongly to each other within a plane, but weakly between adjacent planes. Graphite is soft, electrically conducting and opaque. In diamonds the bonding is strong in all directions. Diamond is the hardest known material, electrically insulating and transparent. Diamond films having excellent protective properties can be produced by vacuum deposition but the optimum substrate temperature for coating is about 900°C, which severely limits the range of substrates to which diamond carbon can be applied.

Near room temperature, a coating containing an amorphous carbon can be produced in which a proportion of the carbon atoms are bonded as in diamond and this resembles diamond in many ways, hence the term Diamond-Like Carbon Coating.

2.2.1 The Coating Process

The samples were initially cleaned in deionised water and placed in an oven at 50°C to remove any moisture. The warm samples were then placed in an atom beam system (figure 3) and pumped to a base pressure of $1x10^{-5}$ mbar. After cleaning in argon plasma and the coating was deposited using acetylene gas as the source of carbon. The argon is ionised by the radio frequency (RF) electromagnetic field and the positive ions bombard and clean the substrates. The cleaning stage is followed by the deposition stage in which a carbon containing gas such as acetylene is introduced to provide the energetic carbon ions. Diamond-like carbon is produced when carbon is deposited under energetic bombardment.

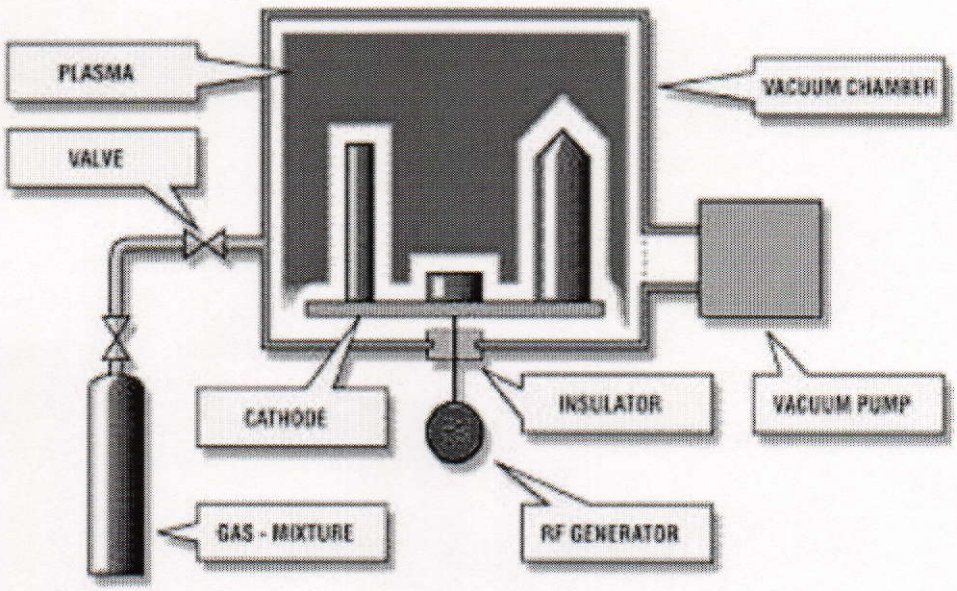

Figure 3. DLC Coating chamber

The instantaneous local high temperature and pressure induce a proportion of the carbon atoms to bond as diamond. These conditions obtain during plasma assisted chemical vapour deposition (PACVD). The samples were rotated during deposition. Coating thickness' were approximately 150nm - 200nm.

2.3 Metrology Methods

White Light Interferometry was used to measure surface roughness in the specimens. Optical methods have long been used for the purpose of surface profiling. One common practice is the inclusion of an interferometric attachment to a microscope to measure surface roughness of a specimen. With the computerisation applied to the technique, full field Phase Shifting Interferometry (PSI) was introduced, resulting in improved accuracy and measurement speed. Surface profiling is required to measure flaws on the surface of EPDM rubber specimens, uncoated and coated with DLC. The surface of each specimen was analysed using a Zygo new View 100 White Light Interferometer. The following results were obtained:

Uncoated dumbbell sample surface roughness is $\mathbf{R_a = 1.047\mu m}$ / Coated dumbbell samples have average roughness of $\mathbf{R_a = 1.023\mu m}$.

Uncoated flat sample surface roughness is $\mathbf{R_a = 0.383\mu m}$ / Coated flat sample surface roughness is $\mathbf{R_a = 0.837\mu m}$.

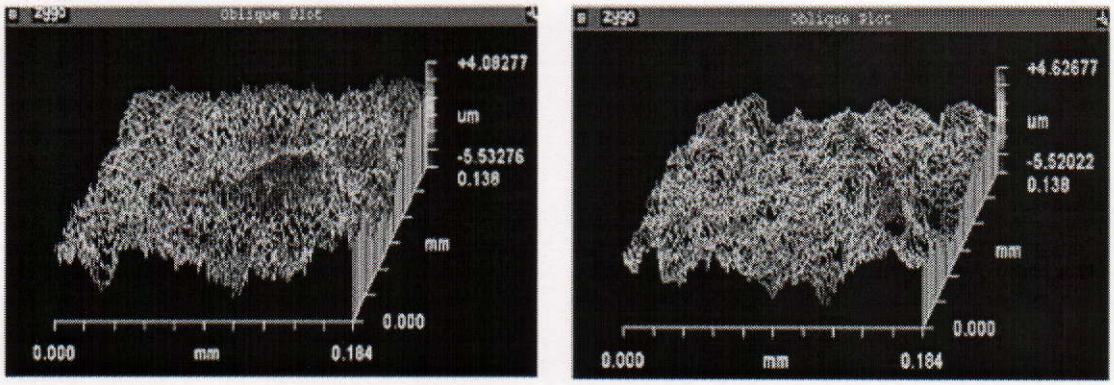

a) b)

Figure 4. Surface impression of a) Uncoated, b) Coated Dumbbell EPDM Rubber taken by White Light Interferometer

2.4 Fatigue Tests

The dynamic loading tests were conducted in the laboratories of the Deutsches Institut für Kautschuktechnologie (DIK), Hannover, Germany. Using a servo hydraulic test system MTS 831.50. Tests were conducted at room temperature and with harmonic loads at a frequency of 1Hz. The 1Hz frequency was chosen to avoid large increases in temperature, which would cause heat build up and consequent thermal break down[12]. The tests were load controlled to failure and six specimens were tested, three coated and three uncoated, though more tests will be required to provide sufficient data. A small number of tests were undertaken due to a shortage of the test equipment in DIT and all tests and materials were dependent on cooperation with two institutions, DIK and Enterprise Ireland. During the fatigue tests, modulus, loss factor and full hysteresis loops were continually recorded for analysis. All specimens were tested under the same conditions and only one procedure was used. A maximum load of 500N was applied from zero (figure 5 and 6). Hence there was no pre-stressing of the samples.

3. Results

The results of the fatigue tests of the coated and uncoated EPDM are shown in figures 5 and 6. Filled EPDM undergoes changes in physical properties during the

load controlled cycles. Dynamic load cycles induce an increased permanent set as the tests progresses. The modulus of the tested specimens decrease as a result of stress softening [13]. The fatigue tests on coated and uncoated samples, show that the stiffness as well as the loss factor (tan δ) of the material decreases throughout until fracture occurs (figure 7-9).

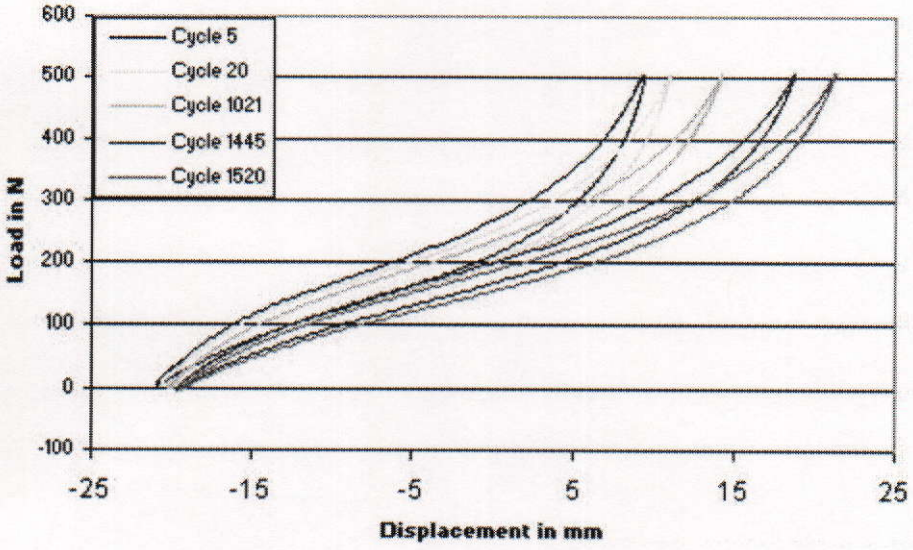

Figure 5. Hysteresis Loops during Fatigue Test, DLC-coated EPDM

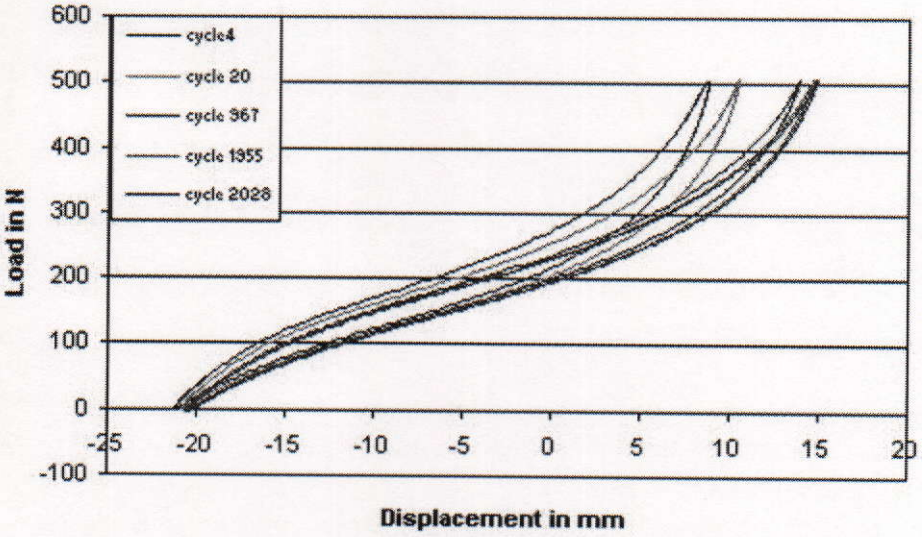

Figure 6. Hysteresis Loops during Fatigue Test, DLC-uncoated EPDM

Test results of coated samples showed that dissipated energy per cycle reaches a plateau after a few hundred cycles as a consequence of the strain behaviour and the change in tan δ. It is only immediately before fracture, as the crack propagates, that

the dissipated energy per cycle and tan δ increase (figure 7.a). The same phenomenon can be observed under less severe conditions when test specimens fail after a thousand cycles[8,14]. Uncoated specimens did not show the same behaviour (figure 7.b).

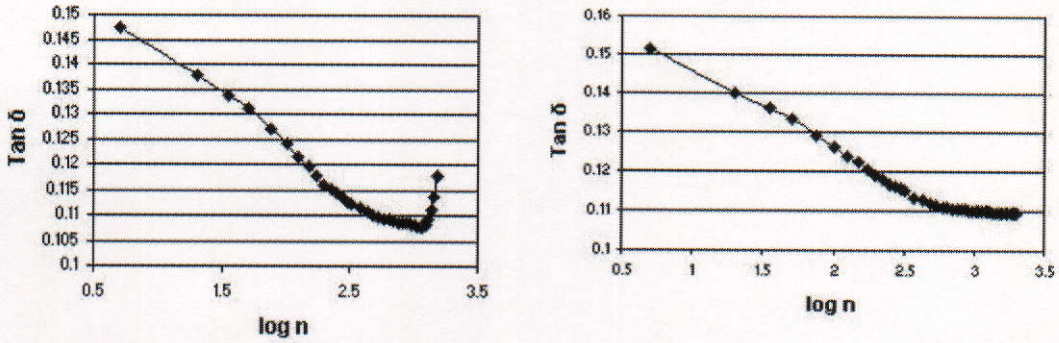

a) b)

Figure 7. Tan δ vs log n cycles a) DLC coated specimen, b) DLC uncoated specimen

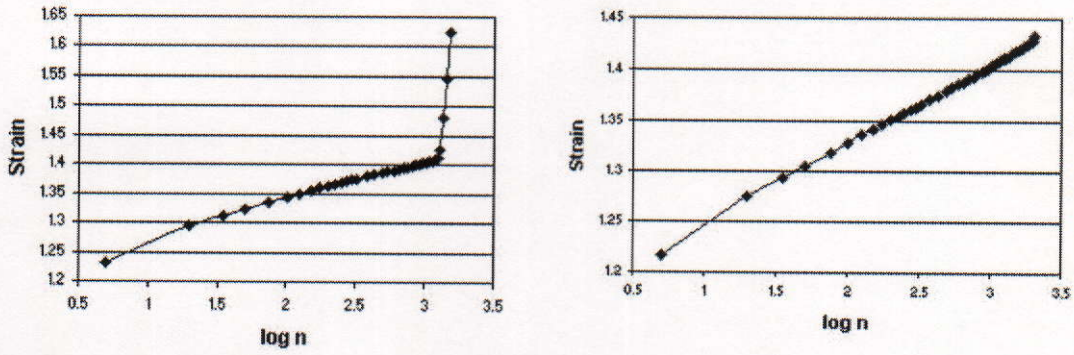

a) b)

Figure 8. Strain vs Ln cycles, a) EPDM Coated, b) EPDM Uncoated

Previous research suggests, that the component will fail when the complex modulus E* has fallen to approximately 76% of the first cycle[8,14]. This can lead to a determination of stiffness loss at which any rubber component manufactured from any particular material will fail. This finding has important consequences for maintenance and replacement of elastomeric components prior to failure. Test results for coated and uncoated specimens confirmed this observation (Figure 9).

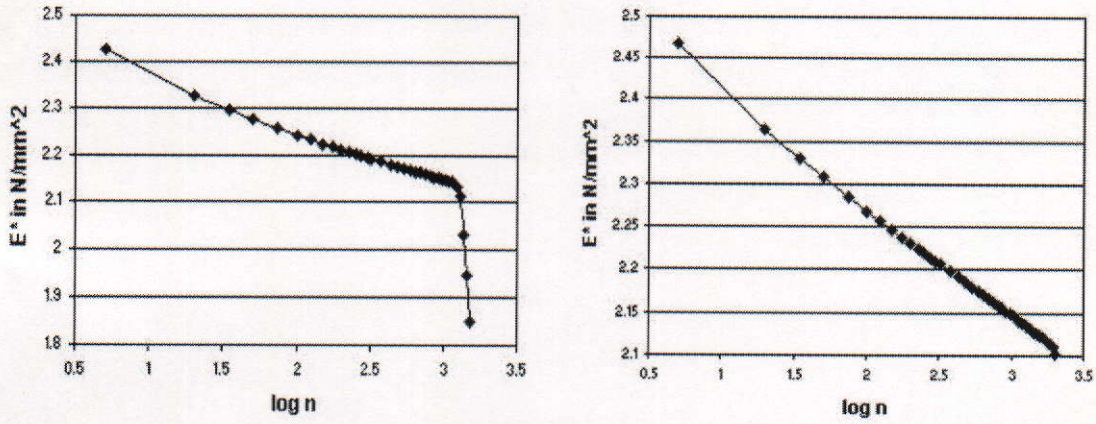

Figure 9. Complex modulus E* vs Ln cycles, a) EPDM Coated, b) EPDM Uncoated

4. Discussion

From the results we can conclude that DLC coating is not a suitable treatment for rubber materials. The procedure does not improve the physical properties and is not economically viable. It is possible that the high temperatures required in the coating procedure alter the properties of the material. However it is advisable to conduct full physical fatigue tests on the samples as to date only one set of results have been obtained and only one procedure was used. Using the metrology methods described, small defects can be detected on the surface of the sample and it might be possible to establish whether correlation between measured surface finish and fatigue life exists.

5. Future Work

Future work will consider different surface treatments. It is proposed to use sol-gel technology with the material Tetraoxysilane, as well as surface blasting with different media. Lack of testing equipment prevents the investigation of the full physical behaviour of the samples. It is also proposed to make simple measurements of surface finish in the rubber samples in order to establish whether a correlation between measured surface finish and fatigue life exists. Using the Finite Element Analysis, elastomeric crack propagation will be modelled, by controlling the notch dimensions and physical properties in order to simulate actual material behaviour. Finite Element Analysis has shown us that it is possible to predict the fatigue behaviour of rubber samples using the proper curve fitting procedures[15].

6. References

1. M. D. Ellul, (Gent A.N. Editor), Chapter 6, "Mechanical Fatigue", Engineering with Rubber to design Rubber components, pp147-148, Hanser(1992)
2. K.-H. Schwalbe, Bruchmechanik metallischer Werkstoffe, Carl Hanser Verlag (1980)
3. J.W. Bergmann, R. Heidenreich, H. Bügler, W. Oberparleiter, IABG-Bericht B-TF-2355 (1988)
4. G. J. Lake and P. B. Lindley, Journal of Applied Polymer Science 10, p 343 (1966)
5. A. N. Gent, "Strength of elastomers" Science and Technology of Rubber 2nd Ed. Academic Press Inc., pp 474-475 (1994)
6. N. Andre, G. Cailletaud and R. Piques, "High diagram for fatigue crack initiation prediction of natural rubber components". KGK Kautschuk gummi Kunststoffe 52 Jahrgang, Nr 2/99 (1999).
7. A. N. Gent, "Strength of elastomers" Science and Technology of Rubber 2nd Ed. Academic Press Inc., p490 (1994)
8. F. Abraham, T. Alshuth, S. J. Jerrams, "The dependence on Minimum Stress and Stress Amplitude of the Fatigue Life of Non Strain Crystallising Elastomers" The International Rubber Conference (IRC2001), Birmingham (2001), Bruchmechanik und Lebensdauer von Elastomeren, Hannover, Germany (2002).
9. A. N. Gent, "Strength of elastomers" Science and Technology of Rubber 2nd Ed. Academic Press Inc., p474 (1994)
10. S. J. jerrams, A. Tabaković, "The Influence of Mean Stress on the Fatigue Properties of Natural Rubber, The International Rubber Conference (IRC2001) Birmingham (2001)
11. http://www.brunel.ac.uk/faculty/tech/systems/groups/dlcc/
12. R. Seldén, Progress in Rubber and Plastics Technology, 11 (1995) 56
13. L. Mullins, Rubber Chemistry and Technology 42, pp339 (1969)

14. T. Alshuth, F. Abraham and S.J. Jerrams, "Parameter Dependence and Prediction of Fatigue Properties of Elastomer Products" Presented at a meeting of the Rubber Division, American Chemical Society, October 2001, Cleveland, Ohio, USA
15. R. Johannknecht, S.J. Jerrams, G. Clauss, "The uncertainty of Implementing Curve-Fitting Procedures in Finite Element Software", Finite Element Analysis of Elastomers, pp.141 (1999)

Acknowlegement

The authors wish to thank Dr. Miriam McConnell of the Enterprise Ireland for assisting in the research process.

The Authors

Amir Tabaković is an MPhil student at the Dublin Institute of Technology (DIT) and is currently researching in the field of elastomeric material behaviour.

Dr. Steve Jerrams is Head of Research and Development in DIT.

Dr. Brian Bowe, works in the field of optics in the School of Physics, Faculty of Science, DIT.

Mr. Frank Abraham is a researcher in elastomeric fatigue at the Deutsches Institut für Kautschuktechnologie.